Faculté des Sciences Appliquées
Université de Liège

Laser cooling of atoms : Monte-Carlo wavefunction simulations

Renaud Chrétien

Mémoire de fin d'études réalisé
en vue de l'obtention du grade de
Master ingénieur civil physicien

Année académique 2013–2014

Acknowledgments

First and foremost, I would like to thank and to express my deep gratitude to my supervisor Prof. John Martin for the exceptional and precious supervision that I received during all the year. His guidance, patience and constant availability have allowed me to perform this master thesis in the best conditions. May this work not be at the antipodes of his expectations and knowledge of physics ...

I also would like to thank Prof. Peter Schlagheck, Prof. Thierry Bastin and Prof. Benoît Vanderheyden for accepting to constitute my reading committee. I wish them the most pleasant reading possible.

This master thesis has made an intensive use of the resources of the "Consortium des Équipements de Calcul Intensif" (`http://www.ceci-hpc.be/`), supported by the FRS-FNRS.

Finally, I would like to thank my family and friends that have supported me all along the way.

Contents

Introduction

The control and manipulation of charged particles by means of external fields has quickly been at the centre of the fundamental knowledge of physics. For example, in high energy physics, one accelerates and collides particles by the use of electric and magnetic fields in order to create new particles with lifetimes so small that they should not be observed naturally. Whereas it is relatively easy to manipulate charged particles, the control of neutral particles is much more limited. Indeed, since those particles are not subject to electromagnetic interaction, except through their possible magnetic moment or polarisation, their manipulation can be quite complex. However, thanks to the recent development of novel laser sources, the remote control of such neutral particles has been greatly enhanced. Lasers are used to slow down and cool neutral particles at temperatures so small that they can easily be manipulated with external electromagnetic fields. The related cooling techniques have allowed one to cool atomic vapours at temperatures very close to the absolute zero and constitute one of the most promising research areas in atomic physics.

The concept of manipulating atoms with light is a source of interest for a long time. Kepler explained the orientation of comets tail with respect to the Sun by introducing what is now called radiation pressure[1]. In 1905, based on the previous works of Max Planck, Einstein postulated that a photon owns a quantised energy : he then explained absorption and emission processes in terms of quantised energy exchanges between light and matter. The subsequent quantisation of the momentum carried by a photon led to a better understandig of radiation pressure. Nonetheless, one had to wait until the advent of tunable lasers to make significant progress in the control of atoms by light. Since then, laser cooling and subsequent cold atoms have become a central research thematic in atomic physics, as the diagram of Figure 1 shows. Indeed, cold atoms can be probed, controlled and manipulated, even individually : they have paved the way for numerous new research prospects both theoretical and experimental.

As Adams and Riis report in their historical sketch of cold atom physics [1], Askar'yan showed in 1962 that a substantial force could be exerted on an atom by applying a laser field with an intensity gradient. In 1968, Letokhov suggested that the force Askar'yan identified could be used to trap atoms at the (anti-) nodes of a standing laser wave which is far detuned from atomic resonance. In the early 1970's, Ashkin accidentally discovered that the light force acting on an atom could be divided into two categories : the radiation pressure that results from linear momentum exchanges between light and matter and the dipole force explained by Askar'yan in 1962.

[1]Though his theory turned out to be incorrect, it highlighted the mechanical action of light on matter and originated subsequent research.

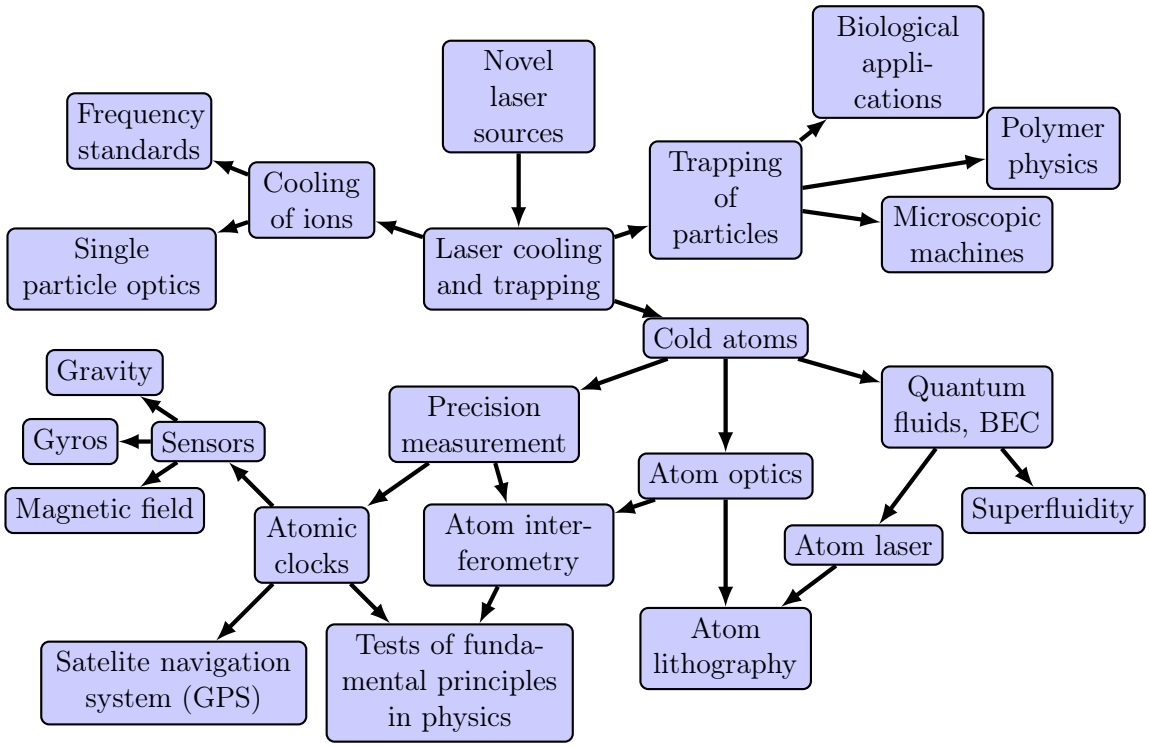

Figure 1: Laser cooling has become one of the most investigated subjects in atomic physics. It is at the origin of plethora of underlying subjects. Figure taken from [1].

It is not until 1975 that Wineland and Dehmelt proposed a cooling scheme for trapped ions [2] and, at the same time, Hänsch and Schawlow proposed a cooling scheme for neutral particles [3]. Both schemes are based on the Doppler effect, hence the name Doppler cooling they received. Theoretical calculations for such a cooling mechanism predict that an atomic vapour could be cooled at hundreds of μK. In 1987, a term working at NIST managed to trap a gas of atoms by using 3 pairs of counterpropagating lasers disposed along 3 orthogonal directions : this is the so-called magneto-optical trap (MOT).

However, in 1988, experiments showed that temperatures much smaller than those predicted by the Doppler cooling theory were obtained, indicating that another mechanism was acting. Such a cooling is closely related to polarisation gradients and is called Sisyphus cooling. Cohen-Tannoudji, Chu and Philipps earned the Nobel prize in 1997 for the explanation of that effect. Aspect *et al.* [4] then showed that it was possible to overcome the so-called recoil limit, corresponding to the velocity kick due to the emission of one photon. Indeed, temperatures below 100 nK have been obtained experimentally, validating the theoretical prediction of Aspect *et al.*. The two most successful cooling schemes to obtain such temperatures are the velocity selective coherent population trapping (VSCPT) and stimulated Raman cooling [1].

A logarithmic thermometer showing the achievable temperatures in various number cooling schemes is illustrated in Figure 2.

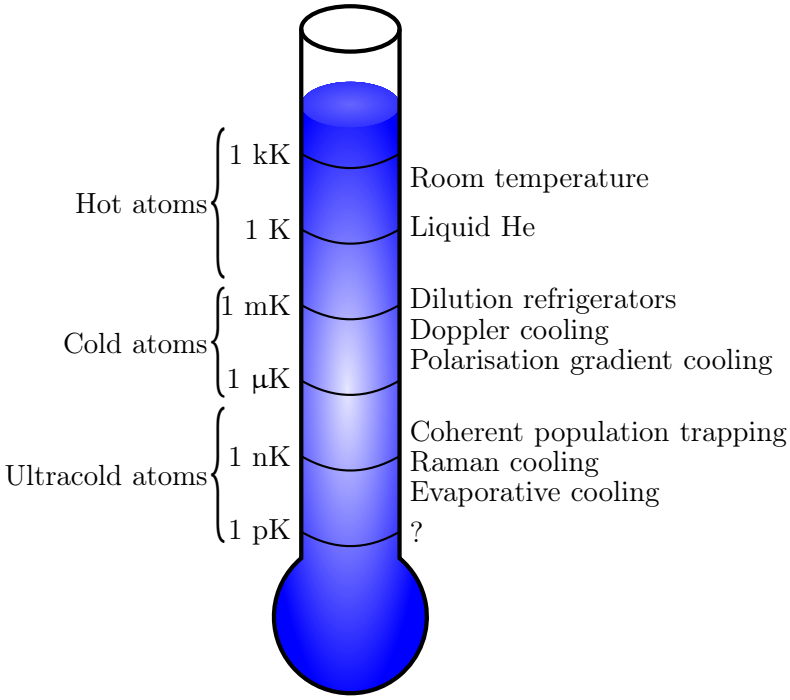

Figure 2: Logarithmic thermometer illustrating relevant orders of magnitude in cold atom physics. Figure taken from [1].

In 1985, concomitantly to the first experimental realisation of an atomic trap [5], Hess [6, 7] suggested an efficient technique called evaporative cooling to cool trapped atoms under the recoil limit. This technique allowed to achieve cooling down to temperatures never reached before and showed significant results, the most astonishing being, without any doubt, the realisation of Bose-Einstein condensation (BEC) in 1995 by Cornell and Wieman [8] which earned them (and also Ketterle) the Nobel prize in physics in 2001. The first BEC was achieved with rubidium atoms [9] and was followed by sodium [10], lithium [11, 12] and hydrogen [13]. As Adams and Riis [1] stress, an ideal BEC, that is a BEC where all atoms are in their ground state, represents a kind of "ultimate" cooling since the temperature, understood in terms of a distribution amongst energy levels, is literally deprived of all substance. For a thorough discussion about BEC, the reader can consult Ref. [14] dealing with this very exciting and versatile research field.

In this master thesis, we present an original synthesis of various works dealing with the numerical simulation of laser cooling within a full quantum approach [15–22]. We perform a detailed study of two distinct laser cooling schemes through full quantum-mechanical simulations using the Monte-Carlo WaveFunction (MCWF) method. We compute the equilibrium properties of a gas of cold atoms treating mechanical effects of light on atoms in an exact manner. We focus on two different cooling mechanisms, Doppler and Sisyphus cooling mechanisms. We thus aim at showing the effects of a laser field characterised by an intensity gradient

and/or a polarisation gradient on the steady state momentum distribution of an atomic gas. We shall compare the results of our simulations treating the atomic motion either classically or quantum-mechanically in order to assess the validity of the semiclassical approach. The MCWF method employed in the following is applied to a $J_g = 1/2 \leftrightarrow J_e = 3/2$ cooling transition, encountered for various atomic species like sodium or rubidium. Hereinbelow, we detail the content of each of the chapters of this work.

In the first chapter, we review laser cooling and we introduce the Doppler and Sisyphus cooling mechanisms. We explain the underlying mechanisms and detail why and how atoms are slowed down and cooled. We also introduce the concept of Doppler temperature, which is the lowest temperature achievable according to the physical mechanisms associated to Doppler cooling. We then discuss about experimental temperatures which turn out to be smaller than the Doppler limit for some laser configurations, indicating that a more subtle mechanism is acting : gradient polarisation cooling.

In the second chapter, we briefly introduce the theory of open quantum systems and master equations which are used to describe the dynamics of open quantum systems. Rather than an explicit derivation of the whole theory, that was incidentally performed by Damanet [23], we explain the main steps of derivation and the underlying hypotheses.

In the third chapter, we present the MCWF method whose aim is to solve master equations. We introduce the principle of the method in details and develop how to use it in practice. We also show the equivalence between the MCWF method and the related master equation, the former yielding the same results as the master equation, in average. We then discuss about the physical meaning of the method. Finally, we illustrate the MCWF method on simple atomic systems showing the saturation of an atomic transition or optical pumping.

In the fourth chapter, we derive the most general form of the system Hamiltonian required by the MCWF method. This derivation is performed in the general case of a $J_g \leftrightarrow J_e$ transition driven by a monochromatic travelling laser wave. More complicated configurations, such as standing waves, are readily obtained by applying the treatment described in this chapter.

Finally, in the fifth and last chapter, we present our numerical results. We present results about Doppler cooling occurring in a σ^+ standing wave. These results are followed by the atomic steady state properties in the case of the lin$\perp$lin configuration, consisting in two crossed linear laser polarisations. We show the significant temperature splitting that occurs between the two laser configurations. We also compare the results of our simulations with the predictions made on the basis of a semiclassical approach.

In the appendix A, we present a (very) short review about Clebsch-Gordan coefficients and we explain how they arise in atomic physics and how to compute them. This appendix allows us to develop some operators appearing in the derivation of the system Hamiltonian.

In the appendix B, we explain how to implement and write in a matrix form a series of quantities appearing in our work, this discussion being as close to the code as possible.

Chapter 1

Semiclassical description of laser cooling of neutral atoms

This first chapter is dedicated to a short review of laser cooling with a particular focus on two well-known types of laser cooling of atoms, namely Doppler and Sisyphus cooling mechanisms. We first present a semiclassical analysis of laser cooling, in which we explain the cooling process in terms of a damping force. Such a picture treats the atomic centre-of-mass motion classically and the atomic internal degrees of freedom quantum-mechanically. We discuss about the validity of such a picture in order to derive its limitations from which a quantum treatment of the external degrees of freedom is required. After that, we present an analysis of the different interacting systems, that is, an atom, the surrounding quantised electromagnetic field and the laser field, under the electric dipole approximation. Under that approximation, two kinds of force are acting on an atom : the radiation pressure force and the dipole force, each one with its own origin and its own physical interpretation. Those forces modify the mean velocity $\langle v \rangle$ and the velocity dispersion Δv of a set of moving atoms. In particular, they allow one to slow down and to cool a set of atoms. We then present Doppler cooling and explain how the non-relativistic Doppler effect modifies the laser frequency perceived by the atom and how this effect can be used to slow down the atomic motion. The Doppler limit, to which one can associate the Doppler temperature T_D, is finally derived. Then, we discuss the Sisyphus cooling mechanism that is responsible for the measured temperatures that are systematically smaller than the Doppler temperature for a particular type of cooling scheme : the polarisation gradient cooling scheme.

1.1 Semiclassical description of laser cooling

One can separate the atomic degrees of freedom (d. f.) into two distinct classes : internal and external ones. Internal d. f. essentially refer to spin polarisation or electronic configuration and are therefore related to the internal dynamics of the atom [24]. They describe the evolution of the population of the various substates of the atoms due to their coupling with external fields such as a laser field or the surrounding quantised electromagnetic field. External d. f. concern the position and the linear momentum of the centre-of-mass of the atom and describe the atomic centre-of-mass motion.

In the semiclassical approach, internal and external d. f. are treated using different descrip-

tions. For external d. f., a classical description is used : the particle is considered as being point-like and therefore, its position and linear momentum are classical variables of time. However, the atomic internal d. f. must be treated using a quantum description. Those two kinds of variables are closely related to one another. For example, due to linear momentum exchanges between light and an atom, the momentum of an atom immersed in a laser field is likely to be modified. Besides, according to the polarisation of the laser, internal variables are likely to be modified by the transfer of angular momentum involving atomic transitions between the various atomic substates. If the laser polarisation is space-varying, the probability of a certain transition to occur is also modified in space. This coupling between internal and external d. f. is at the basis of laser cooling.

For the moment, we do not care about internal sublevels and we consider an atom modelled as a two-level system, with ground state $|g\rangle$ and excited state $|e\rangle$. The ground state stands either for the fundamental (stable) state of the atom or a metastable state whose lifetime is much larger than a characteristic time of observation. The excited state is unstable and every atom in that state tends to come back in the ground state by emission of radiation. The lifetime of the excited state is denoted by Γ^{-1}. The energy separation between the two levels is $\hbar\omega_0$ where ω_0 is the transition frequency. We consider that the atom is interacting with a monochromatic plane laser wave with frequency ω. Unless the explicit mention of the contrary, we assume that only one laser is used in the discussion about the forces acting on an atom. Figure 1.1 shows the two-level model used in the following.

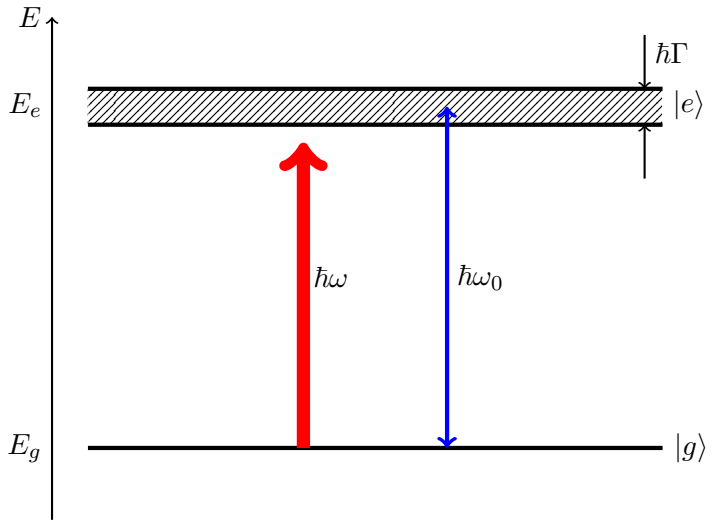

Figure 1.1: Modelling of an atom by a two-level system. The transition frequency is denoted by $\omega_0/2\pi$ and the laser frequency by $\omega/2\pi$.

Of course, such a system does not exist and is an idealisation used to simplify the description. To quote Bill Phillips [25] : "there are no two-level atoms, and sodium is not one of them". Notwithstanding that reality, we shall stick to that model with a pedagogical purpose in mind to present the Doppler cooling scheme. Yet there are some situations where two levels of energy play a distinguishable role apart from the other ones through laser polarisation or frequency. In such cases, the transition may be considered as to occur between the two

remarkable levels aside from degeneracy issues. In the case of optical pumping, where (for a proper laser polarisation) only two states are still coupled together after several cycles of fluorescence, the two-level atom picture works well since those two levels are being uncoupled to the rest of the energy levels.

1.1.1 Validity of the semiclassical approach

In a semiclassical treatment, the atom is considered as sitting at point $\mathbf{r}$, with a well defined velocity $\mathbf{v}$. In a quantum treatment of motion, the position and the momentum must be replaced by their corresponding operators and the atom is described by a wavepacket of spatial extension Δr and linear momentum extension Δp. However, as long as the position and linear momentum extensions are small compared to characteristic quantities of the problem, a point-like description may be used. For such an approach to be valid, two essential conditions must be simultaneously fulfilled :

1. The spatial extension Δr of the wavepacket describing the position spread must be small compared to the laser optical wavelength λ (see [26])

$$\Delta r \ll \lambda. \tag{1.1}$$

   This condition thus requires that the atomic position is well defined with regard to the laser shortest spatial scales of variation of the parameters (intensity, polarisation or phase) [24].

2. The spatial extension Δr of the wavepacket induces a linear momentum uncertainty $\Delta p \sim \hbar/\Delta r$ which in turn involves a velocity dispersion $\Delta v \sim \hbar/(m\Delta r)$. That velocity dispersion must also be well defined with respect to the velocity width resonance [26]. The Doppler shift $k\Delta v$ must be small compared to the natural atomic linewidth Γ

$$k\Delta v \ll \Gamma. \tag{1.2}$$

   This condition expresses that the resonance condition between the light and the atom is the same for all components of the atomic wavefunction.

Using the Heisenberg uncertainty relation and Eqs. (1.1) and (1.2), we arrive at

$$\frac{\hbar k^2}{m\Gamma} \ll 1. \tag{1.3}$$

This is the so-called *broad line condition* that ensures the validity of the semiclassical approach when it is fulfilled, which is the case for most resonant atomic transitions considered in cold atoms experiments. Furthermore, one can show that if Eq. (1.3) is fulfilled, then internal variables follow external variables adiabatically because the internal dynamics is very fast and is nearly instantaneously adapted to the external motion [26].

1.1.2 Treatment of the interacting systems

In order to assess the forces acting on the atom, we first have to model the interaction between the laser field and the atom. In the framework of the dipole approximation, we introduce the reduced electric dipole moment of the $e \leftrightarrow g$ transition by

$$\mathbf{d} = \langle e| \hat{\mathbf{D}} |g\rangle ,$$

which allows one to write the Hermitian electric dipole operator in the form

$$\hat{\mathbf{D}} = \mathbf{d}\,|e\rangle\langle g| + \mathbf{d}^*\,|g\rangle\langle e|\,.$$

Since the laser consists in a densely populated mode of the electric field, containing a huge number of photons, it can be described by a time-dependent classical electromagnetic wave of frequency ω and phase ϕ. The electric field produced by the laser reads

$$\mathbf{E}_L(\mathbf{r},t) = E_0\boldsymbol{\mathcal{E}}\cos\left(\mathbf{k}\cdot\mathbf{r}-\omega t\right), \tag{1.4}$$

where E_0 stands for the electric field amplitude, $\mathbf{k}$ for the laser wavevector and $\boldsymbol{\mathcal{E}}$ for the polarisation vector. The whole system is in fact made of 3 interacting subsystems.

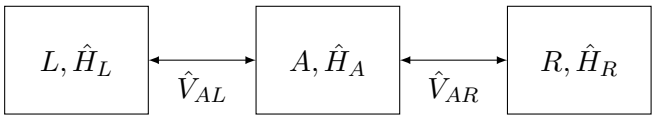

Figure 1.2: Various interacting subsystems with their own Hamiltonian and their coupling Hamiltonian : the atom (A) is coupled to the radiation field (R) and to the laser field(s) (L).

As we already mentioned, the laser is treated classically, *i.e.* as an external field, such that no Hamiltonian should be considered for its description. The laser/atom coupling accounts for absorption and stimulated emission processes. The atom is in turn coupled with all modes of the quantised radiation field R, initially in the vacuum state. That coupling is responsible for spontaneous emission of photons. Since the radiation field is characterised by an infinite number of degrees of freedom, it is considered as a reservoir. Because of the random nature of spontaneous emission, responsible for fluctuations and damping in the atomic evolution, processes in play refer to the class of open quantum systems. Such problems must be treated properly by means of a master equation. In the dedicated chapter, we perform an introduction to master equations and we derive explicitely the treatment to apply in the case of laser cooling.

1.2 Forces acting on an atom

We consider a two-level atom of initial linear momentum $\mathbf{p}$ and initial kinetic energy $E = p^2/2m$ interacting with a monochromatic travelling plane laser wave of wavevector $\mathbf{k}$ and frequency ω, which differs from the atomic transition frequency ω_0 by $\delta = \omega - \omega_0$, the detuning. The detuning is supposed to be small compared to ω_0 and ω, $|\delta| \ll \omega_0, \omega$, in which case the light beam is said to be quasi-resonant. In order to compute the mean spatial force acting on the atom, one has to introduce the Heisenberg equations for $\hat{\mathbf{r}}$ and $\hat{\mathbf{p}}$ and the subsequent force operator. From that operator, it is possible to compute the mean force acting on the atom (that is the expectation value of the force operator at point $\mathbf{r}$ in the internal state) which

turns out to be [27]

$$\begin{aligned}\boldsymbol{\mathcal{F}}(\mathbf{r}) = \langle \hat{\mathbf{F}}(\hat{\mathbf{r}}) \rangle &= -\hbar \left(\boldsymbol{\alpha}(\mathbf{r})\delta + \boldsymbol{\beta}(\mathbf{r})\frac{\Gamma}{2} \right) \frac{s(\mathbf{r})}{1+s(\mathbf{r})} \\ &= \underbrace{-\hbar\boldsymbol{\alpha}(\mathbf{r})\delta\frac{s(\mathbf{r})}{1+s(\mathbf{r})}}_{\boldsymbol{\mathcal{F}}_{\mathrm{dip}}} + \underbrace{-\frac{\hbar\Gamma}{2}\boldsymbol{\beta}(\mathbf{r})\frac{s(\mathbf{r})}{1+s(\mathbf{r})}}_{\boldsymbol{\mathcal{F}}_{\mathrm{RP}}},\end{aligned} \tag{1.5}$$

where we have introduced the vectors

$$\boldsymbol{\alpha}(\mathbf{r}) = \frac{\boldsymbol{\nabla}\Omega(\mathbf{r})}{\Omega(\mathbf{r})}, \qquad \boldsymbol{\beta}(\mathbf{r}) = \boldsymbol{\nabla}\phi(\mathbf{r})$$

and the saturation parameter of the laser wave,

$$s(\mathbf{r}) = \frac{\Omega^2(\mathbf{r})/2}{\delta^2 + \Gamma^2/4}.$$

Therefore, one can decompose the total force acting on the atom into two types of forces : one related to the intensity gradient of the laser field through $\Omega(\mathbf{r})$, the other to its phase gradient.

1.2.1 Radiative forces acting on an atom

The two kinds of forces have a distinct origin and meaning.

1. The force $\boldsymbol{\mathcal{F}}_{\mathrm{RP}}$ is proportional to the phase gradient of the wave and to the oscillating dipole component in quadrature with the laser wave [28] and is called the dissipative force or the radiation pressure force. It is due to the transfer of linear momentum from the incident laser to the atom by quasi-resonant absorption and subsequent emission of light. It is also referred to as scattering force. If we consider a laser wave of constant amplitude, then the mean radiative force is reduced to its dissipative component ($\boldsymbol{\mathcal{F}}_{\mathrm{dip}} = \mathbf{0}$). The general expression of the force is then given by

$$\boldsymbol{\mathcal{F}}_{\mathrm{RP}} = -\frac{\hbar\Gamma}{2}\frac{s}{1+s}\boldsymbol{\nabla}\phi(\mathbf{r}).$$

   In order to assess its properties, we consider a travelling plane wave, for which $\phi(\mathbf{r}) = -\mathbf{k}\cdot\mathbf{r}$ and $\boldsymbol{\beta} = \boldsymbol{\nabla}\phi(\mathbf{r}) = -\mathbf{k}$. In that case, the radiation pressure force reads

$$\boldsymbol{\mathcal{F}}_{\mathrm{RP}} = \frac{\hbar\mathbf{k}\Gamma}{2}\frac{s}{1+s} = \hbar\mathbf{k}\Gamma\frac{\Omega^2/4}{\delta^2 + (\Gamma^2/4) + (\Omega^2/2)}, \tag{1.6}$$

   with the Rabi frequency defined as

$$\Omega = -\frac{(\boldsymbol{\mathcal{E}}\cdot\mathbf{d})E_0}{\hbar}. \tag{1.7}$$

   Equation (1.6) can be cast in the form

$$\boldsymbol{\mathcal{F}}_{\mathrm{RP}} = \hbar\mathbf{k}\left\langle \frac{dN_{\mathrm{spont}}}{dt} \right\rangle,$$

where $\langle dN_{\text{spont}}/dt\rangle$ is the number of fluorescence cycles per unit time[1]. This is the only component of the force that involves energy exchanges between the atom and the surrounding quantised field [28].

2. The force $\boldsymbol{\mathcal{F}}_{\text{dip}}$ is proportional to the amplitude gradient of the wave and to the oscillating dipole component in phase with the laser wave [28] and is called dipole or gradient force. In order to have an amplitude gradient, one has to superpose several plane waves of different wavevectors $\mathbf{k}$. Consider an atom interacting with two counterpropagating plane laser waves. The total laser field is given by the superposition of the two laser fields, that is

$$\mathbf{E}_{\text{tot}}(\mathbf{r},t) = E_0\boldsymbol{\mathcal{E}}\Big(\cos\left(\mathbf{k}\cdot\mathbf{r}-\omega t\right)+\cos\left(-\mathbf{k}\cdot\mathbf{r}-\omega t\right)\Big).$$

For instance, the atom can scatter a photon of wavevector $\mathbf{k}_1 = \mathbf{k}$ from the first laser into the second laser of wavevector $\mathbf{k}_2 = -\mathbf{k}$. The net energy of the laser field remains unchanged whilst the atom experiences a linear momentum variation of $\hbar(\mathbf{k}_1-\mathbf{k}_2)$. This is a redistribution of photons between the components of the global laser field. That process is known for inducing the dipole force [24],

$$\boldsymbol{\mathcal{F}}_{\text{dip}} = -\frac{\hbar\delta}{2}\frac{\nabla s(\mathbf{r})}{1+s(\mathbf{r})} = -\frac{\hbar\delta}{4}\frac{\nabla\Omega(\mathbf{r})^2}{\delta^2+(\Gamma^2/4)+(\Omega(\mathbf{r})^2)/2}.$$

1.3 Doppler cooling

Laser cooling is closely related to the velocity dispersion Δv of an ensemble of atoms. In order to cool a set of atoms, one has to make the velocity spread smaller. With the goal of reducing Δv, the forces applied to the atoms must depend on their velocity. Otherwise, the velocity distribution would be translated as a rigid body, without any modification of its shape. Consider a classical moving atom with velocity $\mathbf{v}$ and position $\mathbf{r}(t) = \mathbf{v}t + \mathbf{r}_0$. Also, consider that the atom travels in a laser field produced by two counterpropagating plane laser waves, slightly detuned to the red of the atomic resonance ($\omega < \omega_0$) as depicted in Figure 1.3.

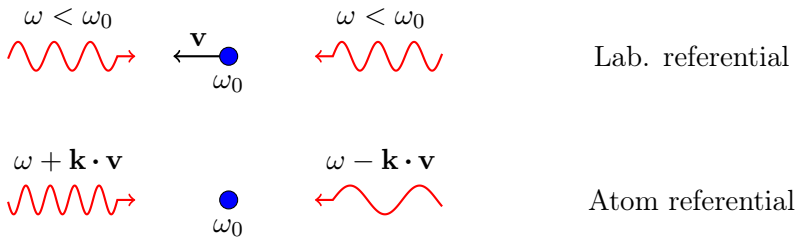

Figure 1.3: For a moving atom, the apparent frequencies are Doppler shifted, resulting in an imbalance between the two radiation forces exerted on the atom.

For an atom at rest, the apparent frequency of both lasers is identical, resulting in a zero net force applied to its centre-of-mass. For a moving atom, those frequencies are Doppler shifted.

[1] A fluorescence cycle is an absorption-spontaneous emission cycle.

The Doppler effect introduces the necessary velocity dependence for the force throughout the detuning δ, as Figure 1.3 illustrates. In this case, the counterpropagating beam is perceived with a frequency closer to the atomic transition frequency whilst the copropagating beam is perceived with a frequency further detuned from the atomic transition frequency. Therefore, a larger number of photons are absorbed from the counterpropagating wave than from the copropagating wave before being emitted by the atom.

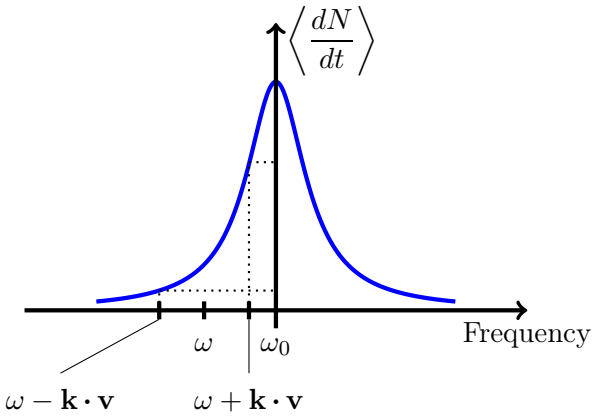

Figure 1.4: Mean scattering rate $\langle dN/dt \rangle$ versus frequency. The apparent frequency of the counterpropagating laser is closer to the atomic transition frequency than the apparent frequency of the copropagating laser. This figure is adapted from [27].

It turns out that the radiation pressure exerted by the counterpropagating beam is greater than the one exerted by the copropagating beam, the result being a net force that induces a deceleration. The force exerted by a single plane laser wave is given by Eq. (1.5) and reads [27]

$$\boldsymbol{\mathcal{F}}(\mathbf{v}) = -\hbar\Gamma \frac{\Omega^2(\mathbf{r})/4}{(\omega + \mathbf{k}\cdot\mathbf{v} - \omega_0^2)^2 + (\Gamma^2/4) + (\Omega^2(\mathbf{r})/2)}\mathbf{k}.$$

For small velocities, it can be interpreted in terms of a viscous force whose expression is obtained by performing a power series expansion of $\boldsymbol{\mathcal{F}}$ around $\mathbf{v} = \mathbf{0}$

$$\boldsymbol{\mathcal{F}} = \boldsymbol{\mathcal{F}}_0 - \alpha\mathbf{v} + \dots.$$

For a red detuned laser, the coefficient α is positive and can be interpreted as a viscosity coefficient, which is given by [27]

$$\alpha = -\hbar k^2 \frac{s}{(1+s)^2} \frac{\delta\Gamma}{\delta^2 + (\Gamma^2/4)}. \tag{1.8}$$

In a Doppler cooling experiment, one wants to maximise that friction coefficient in order to induce the greatest deceleration possible. Clearly, the maximum is reached when $\delta = -\Gamma/2$ and when $s = 1$ (which implies that $\Omega = \Gamma$), in which case one has

$$\alpha_{\max} = \frac{\hbar k^2}{4}.$$

Considering now both the copropagating and the counterpropagating lasers, one can separately add the contribution from the two lasers (ignoring interferences effects) to obtain the net force experienced by the atom (see Figure 1.5) [2].

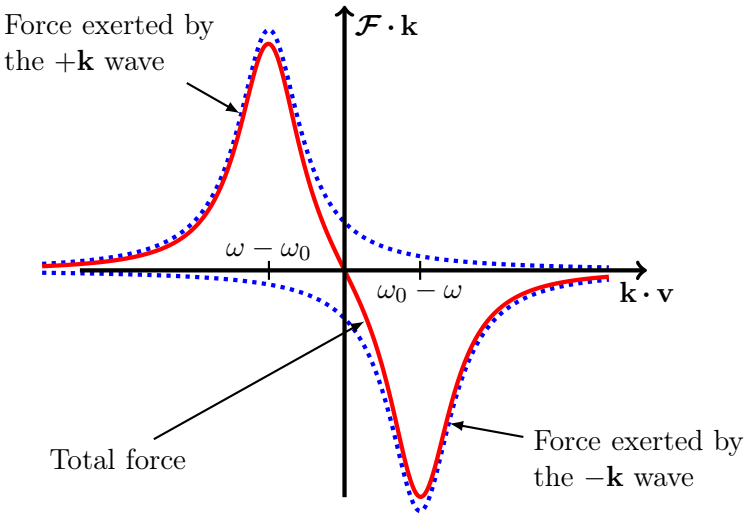

Figure 1.5: Net force (solid curve) experienced by an atom as a result of the superposition of the radiation pressure forces induced by both the copropagating and the counterpropagating waves in the low intensity limit. The force is always opposite to the velocity of the atom, which means that it slows and cools down the atom. This figure is adapted from [27].

Considered independently, the force profiles are Lorentz curves whose maxima are located at $\mathbf{k} \cdot \mathbf{v} = \omega_0 \pm \omega$, that is when the detuning is counterbalanced by the Doppler shift. Considered both together and inspecting Eq. (1.8), one observes that the constant term $\boldsymbol{\mathcal{F}}_0$ in the series expansion of $\boldsymbol{\mathcal{F}}$ of one laser is cancelled out with the same term of the other laser. Close to $\mathbf{v} = \mathbf{0}$, the net force is linear and opposite to the velocity. The generalisation to three dimension is straightforward. Three pairs of laser beams are disposed along three orthogonal directions in order to create a so-called optical molasse.

1.3.1 Energy and momentum budget applied to the photon/atom system

In this subsection, we detail more closely how the momentum transfer can cool the atom. Consider an atom of momentum $\mathbf{p}$ and energy $p^2/2m$ travelling in a counterpropagating laser solely. The coupling between the laser field and the atom is responsible for absorption and stimulated emission processes. However, spontaneous emission may also occur through the coupling with the quantised surrounding field. We consider for the moment that the atom undergoes a fluorescence cycle. Such an absorption-spontaneous emission cycle causes a linear momentum variation equal to the linear momentum of the absorbed photon $\hbar\mathbf{k}$ minus the linear momentum $\hbar\mathbf{k}'$ of the spontaneous emitted photon. After a fluorescence cycle, the

[2] This approach is rigourous for neutral atoms in the low intensity limit and if the total radiation force is spatially averaged (see [27]). At high intensity, interferences between the two lasers are not negligible anymore.

momentum of the atom is thus

$$\mathbf{p}' = \mathbf{p} + \hbar\mathbf{k} - \hbar\mathbf{k}'.$$

The energy after a cycle is then given by

$$\begin{aligned} E' &= \frac{(\mathbf{p} + \hbar\mathbf{k} - \hbar\mathbf{k}')^2}{2m} \\ &= \frac{\mathbf{p}^2 + 2\mathbf{p}\cdot\hbar\mathbf{k} - 2\mathbf{p}\cdot\hbar\mathbf{k}' + (\hbar k)^2 + (\hbar k')^2 - 2\hbar\mathbf{k}\cdot\hbar\mathbf{k}'}{2m}. \end{aligned}$$

Assuming that the wavelength of the emitted photon is close to the one of the absorbed photon[3], one can write

$$(\hbar k')^2 \simeq (\hbar k)^2.$$

Then, the energy variation for one cycle reads

$$\Delta E \simeq \frac{(2\hbar k)^2 + 2\mathbf{p}\cdot\hbar\mathbf{k} - 2\mathbf{p}\cdot\hbar\mathbf{k}' - 2\hbar\mathbf{k}\cdot\hbar\mathbf{k}'}{2m}. \tag{1.9}$$

For the cooling process to be efficient, fluorescence cycles must be repeated several times. Let us consider N of those cycles. At the end of the day, the atom will have absorbed N laser photons of momentum $\hbar\mathbf{k}$ and will have emitted spontaneously N photons of momentum $\hbar\mathbf{k}'_i$ in random directions, as Figure 1.6 illustrates.

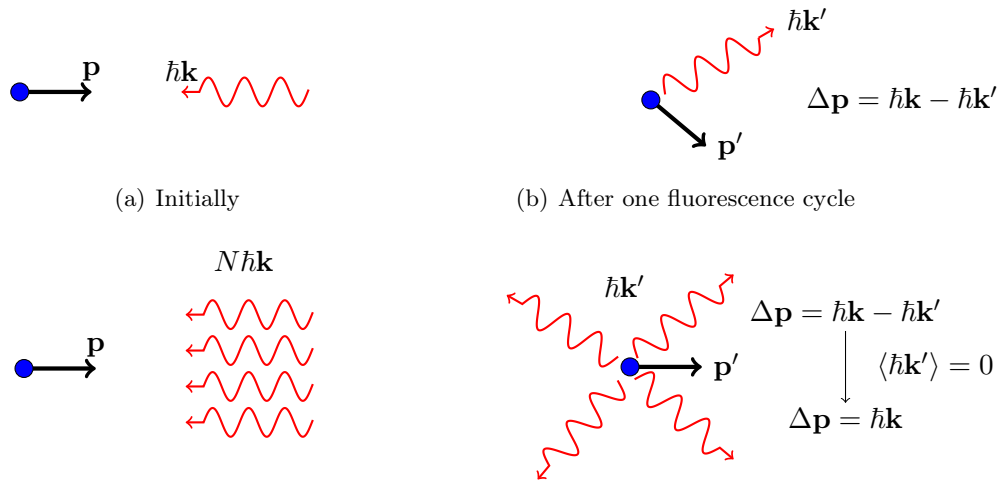

(a) Initially

(b) After one fluorescence cycle

(c) Initially

(d) After N fluorescence cycle

Figure 1.6: Variation of atomic momentum due to fluorescence.

[3]The natural and the Doppler broadenings cause a difference of wavelength between the absorbed and the re-emitted photon. However, the difference is small compared to the wavelengths in play.

Because spontaneous emission is a random process, the wavevectors of the emitted photons have random directions. The atomic momentum after N cycles reads

$$\begin{aligned}\mathbf{p}' &= \mathbf{p} + \left(\hbar\mathbf{k} - \hbar\mathbf{k}'_1\right) + \ldots + \left(\hbar\mathbf{k} - \hbar\mathbf{k}'_N\right) \\ &= \mathbf{p} + \sum_{i=1}^{N}\left(\hbar\mathbf{k} - \hbar\mathbf{k}'_i\right) = N\hbar\mathbf{k} - \underbrace{\sum_{i=1}^{N}\hbar\mathbf{k}'_i}_{\simeq 0} \\ &\simeq \mathbf{p} + N\hbar\mathbf{k}.\end{aligned}$$

Indeed, since the spontaneous emission process is isotropic (when the atom is driven by incoherent unpolarised light), the vector sum of the emitted photons wavevectors over a large number of cycles is close to zero. The momentum variation in one cycle is thus, on average,

$$\langle\Delta\mathbf{p}\rangle\Big|_{1\text{ cycle}} = \hbar\mathbf{k}.$$

Since the laser has been assumed to be counterpropagating, $\mathbf{p}$ and $\hbar\mathbf{k}$ have opposite direction and therefore the net variation of the modulus of the atomic momentum is negative. The absorption of a laser photon corresponds to a reduction of the modulus of the net atomic momentum and thus to a slowing effect. To that momentum variation is associated a variation of velocity given by

$$\langle\Delta\mathbf{v}\rangle\Big|_{1\text{ cycle}} = \frac{\langle\Delta\mathbf{p}\rangle\Big|_{1\text{ cycle}}}{m} = \frac{\hbar\mathbf{k}}{m} = \mathbf{v}_{\text{recoil}},$$

where $\mathbf{v}_{\text{recoil}}$ is the so-called recoil velocity. Since it also has an opposite direction as compared to the atom velocity, it is obvious that the atom is slowed down. The corresponding deceleration is given by, assuming that $\langle dN/dt\rangle$ cycles are realised per unit time,

$$\mathbf{a} = \left\langle\frac{dN}{dt}\right\rangle\langle\Delta\mathbf{v}\rangle\Big|_{1\text{ cycle}} = \left\langle\frac{dN}{dt}\right\rangle\frac{\hbar\mathbf{k}}{m}. \tag{1.10}$$

In terms of energy, since spontaneous emission is an isotropic process, we have for a large number N of cycles

$$\langle\mathbf{p}\cdot\hbar\mathbf{k}'\rangle \simeq 0, \qquad \langle\hbar\mathbf{k}\cdot\hbar\mathbf{k}'\rangle \simeq 0.$$

Thus, Eq. (1.9) for N cycles reads

$$\langle\Delta E\rangle \simeq N\left(\frac{\hbar^2k^2}{m} + \hbar\frac{\mathbf{p}\cdot\mathbf{k}}{m}\right).$$

If the laser and the atom are counterpropagating as assumed, the dot product $\mathbf{p}\cdot\mathbf{k}$ is negative and describes a reduction of the atomic kinetic energy whereas the term $\hbar^2k^2/2m = E_{\text{recoil}}$ is always positive and corresponds to a heating term. This term is called the recoil energy. The corresponding temperature, the recoil temperature, is given by : $T_{\text{recoil}} = E_{\text{recoil}}/k_B$ where k_B is the Boltzmann constant. Hopefully, as long as $|\mathbf{p}| > \hbar|\mathbf{k}|$, the heating term is much smaller than the cooling term which indicates that the atomic kinetic energy decreases on average at each absorption/emission cycle.

When the atom is placed in a field formed by two counterpropagating lasers (or 6 counterpropagating lasers along the three space directions in 3D), the atom will absorb a photon from

one laser or from the other. According to the sign of $\mathbf{p}\cdot\mathbf{k}$, one laser heats and accelerates the atom whereas the other slows down and cools the atom. However, because of the Doppler effect, the counterpropagating laser is perceived with a frequency larger than the frequency of the copropagating laser. Therefore, the atom will absorb much more photons from the counterpropagating laser than from the copropagating one : the cooling contribution from the counterpropagating laser is larger than the heating contribution of the copropagating laser.

One now has to discuss about stimulated emission processes. Contrarily to spontaneous emission which is a random and isotropic process, stimulated emitted photons are only emitted in well defined laser modes. If we only consider one counterpropagating laser and an atom in a 1D situation, this implies that the photons are emitted in the direction of the laser, the atom experiencing a momentum variation of an amount $\hbar k$ per stimulated emitted photon. Combined to the momentum variation $-\hbar k$ experienced at each absorption process, the total atomic momentum variation within such a cycle is equal to zero and there is no cooling effect. The stimulated emission does not contribute to cool the atom but delays the cooling since every stimulated process occurs instead of a possible spontaneous emission.

1.3.2 Efficiency of the process

From Eq. (1.10), one sees that the larger $\langle dN/dt\rangle$ is, the greater the deceleration is. The scattering process is maximum when $\omega = \omega_0$. However, for a slight detuning, it is still possible to observe a scattering process. One can show (see [29]) that the mean number of scattered photons per unit time follows a Lorentzian distribution with respect to the detuning

$$\left\langle \frac{dN}{dt} \right\rangle = \frac{\Gamma}{2}\frac{1}{1+\dfrac{1}{s}}\frac{1}{1+4\left(\dfrac{\omega-\omega_0}{\Gamma\sqrt{1+s}}\right)^2}. \tag{1.11}$$

In Figure 1.7, we plot the corresponding Lorentz curve as a function of the laser frequency ω.

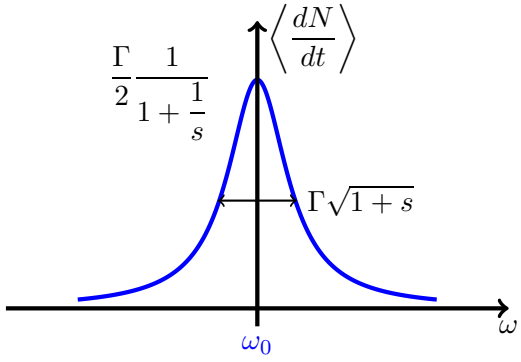

Figure 1.7: Mean scattering rate of photons as a function the incident laser frequency ω. This figure is adapted from [27].

In Eq. (1.11), Γ stands for the spontaneous emission rate from the excited state $|e\rangle$ to the ground state $|g\rangle$ (*i.e.* the Einstein's coefficient A_{eg}) and s stands for the saturation parameter

$s = I/I_s$. The saturation intensity, I_s, is a characteristic quantity of the atomic transition and is given by

$$I_s = \frac{\pi h (2\pi\nu_0)^3 \Gamma}{3c^2}.$$

The maximum number of scattered photons

$$\left\langle \frac{dN}{dt} \right\rangle = \frac{\Gamma}{2} \frac{1}{1 + \frac{1}{s}}$$

is reached at $\omega = \omega_0$. The full width at half maximum (also called the spectral line broadening) of the curve is given by $\Gamma\sqrt{1+s}$. One can also represent the mean number of scattered photons per unit time as a function of the saturation parameter s (for $\omega = \omega_0$), which is given in Figure 1.8 .

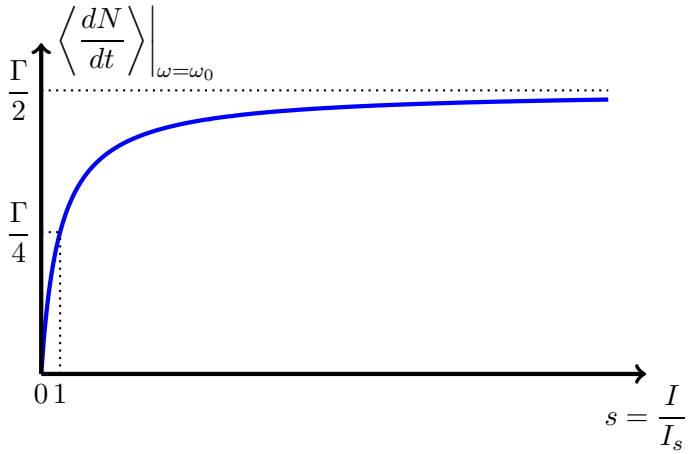

Figure 1.8: Mean number of scattered photons per unit time as a function of the saturation parameter s when the laser frequency ω is tuned to the atomic transition frequency ω_0 (maximum of the Lorentz curve depicted in Figure 1.7). The drawing is not at scale. This figure is adapted from [27].

In the low intensity regime ($s \ll 1$), the spectral line broadening is directly given by the spontaneous emission rate Γ. In such a case, $\langle dN/dt \rangle$ varies linearly with s, which also means that the mean number of scattered photons is proportional to the intensity of the incident light. At higher laser intensity, the spectral line broadening is obtained by weighting the spontaneous emission rate by $\sqrt{1+s}$. Therefore, since the saturation parameter s is proportional to the light intensity I, the width of the distribution increases with the light intensity I. That broadening is called power broadening and is the result of the laser-atom interaction. When $s \gg 1$, the scattering process saturates and $\langle dN/dt \rangle$ tends to $\Gamma/2$: this is called the saturation. The saturation is reached for an intensity several times larger than the saturation intensity. Therefore, it is useless to choose a laser intensity which is arbitrarily high since $\langle dN/dt \rangle$ saturates at a few I_s.

Limits of Doppler cooling

As soon as the apparent frequencies of the copropagating and the counterpropagating lasers are perceived as identical by the atom, the mean number of scattered photons by both lasers is identical, the net force experienced by the atom is equal to zero and the cooling process stops. In such a case, the expectation value for the momentum tends to zero but the expectation value for the energy tends to a non-zero minimal value. The Doppler cooling theory [30–33] predicts a residual energy

$$\langle E\rangle_{\min}(s) = \left(1+\frac{s}{2}\right)\frac{\hbar\Gamma}{4},$$

which is obviously minimum for $s \to 0$: $\langle E\rangle_{\min}(s=0) = \hbar\Gamma/4$. One can associate the so-called Doppler temperature T_D to this energy, through the relation

$$\frac{1}{2}k_B T_D = \frac{\hbar\Gamma}{4}. \tag{1.12}$$

Guéry-Odelin and Cohen-Tannoudji [27] provide a result which takes into account the angular diagram of emission

$$k_B T = \frac{\hbar\Gamma}{4}\left(\frac{2|\delta|}{\Gamma}+\frac{\Gamma}{2|\delta|}\right), \tag{1.13}$$

which is minimum when $\delta = -\Gamma/2$ and which yields the same temperature as Eq. (1.12).

1.4 Sub-Doppler cooling : Sisyphus cooling

In the previous sections, we analysed the Doppler cooling mechanism which led to the Doppler limit to which is associated the Doppler temperature. However, in 1988, Phillips *et al.* performed experiments on sodium atoms cooled in an optical molasse and measurements showed that temperatures far below the Doppler limit and approaching the recoil limit were obtained [34]. Furthermore, the temperature dependence with respect to the detuning δ was not in good agreement with the Doppler cooling predictions, those observations indicating that a more subtle mechanism than Doppler cooling was acting, namely the Sisyphus cooling mechanism (it is also referred to as polarisation gradient cooling in the literature). Its explanation, by Cohen-Tannoudji, Chu and Phillips [35] earned them the Nobel prize in physics in 1997 and is closely related to polarisation gradients [36, 37]. It holds in 5 points :

1. Atomic levels are shifted in a laser field (effect known as AC Stark shift or light shift).
2. Those light shifts depend on the laser polarisation.
3. Two counterpropagating lasers can give rise to a polarisation gradient.
4. In such a polarisation gradient, light shifts are space-varying and describe potential hills and valleys.
5. Due to optical pumping, atoms climb hills more often than they descend valleys.

The purpose of this section is to analyse the physical mechanism of this sub-Doppler cooling scheme.

1.4.1 Light shifts in a laser wave

The interaction between quasi-resonant light with atoms does not only cause transitions between the several Zeeman sublevels but is also responsible for light shift. The oscillating laser electric field acts as a time-dependent perturbation whose result is to shift the energy levels by AC Stark effect. An exact treatment (see for example van der Straten and Metcalf [29]) allows one to compute the shifted energies

$$E_{e/g}^{\text{shifted}} = \frac{\hbar}{2}\left(-\delta \mp \sqrt{\Omega^2 + \delta^2}\right) + E_{e/g}.$$

If the detuning is such that $\Omega \ll |\delta|$, the resulting energies are shifted with respect to $E_g = 0$ and $E_e = \hbar\omega_0$ by

$$\Delta E_{e/g} = \mp\frac{\hbar\Omega^2}{4\delta}.$$

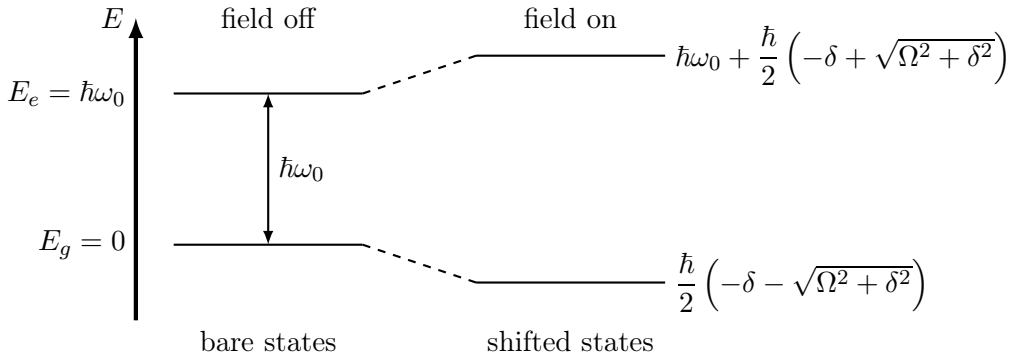

Figure 1.9: Light shifted energy levels due to the atom-light interaction. Figure taken from [29].

Those light shifts are usually neglected when one deals with light of frequency below the megahertz but become important in the case of laser light.

1.4.2 Light shifts of the magnetic sublevels

In the following, we consider the case of a $J_g \leftrightarrow J_e$ transition driven by a laser field where $J_{e/g}$ is the quantum number related to the angular momenta considered in the transition and where we denote by $m_{e/g}$ the magnetic quantum number related to the projection of $J_{e/g}$ onto the quantisation axis. The light shift of a magnetic sublevel depends on the laser polarisation. Depending on the polarisation, substates with magnetic numbers differing by $\Delta m = 0, \pm 1$ are coupled. More precisely, a laser whose polarisation is σ^+ can only couple substates with $\Delta m = 1$. If the polarisation is σ^-, then the laser couples substates with $\Delta m = -1$ and if the polarisation is π, then the laser couples substates with the same magnetic number.

In the following, we clarify the notions of left and right circularly polarised light and linearly polarised light. A linearly polarised beam means that the electric field of the beam oscillates and describes a straight line within a fixed plan perpendicular to the wavevector of the beam.

However, confusions arise when one talks about circularly polarised waves. For such polarisations, the electric field (of constant amplitude) of the propagating wave can be decomposed into two orthogonal components within the plane of oscillation. If those components are out of phase of $\pi/2$, then the global electric field is seen as rolling up around the propagation axis and its projection onto a plane perpendicular to the wavevector is a circle. According to the direction of rotation of the electric field, one talks about left or right circularly polarised wave. In optics, the direction of rotation is described with respect to an observer. If, for an observer sitting in front of the beam and facing it, the electric field is seen as rotating clockwise, then the wave is said to be right circularly polarised. If, for the same observer sitting at the same place, the electric field rotates counterclockwise then the wave is said to be left circularly polarised. Left/right circular polarisation is thus an intrinsic property of light. However, in order to get rid of the direction of propagation of the light, one could also define the polarisation with respect to a well-defined system of reference. We choose that system with the z axis being the motion axis. Any light beam polarised along the z direction will be considered as π-polarised. In order to define $\sigma^{\pm}$-polarised light, we shall use the convention adopted in optics : a clockwise rotating field as seen from the positive z direction (*i.e.* right-circularly polarised light propagating towards $z > 0$ or left-circularly polarised light propagating towards $z < 0$) is called σ^- polarised and a field rotating counterclockwise is called σ^+.

Without entering into details, one can show that the light shift is proportional to $|\langle J_e, m_e|\hat{\mathbf{d}}|J_g, m_g\rangle|^2$ which has to be computed for every possible transition. However, in the context of a qualitative explanation of the Sisyphus effect, we are not interested by the value taken by those shifts but rather by their relative values compared to each other. Since light shifts are proportional to $|\langle J_e, m_e|\hat{\mathbf{d}}|J_g, m_g\rangle|^2$, the square of the Clebsch-Gordan coefficients gives the relative values of the shifts.

Roughly speaking, Clebsch-Gordan coefficients $\langle J_g, m_g, 1, q|J_e, m_e\rangle$, characterise the probability that a transition between two levels takes place. In group theory, such coefficients arise when one wants to compute the inner product of two irreducible representations. That product generally involves a sum of irreducible representations of the studied group : this is the Clebsch-Gordan series. A particular case of those series arises when the sum of irreducible representations reduces to a single term. The proper invariant subspace of that irreducible representation is then spanned by vectors that could be defined, in the Young-Yamanouchi standard basis, as the sum of products of vectors of the two irreducible representations the inner product of which we want to compute. The coefficients of that expansion are called Clebsch-Gordan coefficients [38]. Those coefficients appear in the study of the permutation group S_n or in the study of Lie groups. In our case, they are related to the rotation group $\mathrm{SO}(3, R)$ in which we study the coupling of two angular momenta. The resulting angular momentum can be decomposed onto a basis of tensor product of the two angular momenta. The coefficients of that decomposition are again Clebsch-Gordan coefficients. A discussion about their further meaning, their consequences about transitions and their computation can be found in the Appendix A.

We consider, as an example, the $J_g = 1/2 \leftrightarrow J_g = 3/2$ transition that models the $3s\ ^2S_{1/2} \leftrightarrow 3p\ ^2P^0{}_{3/2}$ transition of Na atoms depicted in Figure 4.4. This is the simplest example but it can be easily generalised to more complicated configurations.

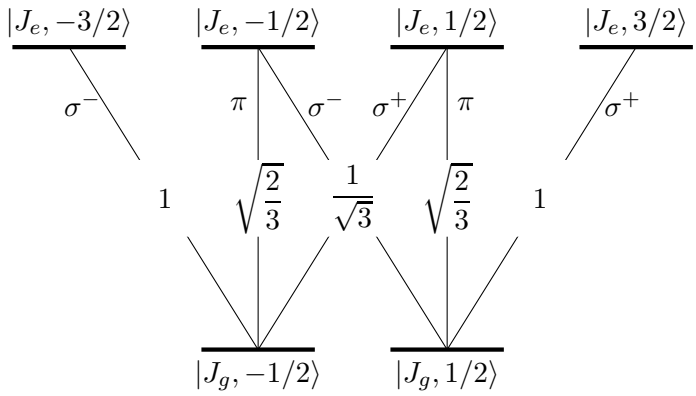

Figure 1.10: Atomic level scheme for a $J_g = 1/2 \leftrightarrow J_e = 3/2$ transition with the associated Clebsch-Gordan coefficients whose square gives the relative values of the light shifts. This figure is adapted from [27].

Because the squares of the Clebsch-Gordan coefficients of the σ^+ transitions are in a $1:3$ ratio, one can say that $|J_g, m_g = 1/2\rangle$ is three times more shifted than $|J_g, m_g = -1/2\rangle$, that conclusion being reversed when one considers σ^- transitions. Invoking symmetry arguments, one finds that the shifts are equal for π polarised light. Therefore, we conclude that depending on the laser polarisation and on the Clebsch-Gordan coefficients, the two ground state sublevels are shifted of a quantity that is in general different and which is crucial for the Sisyphus effect to occur.

1.4.3 Polarisation gradient

Two counterpropagating lasers can give rise to polarisation gradients. In one dimension, essentially two types of polarisation gradients are possible, each of which being associated to different cooling mechanisms [35, 39, 40] :

1. The first configuration, obtained by a superposition of two counterpropagating plane waves of orthogonal linear polarisations is called the lin$\perp$lin configuration. The polarisation switches from σ^- to σ^+ polarisation including π polarisation states. In between, we observe a gradient of ellipticity (Figure 1.11(a)).

2. The second configuration, obtained by a superposition of two orthogonal counterpropagating waves of circular polarisations is called the $\sigma^+ - \sigma^-$ configuration for which a pure rotation of polarisation is observed (Figure 1.11(b)). For such a scheme, the experienced polarisation is linear at any point and we observe a rotation of the polarisation direction in space with a period $\lambda/2$. Therefore, contrarily to the lin$\perp$lin configuration, there is no gradient of ellipticity. This leads to orientational cooling [22].

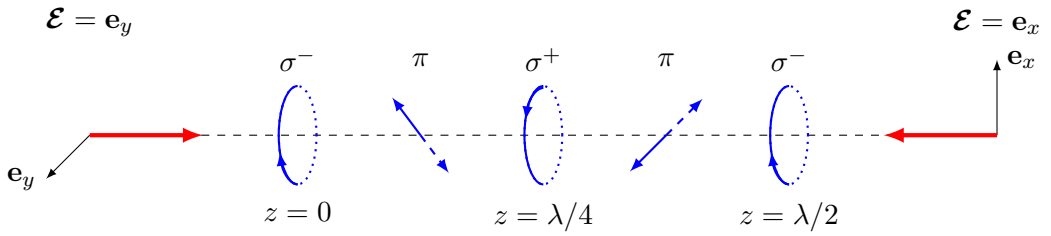

(a) lin⊥lin configuration

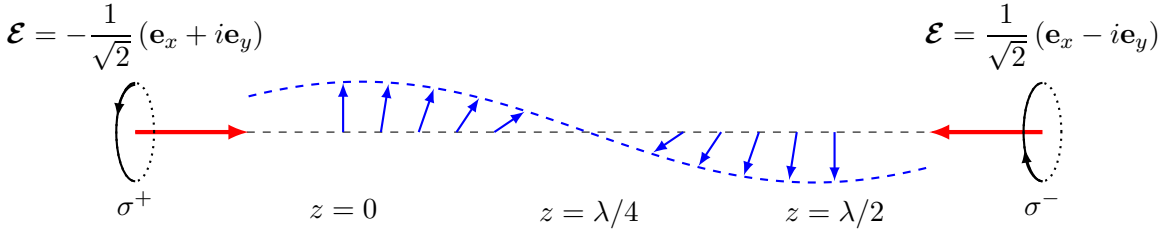

(b) $\sigma^+ - \sigma^-$ configuration

Figure 1.11: Polarisation of the total field resulting from the superposition of two counter-propagating waves with different polarisations. This figure is adapted from [27].

In the following, we mainly focus on the description of the lin⊥lin configuration arising from the superposition of the lasers fields

$$\begin{cases} \mathbf{E}_L(z,t) = E_0 \mathbf{e}_y \left[e^{i(kz-\omega t)} + e^{-i(kz-\omega t)} \right] \\ \mathbf{E}_R(z,t) = E_0 \mathbf{e}_x \left[e^{i(-kz-\omega t-\pi/2)} + e^{-i(-kz-\omega t-\pi/2)} \right] \end{cases},$$

so that the total field reads

$$\boxed{\mathbf{E}(z,t) = E_0 \left(\mathbf{e}_y e^{ikz} - i\mathbf{e}_x e^{-ikz} \right) e^{-i\omega t} + \text{c.c.}}$$

1.4.4 Light shifts in a polarisation gradient and optical pumping : Sisyphus effect

In a σ^+ polarised wave, atoms are pumped from the various ground Zeeman substates to the ground substate with the highest magnetic number whilst the conclusion is reversed in a σ^- polarised wave : this is the optical pumping process due to Kastler in 1950 [41]. The space-varying light shift of the 2 ground state sublevels, which we denote by $\pm\hbar\delta_g/2$ describe potential hills and valleys. Therefore, a moving atom in one of the two sublevels has to climb hills before it has to descend valleys, *i.e.* it periodically loses kinetic energy before regaining it. However, because of optical pumping, the atom has a large probability to be optically pumped from a sublevel to another when it is climbing a hill, that probability reaching a maximum at the top of the hill. If the optical pumping time is long enough, each climbing of a hill will cause an optical pumping from the highest energy ground state sublevel to the lowest one, hence preventing the atom from descending the valley and forcing it to climb another hill (Figure 1.12).

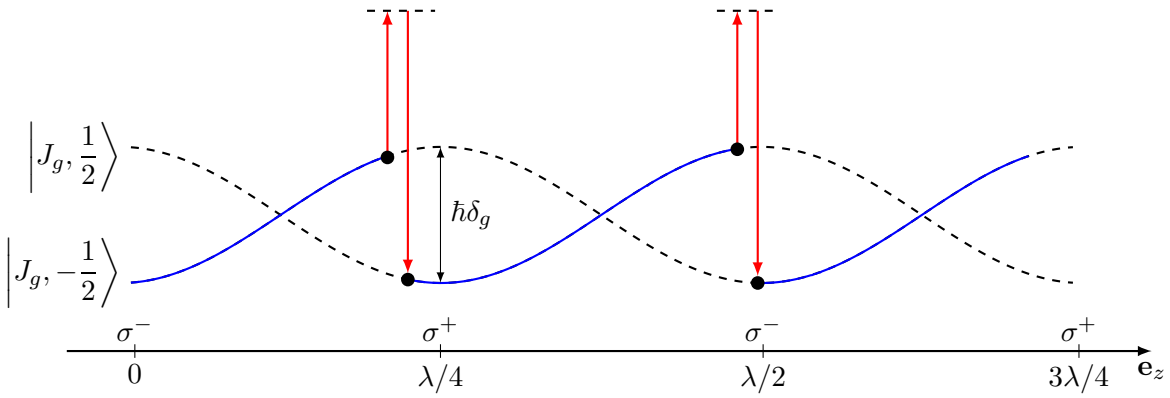

Figure 1.12: Mechanism of the Sisyphus effect : an atom climbing a hill and thus losing kinetic energy ends by being optically pumped to a lower energy ground state sublevel and thus ends by having to climb another hill, which causes another kinetic energy loss.

Therefore, due to the combined action of space-varying light shifts and optical pumping, the atomic kinetic energy gradually lowers until it becomes so small that the atom cannot reach any new hill. Inspired by the Greek mythology where Sisyphus was punished by Zeus to eternally roll, until the top of a moutain, a rock that inescapably comes back down just before reaching the top, Cohen-Tannoudji *et al.* named this mechanism Sisyphus cooling because the atom has to climb hills until its kinetic energy becomes too small to climb yet another hill. Cohen-Tannoudji and Guéry-Odelin [27] provide a simple argument for evaluating the equilibrium temperature. It is clear that the atomic kinetic energy is evacuated through the spontaneous emission of photons with energy higher by an amount $\hbar\delta_g$ (the light shift) than the one of absorbed photons. Therefore, after a fluorescence cycle, the kinetic energy of the atom has decreased by an amount $\hbar\delta_g$ whilst the energy of the quantised field has increased by the same amount. When the kinetic energy has become too small, the atom cannot climb the hill and remains trapped in the optical potential wells induced by the space-varying light shifts. For low laser intensities, the expected equilibrium temperature is [27]

$$T_{\text{sub-Doppler}} \sim \frac{\hbar\delta_g}{k_B} = \frac{1}{k_B}\frac{\hbar\Omega^2|\delta|}{4\delta^2+\Gamma^2}.$$

In the limit of large detunings where $|\delta| \gg \Gamma$, it is given by

$$T_{\text{sub-Doppler}} \sim \frac{\hbar\delta_g}{k_B} = \frac{1}{k_B}\frac{\hbar\Omega^2}{4|\delta|} \propto \frac{\text{Laser intensity}}{\text{Detuning}}.$$

This physical picture is theoretically confirmed by Dalibard and Cohen-Tannoudji [35] and experimentally by Salomon *et al.* [42].

Chapter 2

Open quantum systems and master equations in quantum optics

In this chapter, we introduce the suitable formalism for the description of open quantum systems : the master equations. Master equations are differential equations that aim to describe the evolution of a reduced density operator $\hat{\rho}_S$. We discuss the general hypotheses of derivation of such equations and we also introduce the Lindblad form. Any master equation that can be cast into such a form is guaranteed to preserve the properties of $\hat{\rho}_S$ as a density operator. Finally, we show that the related Lindblad operators are not unique.

2.1 Open quantum systems

Schrödinger's equation describes the time evolution and behaviour of a system which does not exchange any information with its surroundings. In such a case, the system under study is totally decoupled from the rest of the universe : the system is thus said to be closed or isolated from its surroundings. The state of the system can be described by a normalised state vector and the solution of the Schrödinger equation yields the state of the system at any time, provided the initial state is known. However, there are many situations where the system is found interacting with its surroundings, thus exhibiting behaviour and features beyond the Schrödinger equation. Such systems are called open quantum systems. Since open systems cannot be described by normalised state vectors, we have to introduce the suitable formalism for their description as the theory of open quantum systems. According to S. Banerjee and R. Srikanth [43, 44] which are quoted thereafter, the theory of open quantum systems addresses the problems of damping and dephasing in quantum systems by the assertion that all real systems of interest are "open" systems, surrounded by their environments. That is, all open quantum systems can be modelled as being a part of a bigger composite system SR, containing both the system of interest S and a reservoir R to which S is coupled. Mølmer and Castin [15] warn that, in quantum optics, contrarily to other branches in quantum physics, the problem is that the timescale of damping is often comparable to the timescale of coherent processes such as laser excitation. As a consequence, damping cannot be seen as a perturbation of the coherent evolution and perturbation theory cannot be used. One also cannot cast the problem into the determination of the final state of the system after the decay process : the system dynamics in between must be resolved.

A typical example of an open quantum system consists in a set of excited atoms interacting with their surroundings. The theory of open quantum systems also applies to cavity quantum electrodynamics (CQED) and quantum brownian motion (QBM), to mention some well-known research fields. We model such situations as is illustrated in Figure 2.1.

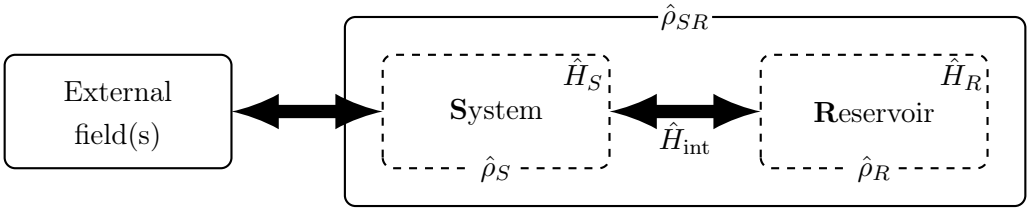

Figure 2.1: Open system(s) coupled to external field(s).

The Hilbert space of the system is denoted by $\mathcal{H}_S$, the Hilbert space of the reservoir by $\mathcal{H}_R$ and the Hilbert space for the whole system by $\mathcal{H}_{SR}$. The composite system SR is defined through the Hamiltonian of the total isolated system

$$\hat{H}_{\text{tot}} = \hat{H}_S \otimes \hat{\mathbb{1}}_R + \hat{\mathbb{1}}_S \otimes \hat{H}_R + \hat{H}_{\text{int}}$$

where

1. $\hat{H}_S$ is the Hamiltonian of the system of interest;
2. $\hat{H}_R$ is the Hamiltonian of the surrounding reservoir;
3. $\hat{H}_{\text{int}}$ is the interaction Hamiltonian between the system and its surroundings;
4. $\hat{\mathbb{1}}_i$ is the identity operator acting on the Hilbert space $\mathcal{H}_i$ $(i = S, R)$.

Amongst open quantum systems, a distinction can be established depending on the commutator of the system Hamiltonian $\hat{H}_S$ and the interaction Hamiltonian $\hat{H}_{\text{int}}$ [43, 44].

- The case of quantum dissipative systems, for which $[\hat{H}_S, \hat{H}_{\text{int}}] \neq 0$, resulting in decoherence with dissipation.
- The case of quantum non-demolition (QND) systems, for which $[\hat{H}_S, \hat{H}_{\text{int}}] = 0$, resulting in decoherence without any dissipation.

In our study, we consider the case where $[\hat{H}_S, \hat{H}_{\text{int}}] \neq 0$ corresponding to a dissipative dynamics.

We assume that the system S is described at the initial time by a density operator $\hat{\rho}_S(0)$ acting on the Hilbert space $\mathcal{H}_S$ of dimension d_S and that the reservoir is described at the same time by a density operator $\hat{\rho}_R(0)$ acting on the Hilbert space $\mathcal{H}_R$ of dimension d_R, that dimension possibly being very large, even infinite. The set "system + reservoir" constitutes a composite system and is therefore described at the initial time in terms of a density operator $\hat{\rho}_{SR}(0)$ acting on the tensor product Hilbert space $\mathcal{H}_{SR} = \mathcal{H}_S \otimes \mathcal{H}_R$ of dimension $d_{SR} = d_S \times d_R$. Since the total composite system is isolated, its evolution is unitary, *i.e.*

$$\hat{\rho}_{SR}(t) = \hat{U}(t)\hat{\rho}_{SR}(0)\hat{U}^\dagger(t) = e^{-i\hat{H}_{\text{tot}}t/\hbar}\hat{\rho}_{SR}(0)e^{i\hat{H}_{\text{tot}}t/\hbar}. \tag{2.1}$$

The state of the system can be alternatively and equivalentely determined with the help of the Liouville-von Neumann equation

$$i\hbar\frac{d\hat{\rho}_{SR}(t)}{dt} = [\hat{H}_{\text{tot}}, \hat{\rho}_{SR}(t)].$$

Generally, due to the large dimension of $\mathcal{H}_R$ (ans thus of $\mathcal{H}_{\text{tot}}$), the density operator $\hat{\rho}_{SR}(t)$ for the whole system (that describes the behaviour of both the system of interest and the reservoir) has a huge number of components, therefore making exact computations expensive, when they are not impossible. The evolution for the system S could of course be deduced from the one of the whole system. However, we are often not interested in the evolution of the reservoir which is not relevant, but rather by the evolution of the system S. Hence, we should derive an equation for the reduced dynamics of S that would take into account the interaction with the surroudings. Therefore, we introduce the reduced density operator as the partial trace of $\hat{\rho}_{SR}(t)$ over the reservoir degrees of freedom

$$\hat{\rho}_S(t) = \text{Tr}_R\left[\hat{\rho}_{SR}(t)\right].$$

This partial trace operation $\text{Tr}_R(\,\cdot\,)$ is the only operation which, for any physical observable O_S of the system S and $O_{SR} = O_S \otimes \mathbb{1}_R$ of both the system and the environment $S+R$ yields the same measurement statistics depending on whether O_{SR} is measured on $S+R$ in the state $\hat{\rho}_{SR}$ or O_S is measured on S in the state $\hat{\rho}_S = \text{Tr}_R(\hat{\rho}_{SR})$. For instance, the expectation value of the physical observable O_S is given by

$$\langle O_S\rangle = \text{Tr}_S\left(\hat{O}_S\hat{\rho}_S\right) = \text{Tr}_{S+R}\left[\left(\hat{O}_S \otimes \hat{\mathbb{1}}_R\right)\hat{\rho}_{SR}\right].$$

Since $\hat{\rho}_S$ is a positive operator ($\langle\phi_S|\hat{\rho}_S|\phi_S\rangle \geq 0$) with unit trace ($\text{Tr}_S(\hat{\rho}_S) = 1$), it can be correctly interpreted as a density operator. The equation describing the evolution of $\hat{\rho}_S$ is then obtained by taking the partial trace of Eq. (2.1) over all reservoir states. Under some suitable approximations, a differential equation describing the evolution of $\hat{\rho}_S$ can be derived, which is called a master equation. The following section will be dedicated to an introduction to master equations.

2.2 Master equations

The equation governing the evolution of the reduced density matrix is called a *master equation*. A whole derivation of such an equation will not be performed in this work but general elements of derivation as well as hypotheses of application and limitations will be discussed. However, the reader might be interested to read Refs. [45–50] if he wants to find a complete derivation. The purpose of this section is to acquire a further physical understanding of master equations. As we mentioned in the previous section, the evolution equation is obtained by taking the partial trace of Eq. (2.1) over all reservoir states

$$\frac{d\hat{\rho}_S(t)}{dt} = \frac{1}{i\hbar}\text{Tr}_R\left([\hat{H}_{\text{tot}}, \hat{\rho}_{SR}(t)]\right).$$

Unfortunately, the right-hand side of that expression still involves the total density operator. We introduce the general form of a master equation by replacing the right-hand side of this equation by [46]

$$\frac{d\hat{\rho}_S(t)}{dt} = \frac{1}{i\hbar}[\hat{H}_S, \hat{\rho}_S(t)] + \hat{\hat{\mathcal{L}}}_{\text{relax}}\left[\hat{\rho}_S(t)\right], \tag{2.2}$$

where $\hat{H}_S$ stands for the system Hamiltonian in the interaction picture. This master equation (2.2) can be written in a more general form

$$\frac{d\hat{\rho}_S(t)}{dt} = \hat{\hat{\mathcal{L}}}(\hat{\rho}_S(t)) \quad \text{with } \hat{\hat{\mathcal{L}}}(\hat{\rho}_S(t)) = \frac{1}{i\hbar}[\hat{H}_S, \hat{\rho}_S(t)] + \hat{\hat{\mathcal{L}}}_{\text{relax}}(\hat{\rho}_S(t)),$$

where we have introduced the Liouvillian $\hat{\hat{\mathcal{L}}}(\,\cdot\,)$ superoperator that acts on an operator and gives back another operator. It can be physically interpreted as being the generator of a quantum dynamical semi-group taking the time as only parameter [23,51,52]. Contrarily to a group, any element of a semi-group does not possess an inverse. Hence, the evolution between two times t_1 and t_2 is irreversible and cannot be inverted, thereby reflecting the irreversible feature of such systems.

Likewise the time-evolution operator which maps the state of a system at time $t = t_0$ to the state of the system at time t, one can also define a superoperator which maps the density matrix describing a system at time t_0 to the one describing the system at time t

$$\hat{\rho}_S(t) = \hat{\hat{\mathcal{M}}}_t(\hat{\rho}_S(t_0)).$$

Such a superoperator acts on a vector space of linear operators. In order to preserve the connection between $\hat{\rho}_S(t_0)$ and $\hat{\rho}_S(t)$ being density operators, the superoperator $\hat{\hat{\mathcal{M}}}_t(\,\cdot\,)$ must be linear, positive and preserve both trace and hermiticity of $\hat{\rho}_S(t_0)$ [53].

2.2.1 Main hypotheses of derivation

In this subsection, we give and detail the Born and the Markov hypotheses for the derivation of a master equation. Together, they constitute the Born-Markov approximation which introduces two distinct timescales, each of which with a precise physical interpretation. However, the following text purposefully focuses on the physical meaning of those approximations rather than on mathematical details which are not the aim of our study.

Born approximation

Born approximation consists in assuming that the reservoir is very slightly influenced by its interaction with the system. As long as the dimension of the Hilbert space of the reservoir $\mathcal{H}_R$ is far larger than that of the Hilbert space of the system $\mathcal{H}_S$, *i.e.* as long as $d_R \gg d_S$, the influence of the system on the reservoir may be assumed negligible. This is the case when one deals with the quantised electromagnetic field. In addition, if the reservoir is stationary, that is, if $[\hat{H}_R, \hat{\rho}_R] = 0$ in which case $\hat{\rho}_R(t) = \hat{\rho}_R(t_0)$, one can perform Born approximation

$$\hat{\rho}_{SR}(t) = \hat{\rho}_S(t) \otimes \hat{\rho}_R + \hat{\rho}_{\text{correlation}}(t) \simeq \hat{\rho}_S(t) \otimes \hat{\rho}_R.$$

This amounts to neglecting the correlation between the system and the reservoir and assuming that S and R are not entangled. This approximation does not imply that the reservoir is insensitive to the system, it rathers means that the modification of the reservoir by the system has no impact on the evolution of the latter [23].

Markov approximation

Markov approximation consists in assuming that the evolution of the reduced density operator can be described in terms of a first-order differential equation in t : the master equation is then local in time. Mathematically speaking, this means that the reduced density operator at time t only depends on the reduced density operator at any previous time t_0

$$\hat{\rho}_S(t) = \hat{\hat{\mathcal{M}}}(\hat{\rho}_S(t_0))$$

and not on $\hat{\rho}_S$ at several times. Such a situation is not general since the reservoir to which the system is coupled has a certain memory. It means that the past interactions between the system and the reservoir are likely to retrospectively influence the system so that the density matrix at time t could be a function of $\hat{\rho}_S$ at several elapsed times. However, within the framework of the Markov approximation, $\hat{\rho}_S(t)$ is entirely determined by the data of $\hat{\rho}_S(t_0)$. Therefore, we introduce the characteristic time τ_B whose meaning is the necessary time for the correlations within the reservoir (resulting of a past interaction with the system) to vanish. For the Markov approximation to be valid, that characteristic time must be small enough (this term is purposefully left vague for the moment).

Justification of the Born-Markov approximation

We have just introduced the characteristic time τ_B for the reservoir to forget the results of its interaction with the system. This quantity is related to the characteristic time of decrease of the correlation function of the reservoir. After such a time τ_B has elapsed, the information the reservoir acquired from the system has vanished and is not likely to feedback the system and thus influence its subsequent evolution. Similarly, we can also introduce a characteristic time τ_{relax} which is the characteristic evolution time of the system as a result of its interaction with the environment. The Born-Markov approximation is justified as long as [23]

$$\boxed{\tau_{\text{relax}} \gg \tau_B}$$

which is the only condition for such an approximation to hold. Therefore, two timescales naturally appear : a small one, corresponding to the decrease of the correlations within the reservoir and another one, larger, corresponding to the typical relaxation time of the system as the result of its coupling with the reservoir. The typical relaxation time τ_{relax} of the system interacting with the reservoir is the time after which a process has a high probability to occur whilst τ_B is the mean duration of that process [27]. Damanet [23] provide a straightforward example of such a typical process : in the case of an atom coupled to the quantised field, that process could happen to be a spontaneous emission of a photon. That is the atom spontaneously emits a photon during a mean time τ_B and is likely to emit another one after a time τ_{relax}.

The introduction of those 2 characteristic timescales allows one to discuss about one of the features of the master equation. The temporal evolution of the system is not continuous, as in an ordinary differential equation, but is rather discretised : one talks about a coarse-grained timescale [51, 54–56].

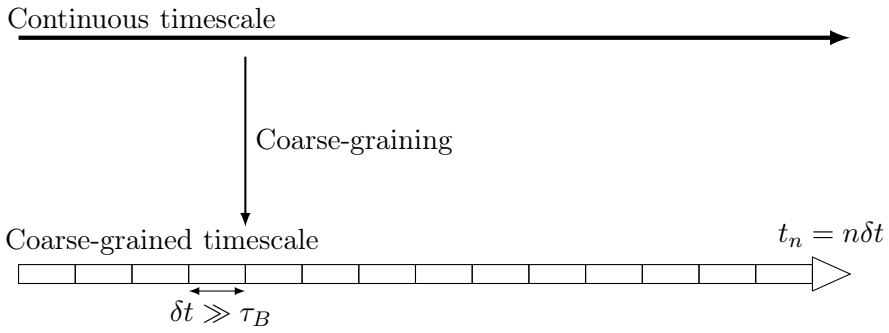

Figure 2.2: Continuous and coarse-grained timescales [23]. The first timescale is continuous and the second, which results from the Markov approximation, is discrete with a discretisation time step δt such that $\tau_{\text{relax}} \gg \delta t \gg \tau_B$. This Figure is adapted from [23].

The master equation gives access to the solution at all multiple integers of δt but does not provide any information in between two subsequent time steps : memory effects are unresolved and thus unknown [23]. Thus, the coarse-graining acts as a low-pass filter that screens out high frequency components of the system dynamics. In fact, fluctuations due to the memory effects are averaged over τ_B yielding a zero contribution [51]. It is obvious that the time step must be chosen greater than the typical time τ_B in order for the correlations within the reservoir to vanish : $\delta t \gg \tau_B$. However, intuitively, the coarse-graining must not affect the system, so that the time step must be small compared to the relaxation time of the system, τ_{relax}. Therefore, the following condition must be fulfilled

$$\tau_{\text{relax}} \gg \delta t \gg \tau_B.$$

If this condition is satisfied, then the system perceives the coarse-grained timescale as a continuous timescale, so that the coarse-graining has no effect on the system. The MCWF method is equivalent to a master equation within the Born-Markov approximation. Whereas the resolution of a master equation gets more accurate as the time step decreases, it should be chosen cautiously in the MCWF method to prevent quantum Zeno type effects [57, 58]. In short, this amounts to satisfy

$$\boxed{\tau_{\text{relax}} \gg \tau_B}, \tag{2.3}$$

which is nothing else than the condition to meet for the Born-Markov approximation to be justified. However, even if the condition (2.3) is fulfilled, the derived master equation is guaranteed to preserve the properties of the reduced density operator along the time only if it can also be cast into a general form derived by Gorini *et al.* [59].

2.2.2 Lindblad form of the master equation

The standard form of the master equation is given by Eq. (2.2). However, any equation that could be written under this form does not necessarily preserve the properties of the density

operator as it evolves in time. Therefore, we have to restrict the set of admissible master equations to those that subscribe to the form

$$\frac{d\hat{\rho}_S(t)}{dt} = \frac{1}{i\hbar}[\hat{H}_S, \hat{\rho}_S(t)] + \sum_m \hat{C}_m \hat{\rho}_S \hat{C}_m^\dagger - \frac{1}{2}\sum_m \left(\hat{C}_m^\dagger \hat{C}_m \hat{\rho}_S + \hat{\rho}_S \hat{C}_m^\dagger \hat{C}_m\right) \tag{2.4}$$

which is called the Lindblad form [60] for which we show that it preserves the density operator properties. At this stage, $\hat{C}_m$ are arbitrary operators.

Proof. The Lindblad form of the master equation (2.4) preserves the properties of any density operator $\hat{\rho}_S$ if the three following conditions are met.

1. The trace of the density operator $\hat{\rho}_S$ must be one at any time. Indeed, taking the trace of equation (2.4) and noting that the trace is invariant under cyclic permutations, we find that $\mathrm{Tr}_S(d\hat{\rho}_S/dt) = 0$ which shows that $\mathrm{Tr}_S\left[\hat{\rho_S}(t)\right] = \mathrm{Tr}_S\left[\hat{\rho}_S(t_0)\right] = 1$.

2. The reduced density operator $\hat{\rho}_S$ must remain Hermitian at any time. Indeed, from Eq. (2.4), we have

$$\begin{aligned}
\frac{d\hat{\rho}_S^\dagger}{dt} &= -\frac{1}{i\hbar}[\hat{H}_S, \hat{\rho}_S(t)]^\dagger + \sum_m \left(\hat{C}_m \hat{\rho}_S \hat{C}_m^\dagger\right)^\dagger - \frac{1}{2}\sum_m \left(\hat{C}_m^\dagger \hat{C}_m \hat{\rho}_S + \hat{\rho}_S \hat{C}_m^\dagger \hat{C}_m\right)^\dagger \\
&= \frac{1}{i\hbar}[\hat{H}_S, \hat{\rho}_S(t)] + \sum_m \hat{C}_m \hat{\rho}_S \hat{C}_m^\dagger - \frac{1}{2}\sum_m \left(\hat{C}_m^\dagger \hat{C}_m \hat{\rho}_S + \hat{\rho}_S \hat{C}_m^\dagger \hat{C}_m\right) \\
&= \frac{d\hat{\rho}_S}{dt}
\end{aligned}$$

   Hence, $d\hat{\rho}_S/dt$ is Hermitian and $\hat{\rho}_S(t)$ is also Hermitian provided $\hat{\rho}_S(t_0)$ is.

3. The reduced density operator $\hat{\rho}_S$ must remain positive at any time. Indeed, consider the reduced density operator at time $t + \delta t$

$$\hat{\rho}_S(t + \delta t) \simeq \hat{\rho}_S(t) + \frac{d\hat{\rho}_S(t)}{dt}\delta t + \mathcal{O}(\delta t^2)$$

   and the following operator

$$\hat{L} = \sum_m \frac{\hat{C}_m^\dagger \hat{C}_m}{2} = \hat{L}^\dagger.$$

   This allows one to write

$$\begin{aligned}
\hat{\rho}_S(t + \delta t) &= \hat{\rho}_S(t) - \frac{i}{\hbar}[\hat{H}_S, \hat{\rho}_S]\delta t - (\hat{L}\hat{\rho}_S + \hat{\rho}_S\hat{L})\delta t + \sum_m \hat{C}_m \hat{\rho}_S \hat{C}_m^\dagger \delta t + \mathcal{O}(\delta t^2) \\
&= \left(\hat{\mathbb{1}} - \frac{i}{\hbar}\hat{H}_S\delta t - \hat{L}\delta t\right)\hat{\rho}_S(t)\left(\hat{\mathbb{1}} + \frac{i}{\hbar}\hat{H}_S\delta t - \hat{L}\delta t\right) + \sum_m \hat{C}_m \hat{\rho}_S \hat{C}_m^\dagger \delta t + \mathcal{O}(\delta t^2).
\end{aligned}$$

   This equation is a sum of contributions of the form $\hat{M}\hat{\rho}_S\hat{M}^\dagger$ each of which being positive as long as $\hat{\rho}_S(t)$ is itself positive. Therefore, the reduced density operator at time $t + \delta t$ is also a positive operator.

A master equation under the Lindblad form preserves the properties of a density operator provided that the superoperator is bounded[1][2]. □

The Lindblad equation (2.4) can be written

$$\frac{d\hat{\rho}_S(t)}{dt} = \hat{\hat{\mathcal{L}}}_{\text{unitary}}\left[\hat{\rho}_S(t)\right] + \hat{\hat{\mathcal{L}}}_{\text{relax}}\left[\hat{\rho}_S(t)\right].$$

This writting emphasises the two main contributions contained in a Lindblad equation. A first term, $\hat{\hat{\mathcal{L}}}_{\text{unitary}}\left[\hat{\rho}_S(t)\right]$, describes the coherent and reversible evolution of the system under an effective and Hermitian Hamiltonian. If this term were to be considered alone, the master equation would reduce to the well-known Liouville-von Neumann equation. The other term $\hat{\hat{\mathcal{L}}}_{\text{relax}}\left[\hat{\rho}_S(t)\right]$ describes the irreversible and non-unitary evolution of the system, as a result of the coupling between the system and the reservoir. As we already mentioned, the dissipator (sometimes called the Lindbladian) takes on the form

$$\hat{\hat{\mathcal{L}}}_{\text{relax}}\left[\hat{\rho}_S(t)\right] = \sum_m \hat{C}_m\hat{\rho}_S\hat{C}_m^\dagger - \frac{1}{2}\sum_m\left(\hat{C}_m^\dagger\hat{C}_m\hat{\rho}_S + \hat{\rho}_S\hat{C}_m^\dagger\hat{C}_m\right). \tag{2.5}$$

As pointed out by Gutmann [61], in this relaxator, appear the $\hat{C}_m$ operators acting on the system Hilbert space $\mathcal{H}_S$. Those operators have dimensions of $1/\sqrt{\text{time}}$ in order to preserve the interpretation of $\hat{\rho}_S$ as a density operator [15]. They form a countable set of positive, bounded operators : the Lindblad operators. The action of those operators and their number (one, several or an infinity) depends on the type of problem treated. They describe how the system is affected by a (fictitious and unread) measurement[3] of the system by the reservoir [54] and thus project the system state on a well-defined state. For that reason, the $\hat{C}_m$ operators are sometimes called the collapse operators since they cause a collapse of the wavefunction due to the fictitious measurement by the reservoir. However, they are more often referred to as jump operators, a terminology we use in the following. They describe how the system states are transformed under the action of a projective measurement of the system and they correspond to an irreversible and instantaneous transformation of the system wavefunction. Their physical meaning is rather obvious : they represent the system contribution to the system-reservoir interaction through the various channels of desexcitations that feed the quantised field [51, 60, 62]. In (2.5), as pointed out in [15], the second sum is an anticommutator which contains terms describing the decay of the total population $\text{Tr}(\hat{\rho}_S)$ of the reduced density operator $\hat{\rho}_S$. The "sandwich" terms in the first sum are source terms contributing to a temporal increase of $\text{Tr}(\hat{\rho}_S)$. A relevant interpretation of those two contributions to $\text{Tr}(\hat{\rho}_S)$ can be drawn out from the two-level atom coupled to the quantised electromagnetic field in the vacuum state

[1] An operator $\hat{A}$ is said to be bounded if, for any $|\psi\rangle$, $\hat{A}|\psi\rangle$ exists in which case we necessarily have $\|\hat{A}|\psi\rangle\| < \infty$. The maximum of $\hat{A}|\psi\rangle / \||\psi\rangle\|$ is called the norm of $\hat{A}$, denoted by $\|\hat{A}\|$

$$\|\hat{A}\| = \sup_{\||\psi\rangle\|=1} \|\hat{A}|\psi\rangle\|.$$

If that quantity does not exist, then the operator is said unbounded [54].

[2] However, Le Bellac [54] informs that this condition is sufficient but not necessary. Indeed, there exist totally valid master equations that involve unbounbed superoperators.

[3] If they were to correspond to physical observables, then such a Lindblad form could be used in order to treat measurement [62].

study. Of course, the subsequent conclusions are more general. We consider a situation where the atom is modelled by its ground state $|g\rangle$ and its excited state $|e\rangle$. This atom is coupled to the quantised electromagnetic field assumed to be initially in a no-photon state. In such a case, the coupling with the vacuum field is described by a dissipator of the form (2.5) with only one jump operator : $\hat{C} = \sqrt{\Gamma}\,|g\rangle\langle e|$, with Γ the spontaneous emission rate. Mølmer and Castin [15] indicate that the anticommutator in (2.5) appears in the derivation of the master equation from the evolution of the component of the atom + field wavefunction in the initial state of the field, that is the zero-photon subspace. In the case of the two-level atom picture, that anticommutator accounts for the decay of the excited state population and describes the coherences between the ground and excited states. Mølmer and Castin [15] also indicate that the sandwich term originates from the trace of the total wavefunction atom + field over the field degrees of freedom (in order to construct the reduced density operator) involving field states different from the initial vacuum state, that is the reservoir states with one fluorescence photon. This term describes the natural feeding of the ground state by spontaneous emission of a photon from the atom to the quantised field.

In a more general problem, as we mentioned previously, conclusions remain unchanged although the interpretation is less straightforward. Indeed, if we consider a $J_g \leftrightarrow J_e$ transition driven by a laser field, with the related degeneracies associated to the angular momenta of the ground and excited states, there are as many jump operators as possible manners for the atom to fall back into the ground state manifold, each of which describing one transition from an excited substate to a ground substate, with a certain polarisation for the spontaneous emitted photon. In such a case, the sums appearing in (2.5) do not reduce anymore to a single term and describe the decay of the excited state population as well as the feeding of the ground state in terms of sums over all possible contributions. Many examples of those Lindblad operators with the related problem can be found in [16].

Non uniqueness of the Lindblad operators

The Lindblad form (2.5) does not determine the quantum jump operators univocally. If there exists an operator $\hat{T}$ acting in $\mathcal{H}_S$ such that the relaxator is left invariant under

$$\hat{T}^\dagger \left[\hat{\hat{\mathcal{L}}}_{\text{relax}}(\hat{\rho}_S)\right] \hat{T} = \hat{\hat{\mathcal{L}}}_{\text{relax}}(\hat{T}^\dagger \hat{\rho}_S \hat{T}),$$

then one can write

$$\hat{\hat{\mathcal{L}}}_{\text{relax}}(\hat{\rho}_S) = \hat{T}^\dagger \left[\hat{\hat{\mathcal{L}}}_{\text{relax}}(\hat{T}^\dagger \hat{\rho}_S \hat{T})\right] \hat{T}.$$

In such a case, the Lindbladian takes the form

$$\hat{\hat{\mathcal{L}}}_{\text{relax}}(\hat{\rho}_S) = \sum_m \hat{D}_m \hat{\rho}_S \hat{D}_m^\dagger - \frac{1}{2}\sum_m \left(\hat{D}_m^\dagger \hat{D}_m \hat{\rho}_S + \hat{\rho}_S \hat{D}_m^\dagger \hat{D}_m\right),$$

where we have defined $\hat{D}_m = \hat{T}^\dagger \hat{C}_m \hat{T}$, which may correspond to a rotation of the basis described by the operator $\hat{T}$. Regardless of the form of the jump operators, the resolution of the Lindblad equation leads to the same results in average. However, the physical picture can be quite different.

Chapter 3

Monte-Carlo wave function method

In the limit of the approximations made to obtain the master equation (2.4) for the reduced density operator $\hat{\rho}_S(t)$, the dynamics of the system of interest is directly obtained by solving that master equation for a given initial state. Unfortunately, the required number of variables for a full density matrix treatment ($\mathcal{O}(N^2_{\text{states}})$) renders realistic problems, such as 3D laser cooling, numerically hard to solve. In a numerical discretisation of the centre-of-mass momentum, for example in the range $|p_i| \leq 50\hbar k$ with $i = x, y, z$ and a discretisation step $\hbar k$, the density matrix contains $(2 \times 50)^6 \simeq 5 \times 10^9$ elements [17]. Moreover, that number must be multiplied by the number of atomic electronic states. In a $J_g \leftrightarrow J_e$ transition, where J_g and J_e are the angular momentum quantum numbers for the ground and excited states, $(2J_g + 1) + (2J_e + 1)$ electronic states must be taken into account. Therefore, a direct integration of the master equation is made impossible by the huge amount of variables to deal with. An approximation, consisting in choosing a proper basis in which only rate equations for the diagonal elements of the density operator are considered, has also been developped in [18, 19] for the 1D and 2D cases. Nevertheless, such an approximation does not work well for a 3D treatment of laser cooling. Klaus Mølmer, Yvan Castin and Jean Dalibard [16, 20] developed a method (which they called the Monte-Carlo wavefunction method) based on the propagation of stochastic wavefunctions rather than on an explicit resolution of the master equation. A wavefunction is a smaller object than a density matrix since it contains $\mathcal{O}(N_{\text{states}})$ elements rather than $\mathcal{O}(N^2_{\text{states}})$ for a density matrix. The MCWF method could be applied in a wide variety of problems in quantum optics including for instance spontaneous emission (with or without Zeeman degeneracy), interaction of an atom with a reservoir at finite temperature, the momentum diffusion in Brownian motion or laser cooling [16]. Let us mention that other equivalent methods have been invented at the same time, driven by the analogy with similar problems in quantum optics. For instance, Carmichael developed the so-called "quantum trajectories" method[1] [63], Zoller et al. [64], Hegerfeldt and Wilser [57] and finally Gisin and Percival [65] all have developed methods based on a stochastic approach of quantum

[1]This method has not to be confused with the De Broglie–Bohm theory which is sometimes referred to as "quantum trajectories". This theory is an alternative formulation to the traditionnal Copenhaguen interpretation of the quantum theory based on a hydrodynamical analogy of the Schrödinger equation. It was first formulated under the name of pilot-wave theory by Louis De Broglie in 1927 at the Solvay Conference before being abandoned due to the reluctances of other physicists. In 1952, David Bohm further developed that theory [66] to give rise to what is now referred to as the De Broglie–Bohm theory and which is nowadays considered as an alternative interpretation of quantum mechanics.

mechanics similar the MCWF method. In this chapter, we first present the principle of the method in the most general case. We also discuss the equivalence between the description of the problem in terms of a master equation and in terms of MCWF. We discuss the physical interpretation of the MCWF method. Finally, we illustrate and present important features of the method by studying the case of an atom at rest.

3.1 Form of the dissipator

The type of relaxation superoperators considered in this work is very general and refers to the Lindblad superoperators introduced previously[2] .

$$\hat{\hat{\mathcal{L}}}_{\text{relax}}(\hat{\rho}_S) = \sum_m \hat{C}_m \hat{\rho}_S \hat{C}_m^\dagger - \frac{1}{2}\sum_m \left(\hat{C}_m^\dagger \hat{C}_m \hat{\rho}_S + \hat{\rho}_S \hat{C}_m^\dagger \hat{C}_m \right). \tag{3.1}$$

As we already mentioned, that kind of relaxator insures that the interpretation of $\hat{\rho}_S$ as a density operator is preserved[3] all along the calculations. Therefore, any dissipator must subscribe to the general form (3.1).

3.2 Principle of the method

The MCWF method allows one to compute expectation values that would otherwise be obtained by solving Eq. (2.4) on the basis of wavefunctions that are propagated in time. Because of the stochastic nature of the method, expectation values computed from a single wavefunction at time t are manifestly vitiated by an error intrinsic to the method. Therefore, it is prescribed to repeat the procedure a large number of times and to average over different realisations so that, in average, MCWF method produces the same results as the master equation. The method for propagating a single wavefunction is quite simple. At initial time t_0, one starts with a normalised wavefunction $|\psi(t_0)\rangle$. The state of the system will be computed at consecutive times separated by a time step δt that must be chosen small enough in order to ensure the validity of the calculations at first order [20]. The state of the system at time $t + \delta t$ is obtained by one of the two evolutions that result from a random choice that will be explained later on :

1. Either the state of the system[4] at time $t + \delta t$, $|\phi(t + \delta t)\rangle$, is obtained by the action of the non-Hermitian Hamiltonian

$$\hat{H} = \hat{H}_S - \frac{i\hbar}{2}\sum_m \hat{C}_m^\dagger \hat{C}_m \tag{3.2}$$

on $|\psi(t)\rangle$. This yields, provided that the time step is small enough

$$|\phi(t + \delta t)\rangle = \left(\hat{\mathbb{1}} - \frac{i\delta t}{\hbar}\hat{H} \right) |\psi(t)\rangle . \tag{3.3}$$

[2]The reader can find the whole demonstration in the text of H. J. Carmichael [63].

[3]Any operator $\hat{\rho}$ which is positive, that is $\langle\psi|\,\hat{\rho}\,|\psi\rangle \geq 0$ for all $|\psi\rangle$ and with unit trace ($\text{Tr}\hat{\rho} = 1$) defines a density operator.

[4]Since the method involves normalised and non-normalised states, one shall denote normalised states by $|\psi\rangle$ whilst non-normalised states shall be denoted by $|\phi\rangle$ in order to avoid any ambiguity.

Since $\hat{H} \neq \hat{H}^\dagger$, its action on a normalised state vector does not produce a normalised state vector. Hence, the resulting state vector $|\phi(t+\delta t)\rangle$ still needs to be normalised in order to preserve the probabilistic interpretation. The square of the norm of $|\phi(t+\delta t)\rangle$ reads

$$\langle\phi(t+\delta t)|\phi(t+\delta t)\rangle = \langle\psi(t)|\left(\hat{\mathbb{1}} + \frac{i\delta t}{\hbar}\hat{H}^\dagger\right)\left(\hat{\mathbb{1}} - \frac{i\delta t}{\hbar}\hat{H}\right)|\psi(t)\rangle = 1 - \delta p + \mathcal{O}(\delta t^2).$$

In this expression, we have introduced the probability δp defined as

$$\delta p = \frac{\delta t}{\hbar} i \langle\psi(t)|\, \hat{H} - \hat{H}^\dagger\, |\psi(t)\rangle = \sum_m \delta p_m$$

with

$$\delta p_m = \delta t \langle\psi(t)|\, \hat{C}_m^\dagger \hat{C}_m\, |\psi(t)\rangle \geq 0.$$

Each of those probabilities δp_m are associated to one of the jump operators $\hat{C}_m$. The total probability δp gives the probability for a quantum jump to occur. Now that the square of the norm of the (non-normalised) resulting wavefunction has been computed, one can normalise it in order to get the next wavefunction

$$|\psi(t+\delta t)\rangle = \frac{|\phi(t+\delta t)\rangle}{\sqrt{\langle\phi(t+\delta t)|\phi(t+\delta t)\rangle}} = \frac{|\phi(t+\delta t)\rangle}{\sqrt{1-\delta p}}.$$

The next evolution of that wavefunction up to time $t + 2\delta t$ is performed either by applying the evolution described hereabove or by performing the evolution described hereafter.

2. Another possibility for evolving the wavefunction is to apply the "quantum jump evolution". The relaxation superoperator involves the jump operators $\hat{C}_m$, describing the possible branching of decay in different channels [15]. The quantum jump evolution consists in applying one of those operators to the wavefunction at time t. As Mølmer, Castin and Dalibard advise [16], the term "quantum jump" is left vague on purpose in the general presentation of the method as it corresponds to a *gedanken experiment process* after which the wavefunction is projected onto the eigenstate corresponding to the measurement result. The meaning of the jump operator will be further investigated through the example given later or through the study of laser cooling. From a practical point of view, one first has to compute the different probabilities δp_m (each of those probabilities is associated to a possible quantum jump, marked by $\hat{C}_m$) that the m^{th} jump occurs and then has to make a random choice to choose which evolution, amongst the non-Hermitian evolution and the jump evolution, is performed. That random choice is performed by picking a pseudo-random number ϵ uniformly distributed in $[0, 1]$ which is then compared to δp. If $\epsilon < \delta p$, then, amongst the m possible jumps, a quantum jump occurs according to the probability law $\Pi_m = \delta p_m / \delta p$. The wavefunction at time $t + \delta t$ is then given by

$$|\phi(t+\delta t)\rangle = \hat{C}_m\, |\psi(t)\rangle \qquad \text{with a probability } \delta p_m.$$

For the same reasons as previously, the resulting wavefunction still needs to be normalised

$$|\psi(t+\delta t)\rangle = \frac{\hat{C}_m\, |\psi(t)\rangle}{\|\hat{C}_m\, |\psi(t)\rangle\,\|} = \frac{\hat{C}_m\, |\psi(t)\rangle}{\sqrt{\delta p_m / \delta t}}.$$

Therefore, starting from a normalised wavefunction $|\psi(t)\rangle$, there are two possible ways for the wavefunction to evolve for a sufficiently small time step δt. The choice between one of those two evolutions is performed by a random choice : the non-Hermitian evolution is realised with a probability $1 - \delta p$ whilst the quantum jump evolution is realised with a probability δp. A second random choice determines which jump occurs being given the different probabilities δp_m, each of which associated with each possible jump obtained by the action of $\hat{C}_m$. Figure 3.1 illustrates the choice one has to deal with when computing a MCWF solution of a master equation.

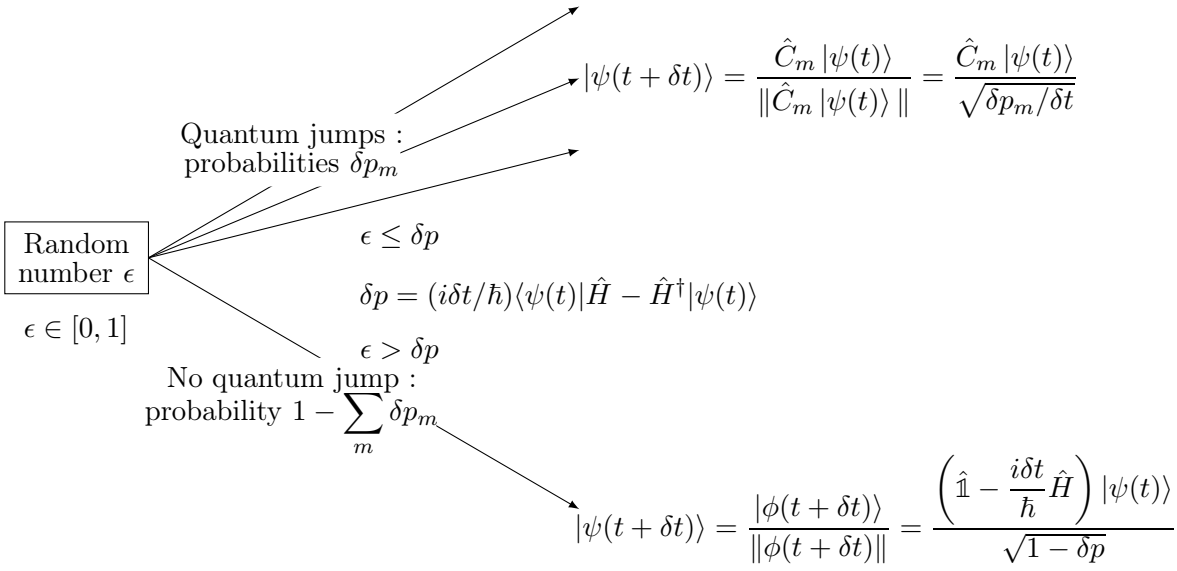

Figure 3.1: The possible branches in the MCWF evolution [16].

Henceforth one knows how to propagate a MWCF in time, one is interested in computing the numerical value of observables. One of the central purposes of the MCWF approach is precisely to give access to average values of physical observables. Following the traditional spirit of a Monte-Carlo like method, one just has to compute the desired observable for each realisation of the method and to average the results over a large number of realisations. That is, consider that N independent[5] MCWF have been propagated until time t and choose a physical observable $\mathcal{A}$ represented by the Hermitian operator $\hat{A}$. One just has to compute the expectation value for the observable $\mathcal{A}$ for all wavefunctions (or trajectories) as it is usually done and to take the average

$$\langle A\rangle_{(N)}(t) = \frac{1}{N}\sum_{i=1}^{N}\langle\psi_i(t)|\hat{A}|\psi_i(t)\rangle. \tag{3.4}$$

Using a master equation approach, one would know the reduced density operator $\hat{\rho}_S$ exactly and could determine the expectation value of any physical observable by computing $\mathrm{Tr}(\hat{\rho}_S\hat{A})$.

[5]The independence of those MCWF is such that the associated propagations in time could be straightforwardly parallelised. Assuming that the material resources are sufficient, the propagation time of N MCWF is the same as the propagation of only one MCWF.

To that extent, Eq. (3.4) is seen as an approximation of $\mathrm{Tr}(\hat{\rho}_S\hat{A})$ which gets more and more accurate as the number of realisations N increases. In statistics, the statistical error related to the mean of a given sample distribution is estimated by

$$\delta A_{(N)}(t) = \frac{\Delta A_{(N)}(t)}{\sqrt{N}},$$

where $\left(\Delta A_{(N)}(t)\right)^2$ is the sample variance at time t of the N expectation values determined previously [15]

$$\left(\Delta A_{(N)}(t)\right)^2 = \frac{1}{N}\left(\sum_{i=1}^{N}\langle\psi_i(t)|\hat{A}|\psi_i(t)\rangle^2\right) - \left(\langle A\rangle_{(N)}(t)\right)^2.$$

Therefore, expectation values for physical observables come with error bars of half width $\Delta A_{(N)}/\sqrt{N}$. For large N, $\langle A\rangle_{(N)}(t) \simeq \langle A\rangle(t) = \mathrm{Tr}[\hat{\rho}_S(t)\hat{A}]$. In the following section, we prove and quantify how the approximate value computed by the MCWF method converges to the real expectation value. In the following, we define the signal-to-noise ratio as $\langle A\rangle/\Delta A_{(N)}$. Such a ratio provides a criterion for determining the quality of the produced average value of $\mathcal{A}$. The condition for having a good signal-to-noise ratio is [16]

$$\sqrt{N} \gg \frac{\Delta A_{(N)}(t)}{\langle A\rangle(t)}. \tag{3.5}$$

This relation suggests that the larger N is, the better the results are. However, beyond a certain value of N, results stop improving convincingly so that one might wonder what are the requirements imposed by Eq. (3.5). To that purpose, we separate operators in 2 categories consisting in "local" and "global" operators [16]. An example of global operator is given by the average kinetic energy whilst an example of local operator is given by the population of a particular state $|i\rangle$. For the latter, it is shown that such operators have fluctuations (related to their expectation values) larger than the ones of the former [15]. In fact, for those local operators, denoting by N_{states} the number of electronic states involved in a realisation of the method, it is expected that [16]

$$\langle A\rangle(t) \sim \frac{1}{N_{\text{states}}}, \quad (\Delta A)^2(t) \sim \frac{1}{N_{\text{states}}}, \quad \text{when } N_{\text{states}} \gg 1.$$

Inserting those expectations into Eq. (3.5), we see that

$$N \gg N_{\text{states}}.$$

As we already knew, the larger the number of realisations, the better the signal-to-noise ratio. However, we have to perform at least N_{states} simulations of wavefunctions ($N \geq N_{\text{states}}$) involving N_{states} which amounts to dealing with a method of (at least) complexity $\mathcal{O}(N_{\text{states}}^2)$. In conclusion, for local operators, the MCWF approach is not efficient compared to a density matrix treatment of the problem. For global operators, the situation is better since we expect [15]

$$\Delta A(t) \sim \langle A\rangle(t).$$

Inserting this expectation into Eq. (3.5), we observe that

$$\sqrt{N} \gg 1,$$

so that the method provides good results for global operators as soon as the number of realisations is much larger than one. As Mølmer pointed out, if one wants a 10% accuracy on the expectation value of such an operator, Eq. (3.5) indicates that 100 realisations must be performed in order to reach such an accuracy. Therefore, as long as the number of realisations associated to a given accuracy is larger than the number of electronic states to deal with, the MCWF approach is more efficient than a density matrix treatment.

3.3 Equivalence between the MCWF and the master equation approaches

Because of the statistical uncertainty intrinsically linked to the MCWF method, one must propagate a certain number of wavefunctions in time and average the produced results. As the previous section showed, the larger the number of wavefunctions propagated, the smaller the statistical error. In order to prove the equivalence with a master equation, we consider a set of N simulations all starting from the same wavefunction : $|\psi_i(0)\rangle = |\psi(0)\rangle\,, \forall i$. At time t, we consider

$$\hat{\bar{\sigma}}(t) = \frac{1}{N}\sum_{i=1}^{N} |\psi_i(t)\rangle \langle\psi_i(t)|\,,$$

which is the average reduced density operator at time t obtained from all wavefunctions propagated by the MCWF method. The proof of the equivalence consists in showing that, assuming that the average reduced density matrix at time $t = 0$, $\bar{\sigma}(0)$, coincide with the reduced density matrix at the same time, $\hat{\rho}_S(0)$[6]

$$\hat{\rho}_S(0) = |\psi(0)\rangle \langle\psi(0)|\,,$$

it is true at all times. That is, if $\hat{\bar{\sigma}}(0)$ and $\hat{\rho}_S(0)$ have identical expressions, they still will coincide at any future time t in the limit $N \to \infty$. If such a point is to be demonstrated, then one will have proved the equivalence between MCWF approach and a density matrix approach. Consider at time t the result of the propagation of $|\psi(0)\rangle$ from time $t = 0$, that is $|\psi(t)\rangle$ and write the average value of $\bar{\sigma}(t)$ at the next time step

$$\hat{\bar{\sigma}}(t+\delta t) = (1-\delta p)\frac{|\phi(t+\delta t)\rangle}{\||\phi(t+\delta t)\rangle\|}\frac{\langle\phi(t+\delta t)|}{\|\langle\phi(t+\delta t)|\|} + \sum_m \delta p_m \frac{\hat{C}_m|\psi(t)\rangle}{\|\hat{C}_m|\psi(t)\rangle\|}\frac{\langle\psi(t)|\hat{C}_m^\dagger}{\|\langle\psi(t)|\hat{C}_m^\dagger\|}. \quad (3.6)$$

Since the wavefunction evolving under the action of non-Hermitian Hamiltonian reads

$$|\phi(t+\delta t)\rangle = \left(\hat{\mathbb{1}} - \frac{i\hat{H}\delta t}{\hbar}\right)|\psi(t)\rangle\,,$$

one can rewrite Eq. (3.6) as [16]

$$\hat{\bar{\sigma}}(t+\delta t) = \hat{\sigma}(t) + \frac{i\delta t}{\hbar}[\hat{\sigma}(t), \hat{H}_S] + \delta t\hat{\bar{\mathcal{L}}}_{\text{relax}}[\hat{\sigma}(t)]\,,$$

[6] If the reduced density operator $\hat{\rho}_S(0)$ were not to correspond to a pure state, one has to express it as a statistical mixture of pure states $\hat{\rho}_S(0) = \sum_i p_i |\chi_i\rangle\langle\chi_i|$ and perform a random choice based on the probability law p_i in order to determine which of the $|\chi_i\rangle$'s is chosen as initial state for the MCWF resolution.

with

$$\hat{\hat{\mathcal{L}}}_{\text{relax}}\left[\hat{\sigma}(t)\right] = \sum_m \hat{C}_m \hat{\sigma}(t) \hat{C}_m^\dagger - \frac{1}{2}\sum_m \left(\hat{C}_m^\dagger \hat{C}_m \hat{\sigma}(t) + \hat{\sigma}(t)\hat{C}_m^\dagger \hat{C}_m\right),$$

which yields, after averaging over many trajectories

$$\frac{d\hat{\bar{\sigma}}}{dt} = \frac{i}{\hbar}[\hat{\bar{\sigma}}, \hat{H}_S] + \hat{\bar{\mathcal{L}}}_{\text{relax}}(\hat{\bar{\sigma}}). \tag{3.7}$$

Equation (3.7) is the master equation the MCWF method is solving. The time step δt should be chosen neither too large[7] nor too small [16]. On the one hand, denoting by $\hbar\eta_i$ the eigenvalues of the Hamiltonian, the time step should be such that $\eta_i \delta t \ll 1$. On the other hand, denoting by τ_B the correlation time of the reservoir, δt should be such that $\delta t \gg \tau_B$ in order to prevent quantum Zeno-type effects[8] [57, 58]. This comes from the coarse-grain average in the derivation of the master equation.

3.4 Physical content of the MCWF method in the case of spontaneous emission

In this section, we study the method in details through one of the simplest example (for which an analytical study is readily performed) : the spontaneous emission of a photon by a two-level atom. As a reminder, such an atom consists of a ground state $|g\rangle$ and an excited state $|e\rangle$. The master equation to solve reads

$$\frac{d\hat{\rho}_S}{dt} = \frac{i}{\hbar}\left[\hat{\rho}_S, \hat{H}_S\right] + \hat{\bar{\mathcal{L}}}_{\text{relax}}(\hat{\rho}_S).$$

In the case of spontaneous emission, there is only one jump operator $\hat{C} = \sqrt{\Gamma}\,|g\rangle\langle e| = \sqrt{\Gamma}\hat{\sigma}^-$, with Γ the spontaneous emission rate. Therefore, the associated Lindblad relaxation superoperator reads [20]

$$\begin{aligned}\hat{\bar{\mathcal{L}}}_{\text{relax}}(\hat{\rho}_S) &= \sum_m \hat{C}_m \hat{\rho}_S \hat{C}_m^\dagger - \frac{1}{2}\sum_m \left(\hat{C}_m^\dagger \hat{C}_m \hat{\rho}_S + \hat{\rho}_S \hat{C}_m^\dagger \hat{C}_m\right) \\ &= \Gamma\left(\hat{\sigma}^- \hat{\rho}_S \hat{\sigma}^+\right) - \frac{\Gamma}{2}\left(\hat{\sigma}^+\hat{\sigma}^-\hat{\rho}_S + \hat{\rho}_S\hat{\sigma}^+\hat{\sigma}^-\right).\end{aligned}$$

In the $\{|e\rangle, |g\rangle\}$ basis, we have

$$\hat{C} = \sqrt{\Gamma}\begin{pmatrix} 0 & 0 \\ 1 & 0 \end{pmatrix}, \qquad \hat{C}^\dagger = \sqrt{\Gamma}\begin{pmatrix} 0 & 1 \\ 0 & 0 \end{pmatrix}.$$

[7] We have already mentioned that δt is chosen such that calculations remain valid at first order.

[8] Such effects refer to a situation where the observation of a system with a frequency high enough freezes its evolution from or towards a certain state. It can lead to paradoxical situations such as the one of a particle in an unstable state which it never decays from because of the too high frequency measurement.

Such a dissipator leads to the Optical Bloch Equations (OBE)

$$\begin{cases} \left.\dfrac{d\hat{\rho}_S}{dt}\right|_{ee} = -\Gamma\hat{\rho}_S\Big|_{ee} \\ \left.\dfrac{d\hat{\rho}_S}{dt}\right|_{ge} = -\dfrac{\Gamma}{2}\hat{\rho}_S\Big|_{ge} \\ \left.\dfrac{d\hat{\rho}_S}{dt}\right|_{eg} = -\dfrac{\Gamma}{2}\hat{\rho}_S\Big|_{eg} \\ \left.\dfrac{d\hat{\rho}_S}{dt}\right|_{gg} = \Gamma\hat{\rho}_S\Big|_{ee} \end{cases}.$$

We consider as initial state a coherent superposition of the excited and ground states

$$|\psi(0)\rangle = c_g\,|g\rangle + c_e\,|e\rangle \qquad \text{with} \qquad |c_g|^2 + |c_e|^2 = 1.$$

The state of the wavefunction at time δt is obtained by the result of one of the two procedures.

1. We evolve $|\psi(0)\rangle$ under the action of

$$\begin{aligned} \hat{H} &= \hat{H}_S - \frac{i\hbar}{2}\sum_m \hat{C}_m^\dagger \hat{C}_m \\ &= \hat{H}_S - \frac{i\hbar\Gamma}{2}\hat{P}_e, \end{aligned}$$

where $\hat{P}_e$ is the projector onto the excited state. As in scattering theory, the excited state energy has an imaginary part which describes the decay of the excited state population. In the absence of laser, $\hat{H}_S = \hbar\omega_0\hat{P}_e$ and in the $\{|e\rangle, |g\rangle\}$ basis, $\hat{H}$ reads

$$\hat{H} = \hbar\omega_0\hat{P}_e - \frac{i\hbar\Gamma}{2}\begin{pmatrix}1 & 0\\ 0 & 0\end{pmatrix}.$$

Therefore, after being evolved through Eq. (3.3), $|\psi(0)\rangle$ becomes

$$|\phi(\delta t)\rangle = c_g\,|g\rangle + c_e\left(1 - \frac{\Gamma\delta t}{2}\right)|e\rangle \simeq c_g\,|g\rangle + c_e e^{-\Gamma\delta t/2}\,|e\rangle\,.$$

The amplitude of c_e has been reduced by the $e^{-\Gamma\delta t/2}$ factor whilst c_g remains unchanged, which clearly indicates that $|\phi(\delta t)\rangle$ is not normalised, as expected. After normalisation, the wavefunction reads

$$|\psi(\delta t)\rangle = c_g\left(1 + \frac{\Gamma\delta t}{2}|c_e|^2\right)|g\rangle + c_e\left(1 - \frac{\Gamma\delta t}{2}|c_g|^2\right)e^{-\Gamma\delta t/2}\,|e\rangle\,. \tag{3.8}$$

That evolution occurs with a probability $1 - \delta p$ where

$$\delta p = \frac{\delta t}{\hbar} i\,\langle\psi(t)|\,\hat{H} - \hat{H}^\dagger\,|\psi(t)\rangle = \Gamma|c_e|^2\delta t,$$

is the probability for performing a quantum jump.

2. We perform a quantum jump under the action of $\hat{C} = \sqrt{\Gamma}\,|g\rangle\langle e|$ and the state of the atom after such a jump is $|\psi(\delta t)\rangle = |g\rangle$.

The probability δp can be interpreted as the probability for emitting a spontaneous photon between $t = 0$ and $t = \delta t$. As Mølmer pointed out [21], $|\phi(\delta t)\rangle$ is the zero-photon component of the total atom+field wavefunction and $1-\langle\phi(\delta t)|\phi(\delta t)\rangle \simeq \Gamma|c_e|^2\delta t$ is the norm of the remaining one photon component. Using an analogy with the quantum measurement theory and positive-operator valued measure (POVM), the pseudo-random number ϵ simulates whether or not a photon has been detected during δt and the jump operators are the projective operators associated with the measurement of one spontaneous photon. In fact, the MCWF procedure can be seen as a tracking of the wavefunction history through a continuous measurement process [20, 67, 68]. When no photon is detected, a slight rotation of the wavefunction occurs. Indeed, the excited state population has decreased just as much as the ground state population has increased. Imagining that the wavefunction were in the eigenstate $|e\rangle$ at the beginning and that no photon is detected through the whole process, the wavefunction would continuously rotate from $|e\rangle$ to fall back into its ground state $|g\rangle$. Such a situation has been theoretically analysed by Dicke [69]. This rotation is crucial inasmuch it affects the probability for detecting a photon. Without such a rotation, the wavefunction would irremediably remain in its initial state until a photon is finally detected in which case it would be projected onto its ground state. This means that one is sure to detect such a photon if one waits a sufficiently long time, provided the excited state population is not zero (but could be arbitrarily small), which clearly appears to be wrong. However, as (3.8) demonstrates, the excited state population is decreased by the rotation, thereby also decreasing the probability for detecting a spontaneous photon. Actually, assuming that no photon has been detected between $t = 0$ and t, then the normalised wavefunction reads

$$|\psi(t)\rangle = \frac{c_g\,|g\rangle + c_e e^{-\Gamma t/2}\,|e\rangle}{\sqrt{|c_g|^2 + |c_e|^2 e^{-\Gamma t}}}.$$

The probability for detecting no photon must fulfil [21]

$$P(t+\delta t) = P(t)\frac{1-\Gamma\delta t|c_e|^2 e^{-\Gamma t}}{|c_g|^2 + |c_e|^2 e^{-\Gamma t}},$$

whose solution is

$$P(t) = |c_g|^2 + |c_e|^2 e^{-\Gamma t} \overset{t\to\infty}{=} |c_g|^2. \tag{3.9}$$

This equation clearly shows that the probability for detecting no photon decreases with time but is not zero[9] when $t \to \infty$. That is, the more one waits, the more one is likely to detect a photon. It also shows that the detection of a photon depends upon the initial population of both atomic internal states. For instance, if the excited state population is initially small but not zero, one should not detect[10] any spontaneous photon when $t \to \infty$. As Mølmer advised [21], the treatment of the no jump periods could be further investigated. If no jump

[9] Provided $|c_g|^2 \neq 0$.

[10] Such a detection is not forbidden by the rotation of the wavefunction, but the spontaneous emission probabity decreases with time.

occured during the period $[0,t]$, the behaviour of the wavefunction is then governed by

$$i\hbar\frac{d\left|\phi(t)\right\rangle}{dt} = \left(\hat{H} + \langle\phi(t)|\frac{\hat{H}^\dagger - \hat{H}}{2}|\phi(t)\rangle\right)|\phi(t)\rangle\,,$$

whose normalised solution is (provided the Hamiltonian does not explicitely depend upon time)[11]

$$|\phi(t)\rangle = \frac{e^{-i\hat{H}t/\hbar}\,|\phi(0)\rangle}{\sqrt{\langle\phi(0)|e^{i\hat{H}^\dagger t/\hbar}e^{-i\hat{H}t/\hbar}|\phi(0)\rangle}}.$$

This is nothing else than the traditionnal evolution through the Schrödinger equation (although the Hamiltonian is non-Hermitian) followed by the proper renormalisation. Cohen-Tannoudji and Dalibard [70] interpreted the probability for detecting no photon defined in (3.9) as a delay function which provides the statistics of the time intervals between subsequent emission events [21]. Such an interpretation allowed them to provide further insight into the fluorescence signal and they identified bright and dark periods, which has been proven in [71]. This may constitute an alternative way to use the MCWF procedure. Instead of realising a pseudo-random choice every time step to know whether or not a photon is detected, one chooses a pseudo-random ϵ and compare it to the value of the delay function $P(t)$ which is actualised each time step. That is, as soon as the delay function is smaller than ϵ, a jump occurs and immediately after, the delay function is set to $P(t) = 1$. In each future time steps, this function is multiplied by $1 - \delta p$: it accumulates the probability that no photon had been detected. When $P(t) < \epsilon$, a jump occurs and the procedure is repeated. Such an approach has been carried on in [64, 72]. This function is analytically reachable for simple systems but unfortunately cannot be accessed for systems with a large number of states. In such a case, it is computed numerically. The delay function (which gives the probability that no photon had been detected until time t) decreases as time increases. When this function crosses the pseudo-random number, a jump operator is applied and a new pseudo-random number is drawn. The procedure is then repeated again as many times as necessary. This kind of simulation has been used in [73] to simulate an atomic-beam cooling experiment, in [74] for laser cooling of atoms using velocity-selective coherent population trapping and finally for lasing without inversion in [75]. It has also been applied for studying the Sisyphus cooling in 2D [76] and to study the spectrum of light emitted by an assembly of cold atoms [77].

3.5 Illustration of the MCWF method through an atom a rest driven by a laser field

In this section, we present our numerical results related to atoms at rest driven by a laser field to illustrate the phenomena of saturation and optical pumping.

3.5.1 Master equation for an atom at rest driven by a laser field

The master equation to solve reads

$$\frac{d\hat{\rho}_S}{dt} = \frac{i}{\hbar}[\hat{\rho}_S, \hat{H}_S] + \hat{\hat{\mathcal{L}}}_{\text{relax}}(\hat{\rho}_S), \tag{3.10}$$

[11] Exceptionally, the notations $|\psi(t)\rangle$ and $|\phi(t)\rangle$ for normalised and not normalised states are not used.

where, when no motion is considered, the system Hamiltonian $\hat{H}_S$ has the simple form

$$\hat{H}_S = \frac{\hbar\Omega}{2}\left(\hat{S}^+ + \hat{S}^-\right) - \hbar\delta\hat{P}_e.$$

We have obtained this Hamiltonian by applying our generic derivation (4.25), which is thoroughly described in chapter 4, particularised when the atom is at rest, which explains there is no term related to the atomic kinetic energy. Operators $\hat{S}^+$ and $\hat{S}^-$ are defined in Eq. (4.24). The dissipator $\hat{\hat{\mathcal{L}}}_{\text{relax}}(\hat{\rho}_S)$ in Eq. (3.10) reads

$$\hat{\hat{\mathcal{L}}}_{\text{relax}}(\hat{\rho}_S) = -\frac{\Gamma}{2}\left(\hat{P}_e\hat{\rho}_S + \hat{\rho}_S\hat{P}_e\right) + \Gamma\sum_{q=0,\pm}\left(\boldsymbol{\epsilon}_q^*\cdot\hat{\mathbf{S}}^-\right)\hat{\rho}_S\left(\boldsymbol{\epsilon}_q\cdot\hat{\mathbf{S}}^+\right),$$

where we have introduced the spherical standard basis

$$\begin{cases}\boldsymbol{\epsilon}_\pm = \mp\dfrac{1}{\sqrt{2}}(\mathbf{e}_x \pm i\mathbf{e}_y)\\ \boldsymbol{\epsilon}_0 = \mathbf{e}_z\end{cases}. \tag{3.11}$$

We choose the jump operators as [16]

$$\hat{C}_q = \sqrt{\Gamma}\left(\boldsymbol{\epsilon}_q^*\cdot\hat{\mathbf{S}}^-\right) \quad \text{with } q = 0,\pm,$$

that is, a form that manifestly subscribes to the Lindblad form (2.4) since

$$\sum_{q=0,\pm1}\hat{C}_q^\dagger\hat{C}_q = \Gamma\hat{\mathbf{S}}^+\cdot\hat{\mathbf{S}}^- = \Gamma\hat{P}_e.$$

Operators $\mathbf{S}^+$ and $\mathbf{S}^-$ are defined through their action on internal states [16]

$$\begin{aligned}\boldsymbol{\epsilon}_q\cdot\hat{\mathbf{S}}^+\left|J_g, m_g\right\rangle &= \langle 1, J_g, q, m_g | J_e, m_e = m_g + q\rangle \left|J_e, m_e = m_g + q\right\rangle\\ \boldsymbol{\epsilon}_q\cdot\hat{\mathbf{S}}^+\left|J_e, m_e\right\rangle &= 0\\ \boldsymbol{\epsilon}_q^*\cdot\hat{\mathbf{S}}^- &= \left(\boldsymbol{\epsilon}_q\cdot\mathbf{S}^+\right)^\dagger,\end{aligned}$$

with $\langle 1, J_g, q, m_g | J_e, m_e = m_g + q\rangle$ being the Clebsch-Gordan coefficient related to the $|J_e, m_e = m_g + q\rangle \leftrightarrow |J_g, m_g\rangle$ transition. All desexcitation channels are characterised by their Clebsch-Gordan coefficient whose square gives the probability that the related channel is chosen in the MCWF method.

3.5.2 Saturation of an atomic transition

First, we present results that illustrate how the method works. In steady state, the population of all states involved in the atomic transition have a well defined value, apart from fluctuations around this value, which depends on the saturation parameter of the laser. This is the saturation phenomenon which we study in the following. In Figure 3.2, we plot the excited state population of a two-level atom (for instance an atom with a transition $|J_g = 0, m_g = 0\rangle \leftrightarrow |J_e = 1, m_e = 0\rangle$ driven by π-polarised light in which case the only non-vanishing jump operator is $\hat{C}_0 = \sqrt{\Gamma}(\boldsymbol{\epsilon}_0^* \cdot \hat{\mathbf{S}}^-)$) as a function of time for one MCWF.

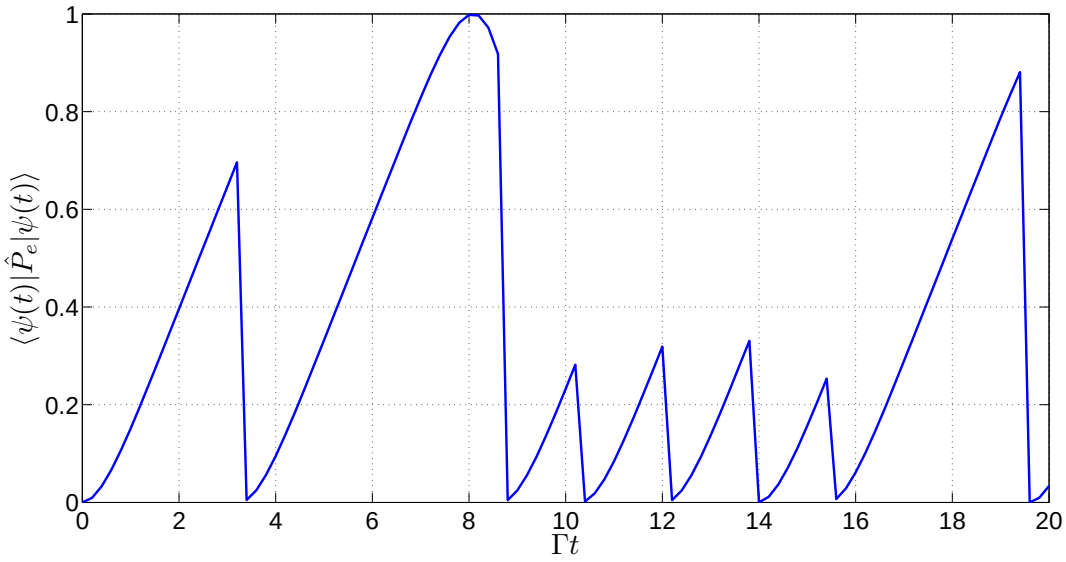

Figure 3.2: Excited state population of a two-level atom as a function of time for one MCWF. Simulation parameters are : $\Omega = \Gamma$, $\delta = -\Gamma/2$, $\Gamma\delta t = 0.0025$, $\Gamma t_f = 20$ and $|\psi(0)\rangle = |g\rangle$.

The excited state population undergoes Rabi oscillations : it oscillates back and forth between 0 and 1 at the Rabi frequency. Those oscillations are interrupted by quantum jumps occuring at random times, those jumps projecting the wavefunction onto the ground state. In Figure 3.3, we show the excited and ground state populations averaged over 500 MCWF as a function of time.

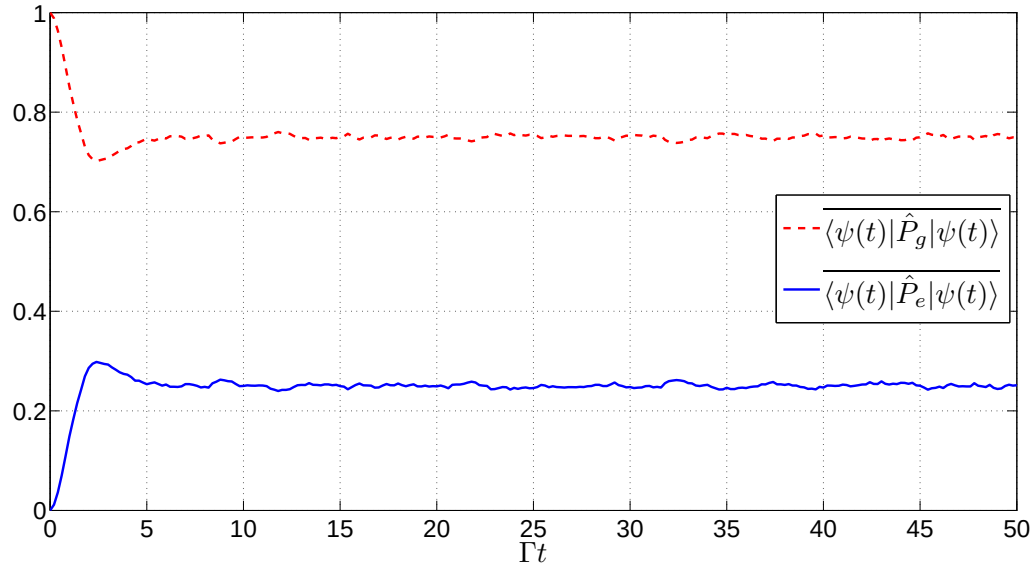

Figure 3.3: Averaged excited and ground state populations of a two-level atom as a function of time averaged over 500 MCWF. Simulation parameters are : $\Omega = \Gamma$, $\delta = -\Gamma/2$, $\Gamma\delta t = 0.0025$, $\Gamma t_f = 50$ and $|\psi(0)\rangle = |g\rangle$.

After a short transient period of about $5\Gamma^{-1}$, both populations reach a steady value with fluctuations around the mean due to the finite number of trajectories. When the steady state is reached, an analytical solution to the master equation (3.10) shows that the excited state population saturates at [29]

$$\rho_{ee}^{\infty} = \frac{s}{2(s+1)} \tag{3.12}$$

In Figure 3.4, we compare the theoretical expression (3.12) with the values obtained with the MCWF method in steady state.

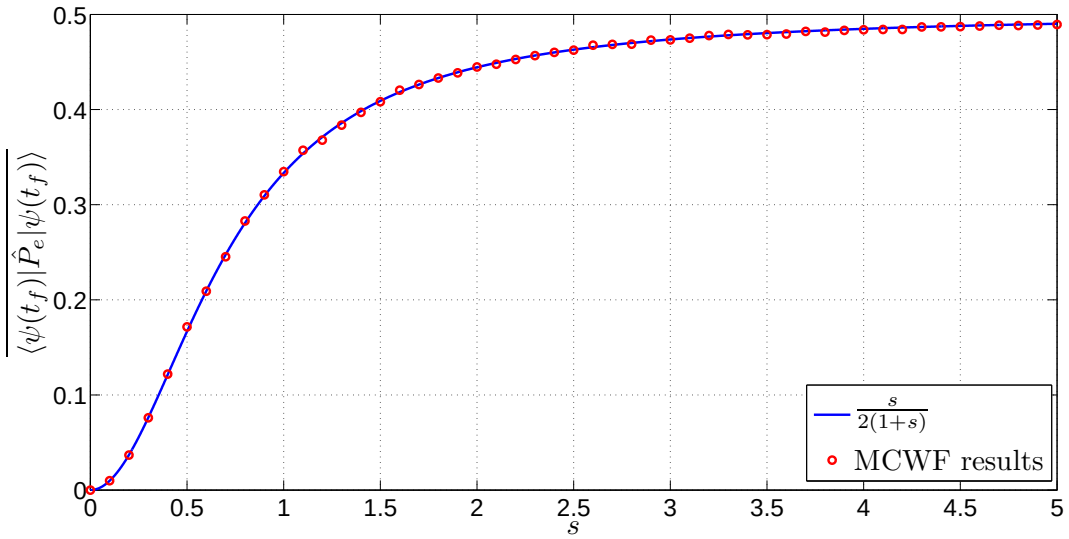

Figure 3.4: Saturated population of the excited state in steady state. Numerical results are averaged over 100 MCWF and have been obtained by keeping δ fixed and varying Ω. Simulation parameters are : $\delta = 0$, $\Gamma\delta t = 0.0025$, $\Gamma t_f = 50$ and $|\psi(0)\rangle = |g\rangle$.

We see that, except for some imperfections hither and thither still due to the finite number of trajectories, the results are in very good agreement with Eq. (3.12). When degeneracy is taken into account, because of optical pumping occurring in the case of $\sigma^{\pm}$-polarised light, only the levels whose quantum numbers $m_{e/g}$ related to the projection of the angular momentum onto the quantisation axis is maximum (for σ^{+}-polarised light) or minimum (for σ^{-}-polarised light) play a role when the system is in steady state.

3.5.3 Optical pumping

By the use of light with polarisation σ^+, it is possible to transfer the population from the low energy states to the high energy states or conversely (one then has to use σ^--polarised light) : this is the optical pumping phenomenon. It is responsible for coupling only two states of the ground and excited state manifolds for a proper choice of light polarisation. We have analysed the transient regime in which optical pumping occurs and we present a single MCWF trajectory in Figure 3.5(a) and an averaged result in Figure 3.5(b) for an atom starting in the $|J_e, m_e = -3/2\rangle$ state and driven by σ^+-polarised light.

In Figure 3.5, we analyse the populations of each substate involved in the $J_g = 1/2 \leftrightarrow J_e = 3/2$ transition, those populations being the expectation values of the related operators, which we define as

$$\hat{P}_{e/g,m_{e/g}} = |J_{e/g}, m_{e/g}\rangle \langle J_{e/g}, m_{e/g}| .$$

In Figure 3.5(a), we see that the first quantum jump completely depopulates the $|J_e, m_e = -3/2\rangle$ substate and the wavefunction is projected onto the $|J_g, m_g = -1/2\rangle$ substate : the $|J_e, m_e = -3/2\rangle$ substate has gone out of the picture. Because the polarisation of the laser is σ^+, the $|J_e, m_e = -1/2\rangle$ substate cannot be reached since it involves π transitions and $|J_g, m_g = -1/2\rangle$ is now coupled to $|J_e, m_e = 1/2\rangle$. The population is then transferred from $|J_g, m_g = -1/2\rangle$ and $|J_e, m_e = 1/2\rangle$ to $|J_g, m_g = 1/2\rangle$ and $|J_e, m_e = 3/2\rangle$ so that after several fluorescence cycles, only the $|J_g, m_g = 1/2\rangle$ and $|J_e, m_e = 3/2\rangle$ substates are still coupled, all other substates being unoccupied and uncoupled from those two substates for the rest of the simulation.

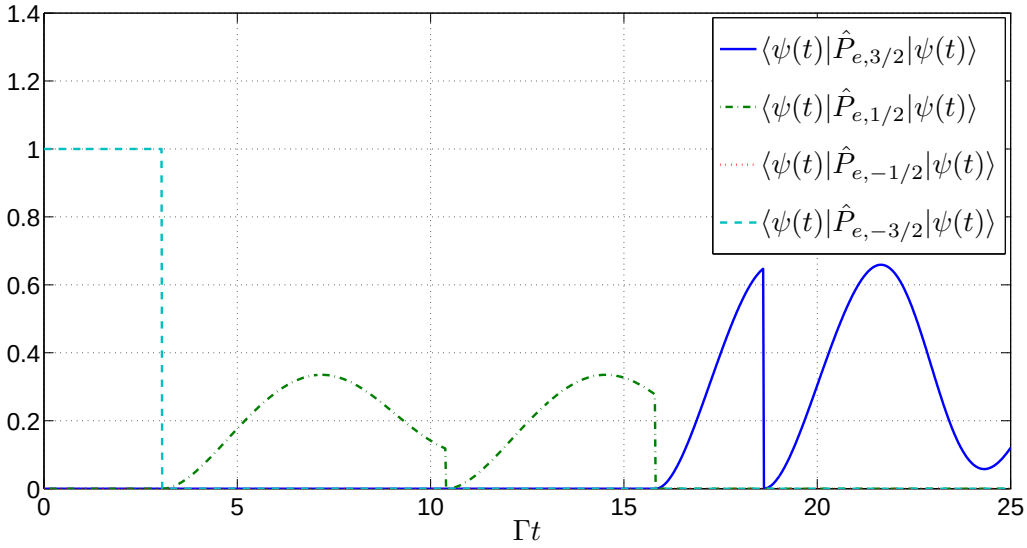

(a) Excited states populations as a function of time for one MCWF ($\Gamma t_f = 25$).

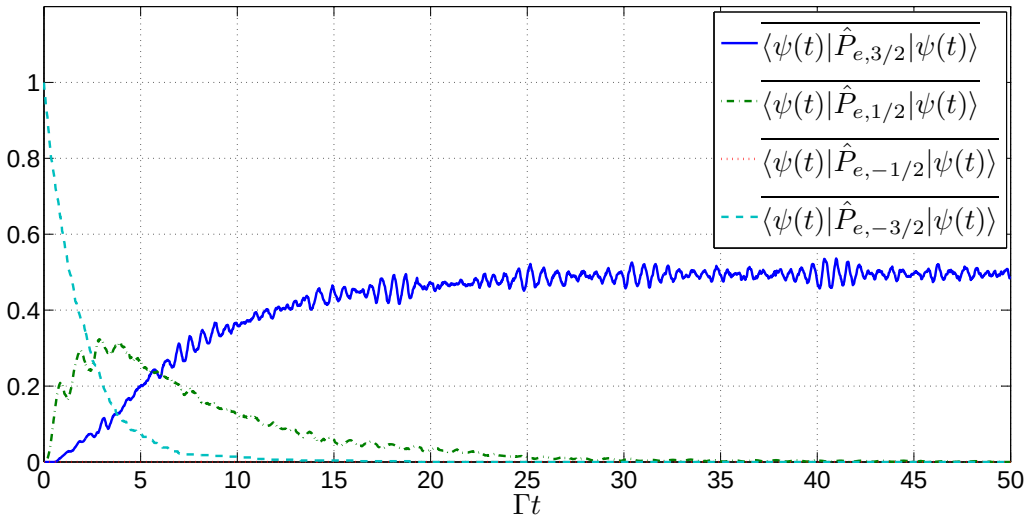

(b) Excited states populations as a function of time averaged over 500 MCWF ($\Gamma t_f = 50$).

Figure 3.5: Populations of excited substates involved in an atomic transition $J_g = 1/2 \leftrightarrow J_e = 3/2$ driven by σ^+ polarised light. Simulation parameters are : $\Omega = \Gamma$, $\delta = -\Gamma/2$, $\Gamma\delta t = 0.0025$ and $|\psi(0)\rangle = |J_e, m_e = -3/2\rangle$.

Chapter 4

Full quantum-mechanical treatment of laser cooling

In this chapter, we apply the MCWF method described in chapter 2 to laser cooling. We first present the master equation to solve in its most general form. Then, we explain how it can be greatly simplified by imposing some reasonable restrictions about the direction of emission of photons. After that, we derive the system Hamiltonian appearing in the master equation very generally such that all system Hamiltonians related to future simulations appearing in the following are special cases of our treatment. In an (ionic or atomic) trap, the density of particles is very small so that the mean free path of each particle is much larger than the dimension of the trap. Thus, the collision probability is virtually equal to zero so that the set of interacting particles is mapped into a set of non-interacting particles. Consequently, since the medium is so dilute that we can neglect the atom/atom interactions, the total Hamiltonian is simply obtained by performing the sum of all single-atom Hamiltonians.

4.1 Master equation with quantisation of the atomic centre-of-mass motion

The semiclassical description of laser cooling presented in chapter 1 works well at high temperature but becomes less reliable as soon as the atomic momentum is small. To predict the temperature of a cooled gas, a quantum description of the centre-of-mass motion is required, especially regarding the recoil due to spontaneous emission. In this case, the master equation to solve for the (reduced) atomic density operator $\hat{\rho}_S$ reads

$$\frac{d\hat{\rho}_S}{dt} = \frac{i}{\hbar}[\hat{\rho}_S, \hat{H}_S] + \hat{\hat{\mathcal{L}}}_{\text{relax}}(\hat{\rho}_S),$$

with the dissipator [16, 28, 78]

$$\hat{\hat{\mathcal{L}}}_{\text{relax}}(\hat{\rho}_S) = -\frac{\Gamma}{2}\left(\hat{P}_e\hat{\rho}_S + \hat{\rho}_S\hat{P}_e\right) + \frac{3\Gamma}{8\pi}\int \mathrm{d}^2\Omega \sum_{\boldsymbol{\epsilon}\perp\mathbf{k}} e^{-i\mathbf{k}\cdot\hat{\mathbf{r}}}(\boldsymbol{\epsilon}^*\cdot\hat{\mathbf{S}}^-)\hat{\rho}_S(\boldsymbol{\epsilon}\cdot\hat{\mathbf{S}}^+)e^{i\mathbf{k}\cdot\hat{\mathbf{r}}}, \qquad (4.1)$$

where Γ is the total spontaneous emission rate, $\hat{P}_e$ is the projector onto the excited state manifold, the wavevector $\mathbf{k}$ points in the direction of the solid angle Ω, the integral runs over all possible directions for the spontaneously emitted photon and the sum is performed over

two polarisations $\boldsymbol{\epsilon}$ orthogonal to $\mathbf{k}$ and forming a basis set for the polarisation vector $\boldsymbol{\mathcal{E}}$. In the dissipator (4.1), $\exp(\pm i\mathbf{k}\cdot\hat{\mathbf{r}})$ are translation operators and $\boldsymbol{\epsilon}^*\cdot\hat{\mathbf{S}}^-$ (resp. $\boldsymbol{\epsilon}\cdot\hat{\mathbf{S}}^+$) are operators acting on internal states that project the wavefunction from an excited substate (resp. a ground substate) to the proper ground substate (resp. the proper excited substate) whose expression is given below. The dissipator (4.1) suggests to choose the jump operators as follows [16]

$$\hat{C}_{\Omega,\boldsymbol{\epsilon}} = \sqrt{\frac{3\Gamma}{8\pi}} e^{-i\mathbf{k}\cdot\hat{\mathbf{r}}}(\boldsymbol{\epsilon}^*\cdot\hat{\mathbf{S}}^-). \tag{4.2}$$

The dissipator (4.1) subscribes to the Lindblad form and thereby preserves the properties of $\hat{\rho}_S$ as a density operator. This can be seen through the following identity [16]

$$\begin{aligned}\int \mathrm{d}^2\Omega \sum_{\boldsymbol{\epsilon}\perp\mathbf{k}} \hat{C}^\dagger_{\Omega,\boldsymbol{\epsilon}}\hat{C}_{\Omega,\boldsymbol{\epsilon}} &= \frac{3\Gamma}{8\pi}\int \mathrm{d}^2\Omega \sum_{\boldsymbol{\epsilon}\perp\mathbf{k}} (\boldsymbol{\epsilon}\cdot\hat{\mathbf{S}}^+)(\boldsymbol{\epsilon}^*\cdot\hat{\mathbf{S}}^-) \\ &= \Gamma\hat{\mathbf{S}}^+\cdot\hat{\mathbf{S}}^- = \Gamma\hat{P}_e,\end{aligned}$$

which guarantees that the dissipator is under the suitable form (2.4).

A rather tedious procedure, which amounts to choosing the direction and polarisation of the emitted photon, must then be performed to choose which jump operators, amongst the infinite set of jump operators (4.2), must be applied to the wavefunction. However, as Mølmer *et al.* [16] stress, when one is not interested in the detailed effect of the spontaneous emission pattern on the atomic dynamics, one can restrict the discussion to a much simplified spontaneous emission pattern and only consider emission along a given set of coordinates specified by the basis vectors $\mathbf{e}_x$, $\mathbf{e}_y$ and $\mathbf{e}_z$. These basis vectors can also be used as a polarisation basis for the polarisation vectors : a photon whose wavevector is along $\mathbf{e}_z$ may have polarisation $\mathbf{e}_x$ or $\mathbf{e}_y$. We note that this simplification drastically reduces the number of jump operators since from an infinite set of jump operators we now deal with a finite set of such operators. Indeed, in the dissipator (4.1), the integral running over all possible directions of emission is now replaced by a summation over all new possible directions of emission [16], that is $\mathbf{k} = \pm k\mathbf{e}_i$, with $i = x, y, z$

$$\frac{\Gamma}{2}\sum_{\mathbf{k}/k=\mathbf{e}_x,\mathbf{e}_y,\mathbf{e}_z}\sum_{\boldsymbol{\epsilon}\perp\mathbf{k}} e^{-i\mathbf{k}\cdot\hat{\mathbf{r}}}(\boldsymbol{\epsilon}^*\cdot\hat{\mathbf{S}}^-)\hat{\rho}_S(\boldsymbol{\epsilon}\cdot\hat{\mathbf{S}}^+)e^{i\mathbf{k}\cdot\hat{\mathbf{r}}},$$

so that the dissipator now reads

$$\hat{\hat{\mathcal{L}}}_{\mathrm{relax}}(\hat{\rho}_S) = -\frac{\Gamma}{2}\left(\hat{P}_e\hat{\rho}_S + \hat{\rho}_S\hat{P}_e\right) + \frac{\Gamma}{2}\sum_{\mathbf{k}/k=\mathbf{e}_x,\mathbf{e}_y,\mathbf{e}_z}\sum_{\boldsymbol{\epsilon}\perp\mathbf{k}} e^{-i\mathbf{k}\cdot\hat{\mathbf{r}}}(\boldsymbol{\epsilon}^*\cdot\hat{\mathbf{S}}^-)\hat{\rho}_S(\boldsymbol{\epsilon}\cdot\hat{\mathbf{S}}^+)e^{i\mathbf{k}\cdot\hat{\mathbf{r}}}. \tag{4.3}$$

When one restricts the discussion to 1D cooling along the z direction, which amounts to taking the trace over x and y in equation (4.3), the dissipator reads [16]

$$\hat{\hat{\mathcal{L}}}_{\mathrm{relax}}(\hat{\rho}_S) = -\frac{\Gamma}{2}\left(\hat{P}_e\hat{\rho}_S + \hat{\rho}_S\hat{P}_e\right) + \Gamma\sum_{q=0,\pm}\sum_{k'=0,\pm k}\bar{p}_q(k')e^{-ik'\hat{z}}(\boldsymbol{\epsilon}^*\cdot\hat{\mathbf{S}}^-)\hat{\rho}_S(\boldsymbol{\epsilon}\cdot\hat{\mathbf{S}}^+)e^{ik'\hat{z}}, \tag{4.4}$$

with $\bar{p}_q(k')$ the probability for having a spontaneous photon with linear momentum $\hbar\mathbf{k}'$ along the motion axis and angular momentum $\hbar\mathbf{q}$ [16] and vectors $\boldsymbol{\epsilon}_q$, forming the standard spherical basis, have been defined in Eq. (3.11). For 1D cooling, we thus restrict the discussion to

spontaneous emission along $\pm\mathbf{e}_z$ or in the $xy-$plane. Because of this restriction to 1D cooling, we now deal with 9 quantum jump operators which read

$$\hat{C}_{k',q} = \sqrt{\Gamma \bar{p}_q(k')} e^{-ik'\hat{z}} \left(\boldsymbol{\epsilon}_q^* \cdot \hat{\mathbf{S}}^- \right),$$

that is a form totally analogous to (4.2). Operators $\hat{\mathbf{S}}^+$ and $\hat{\mathbf{S}}^-$ are defined through their action on internal states [16]

$$\begin{aligned} \boldsymbol{\epsilon}_q \cdot \hat{\mathbf{S}}^+ |J_g, m_g\rangle &= \langle 1, J_g, q, m_g | J_e, m_e = m_g + q \rangle \, |J_e, m_e = m_g + q\rangle \\ \boldsymbol{\epsilon}_q \cdot \hat{\mathbf{S}}^+ |J_e, m_e\rangle &= 0 \\ \boldsymbol{\epsilon}_q^* \cdot \hat{\mathbf{S}}^- &= \left(\boldsymbol{\epsilon}_q \cdot \hat{\mathbf{S}}^+ \right)^\dagger, \end{aligned}$$

with $\langle 1, J_g, q, m_g | J_e, m_e = m_g + q \rangle$ being the Clebsch-Gordan coefficient related to the $|J_e, m_e = m_g + q\rangle \leftrightarrow |J_g, m_g\rangle$ transition. In the following subsection, we derive the probabilities $\bar{p}_q(k')$ based on the angular distribution of intensity of classical electric dipoles.

4.1.1 Discrete probabilities of emission in a given direction and angular distribution of atomic fluorescence

In the definition of the jump operators, one is interested in the probability of emitting a photon along $\pm\mathbf{e}_z$ or in the $xy-$plane with a well defined polarisation. For that purpose, we first present the angular distribution of the emitted light intensity. Let us choose a Cartesian coordinate system such that the atoms are located at the origin. Since the problem is axial symmetric with respect to the z axis, one can restrict the discussion to light emitted with a wavevector lying in the $x > 0$, $xz-$semiplane [79]. Therefore, the polar angle θ univocally defines the direction of emission of radiation.

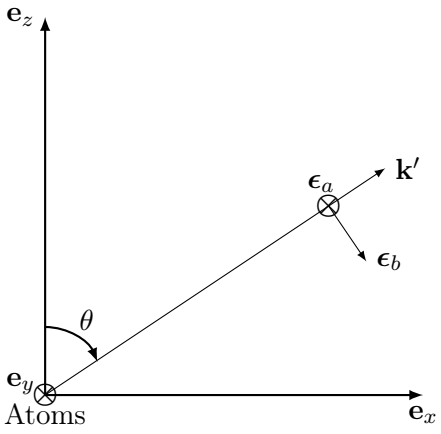

Figure 4.1: Coordinate system centered on the atoms, where $\mathbf{k}'$ is the wavevector of the emitted light, $\boldsymbol{\epsilon}_a$ and $\boldsymbol{\epsilon}_b$ are two possible orthogonal directions for the light polarisation. Figure adapted from [79].

For a given direction of emission specified by the wavevector $\mathbf{k}'$, two possible orthogonal light polarisation vectors are

$$\begin{cases} \boldsymbol{\epsilon}_a = \mathbf{e}_y, \\ \boldsymbol{\epsilon}_b = \cos\theta\,\mathbf{e}_x - \sin\theta\,\mathbf{e}_z \end{cases}.$$

When spontaneous emission occurs, an atom has 3 possible decay channels, each of which related to a particular spontaneous photon polarisation ($\sigma^{\pm}$ or π). The probabilities associated to such decay channels are proportional to the square of Clebsch-Gordan coefficients. According to the polarisation of the emitted photon, the angular pattern of emission is different. In a classical picture, a dipole oscillating along the z direction with dipole moment

$$\mathbf{d}_0(t) = d_0\cos(\omega_0 t)\mathbf{e}_z = d_0\cos(\omega_0 t)\boldsymbol{\epsilon}_0$$

produces light with π polarisation and frequency ω_0 whilst a dipole rotating in $x-y$ plane with dipole moment

$$\mathbf{d}_{\pm}(t) = d_0\Big(\cos(\omega_0 t)\mathbf{e}_x \mp \sin(\omega_0 t)\mathbf{e}_y\Big) = \Re\left[\sqrt{2}d_0\boldsymbol{\epsilon}_{\pm}e^{\mp i\omega_0 t}\right]$$

produces light with $\sigma^{\pm}$ polarisation and frequency ω_0. For a given direction of emission specified by θ and a polarisation vector $\boldsymbol{\epsilon}_i$ with $i = a, b$, the intensity of the emitted light is proportional to the square of the modulus of the dot product between the corresponding polarisation vector $\boldsymbol{\epsilon}_i$ and the direction of oscillation of $\mathbf{d}_q(t)$ [79]. In the case of π light produced by a dipole oscillating along the z axis, the direction of oscillation is $\mathbf{e}_z$ which yields

$$\begin{cases} I^{(\pi)}_{\boldsymbol{\epsilon}_a}(\theta) \propto |\boldsymbol{\epsilon}_a \cdot \mathbf{e}_z|^2 = 0 \\ I^{(\pi)}_{\boldsymbol{\epsilon}_b}(\theta) \propto |\boldsymbol{\epsilon}_b \cdot \mathbf{e}_z|^2 = |(\cos\theta\,\mathbf{e}_x - \sin\theta\,\mathbf{e}_z)\cdot\mathbf{e}_z|^2 = \sin^2\theta \end{cases}.$$

The total intensity is therefore proportional to $I^{(\pi)}_{\text{tot}}(\theta) \propto \sin^2\theta$, that is no emission along the z axis and a large emission in the equatorial plane (maximum for $\theta = \pi/2$). In the case of $\sigma^{\pm}$ light produced by a dipole rotating clockwise or counterclockwise in the $xy-$plane, the direction of oscillation is

$$\boldsymbol{\epsilon}_{\pm} = \mp\frac{1}{\sqrt{2}}(\mathbf{e}_x \pm i\mathbf{e}_y),$$

which yields

$$\begin{cases} I^{(\sigma^{\pm})}_{\boldsymbol{\epsilon}_a}(\theta) \propto |\boldsymbol{\epsilon}_a \cdot \boldsymbol{\epsilon}_{\pm}|^2 = \left|\mathbf{e}_y \cdot \mp\frac{1}{\sqrt{2}}(\mathbf{e}_x \pm i\mathbf{e}_y)\right|^2 = \frac{1}{2} \\ I^{(\sigma^{\pm})}_{\boldsymbol{\epsilon}_b}(\theta) \propto |\boldsymbol{\epsilon}_b \cdot \boldsymbol{\epsilon}_{\pm}|^2 = \left|(\cos\theta\,\mathbf{e}_x - \sin\theta\,\mathbf{e}_z)\cdot \mp\frac{1}{\sqrt{2}}(\mathbf{e}_x \pm i\mathbf{e}_y)\right|^2 = \frac{\cos^2\theta}{2} \end{cases}.$$

The total intensity is therefore proportional to $I^{(\sigma^{\pm})}_{\text{tot}}(\theta) \propto (1+\cos^2\theta)/2$, that is an intense emission along the z axis and a weaker emission in the equatorial plane.

The normalised angular patterns for π or $\sigma^{\pm}$ lights are given in Figure 4.2.

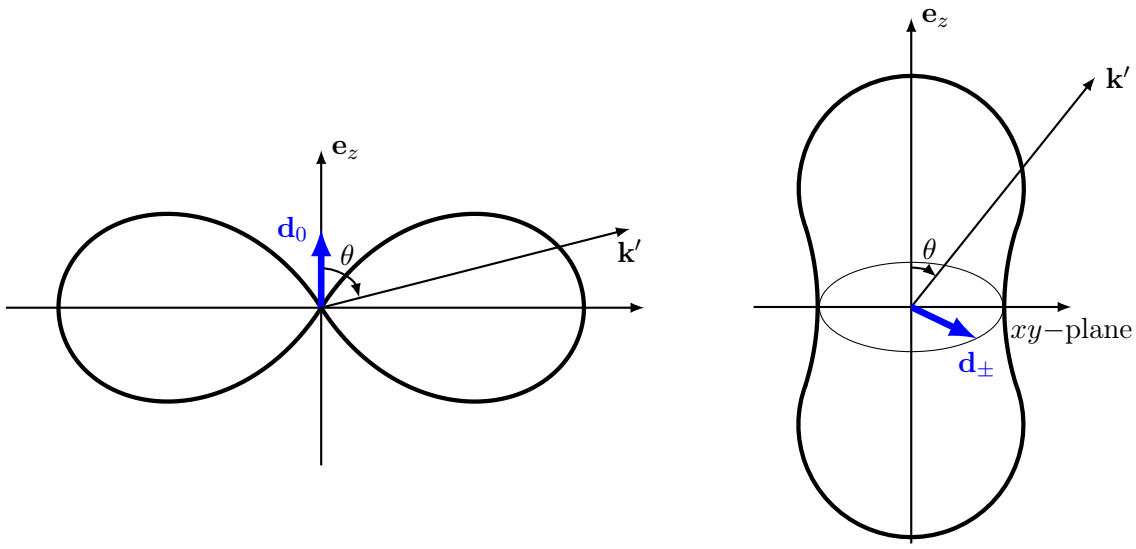

$\mathbf{d}_0(t) = d_0 \cos(\omega_0 t)\mathbf{e}_z$

(a) $I_{\text{tot}}^{(\pi)}(\theta) \propto \sin^2\theta$

$\mathbf{d}_{\pm}(t) = d_0 \left(\cos(\omega_0 t)\mathbf{e}_x \mp \sin(\omega_0 t)\mathbf{e}_y\right)$

(b) $I_{\text{tot}}^{(\sigma^{\pm})}(\theta) \propto (1+\cos^2\theta)/2$

Figure 4.2: Normalised angular patterns of light emitted by (a) a dipole oscillating along the z axis and (b) a dipole rotating in the $xy-$plane. Figure adapted from [79].

The classical discussion we have led hereinbefore allowed us to introduce the angular patterns of emission, which result we apply to spontaneous emission of photons by atoms in the following. The total intensity of radiation in a given direction is obtained by adding the angular patterns for each type of transition, weighted by the square of the proper Clebsch-Gordan coefficient. It can be shown that when an atom is driven by unpolarised light [79], the result has no angular dependence indicating that the total light intensity is isotropic. Finally, after computing the normalisation constant, the normalised angular probability distributions read

$$\begin{cases} I_{\text{tot}}^{(\sigma^{\pm})}(\theta) = \dfrac{3}{4}\left(\dfrac{1+\cos^2\theta}{2}\right) \\ I_{\text{tot}}^{(\pi)}(\theta) = \dfrac{3}{4}\sin^2\theta \end{cases} . \tag{4.5}$$

As we have already mentioned earlier, when one restricts to a simplified procedure consisting in choosing a set of unit vectors $\mathbf{e}_x, \mathbf{e}_y, \mathbf{e}_z$ accounting for the only possible directions of spontaneous emission and when the atomic motion is unidimensional, one has to convert the continuous probability densities into corresponding discrete probabilities. The problem we have in mind is the elastic scattering of a photon of wavevector $\mathbf{k}$ into a photon of wavevector $\mathbf{k}' : |\mathbf{k}'| = |\mathbf{k}|$.

We choose the set of coordinates with $\mathbf{e}_z$ in the same direction as $\mathbf{k}$, the $xy-$plane being perpendicular to $\mathbf{k}$, as shown in Figure 4.3.

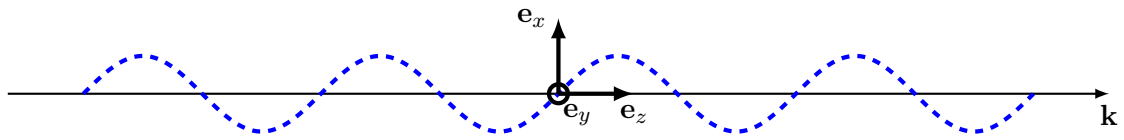

Figure 4.3: Unit vectors with $\mathbf{e}_z$ in the same direction as $\mathbf{k}$, the laser wave being depicted in dashed blue.

In order to assess the equivalent discrete probabilities, we define κ as the projection of $\mathbf{k}'$ onto $\mathbf{e}_z$

$$\kappa = \mathbf{k}' \cdot \mathbf{e}_z = \mathbf{k}' \cdot \frac{\mathbf{k}}{k} = k \cos\theta.$$

Therefore, in terms of κ, the angular profiles of emission from classical electrodynamics (4.5) read

$$\begin{cases} I_{\text{tot}}^{(\sigma^\pm)}(\kappa/k) = \dfrac{3}{8}\left[1 + \left(\dfrac{\kappa}{k}\right)^2\right] \\ I_{\text{tot}}^{(\pi)}(\kappa/k) = \dfrac{3}{4}\left[1 - \left(\dfrac{\kappa}{k}\right)^2\right] \end{cases} . \tag{4.6}$$

We can associate to these angular patterns normalised probability densities for having a photon with angular momentum $\hbar\mathbf{q} = 0, \pm\hbar\mathbf{e}_z$ and linear momentum $\hbar\boldsymbol{\kappa}$ along the motion axis $\mathbf{e}_z$

$$\begin{cases} \mathcal{N}_{\pm}^{(\sigma^\pm)}(\kappa/k) = \dfrac{3}{8k}\left[1 + \left(\dfrac{\kappa}{k}\right)^2\right] \\ \mathcal{N}_{0}^{(\pi)}(\kappa/k) = \dfrac{3}{4k}\left[1 - \left(\dfrac{\kappa}{k}\right)^2\right] \end{cases} . \tag{4.7}$$

Since $\cos\theta \in [-1, 1]$, then $\kappa \in [-k, k]$ and one easily checks the normalisation of those probability densities by integrating over all possible values for κ

$$\int_{-k}^{k} \mathcal{N}_q(\kappa) \mathrm{d}\kappa = 1, \quad q = 0, \pm.$$

Now that we have successfully computed the angular distribution of the emitted light intensity and that we have deduced normalised probability densities for having a photon with a given polarisation in a given direction, we have to convert those continuous probability densities into corresponding discrete probabilities. Whatever its direction, we can always decompose $\mathbf{k}'$ onto the basis we introduced earlier, which yields

$$\mathbf{k}' = \kappa\mathbf{e}_z + \mathbf{k}_{xy},$$

that is, a part belonging to a plane perpendicular to $\mathbf{k}$ and another one along $\mathbf{k}$. Therefore, following the prescription of quantum mechanics, the discrete probabilities p_{xy} and p_z for measuring $\mathbf{k}'$ in the xy plane and along the z direction respectively, are given by

$$p_{xy} = \frac{|\mathbf{k}_{xy}|^2}{|\kappa|^2 + |\mathbf{k}_{xy}|^2} = \sin^2\theta$$
$$p_z = \frac{|\kappa|^2}{|\kappa|^2 + |\mathbf{k}_{xy}|^2} = \cos^2\theta.$$

Averaging those probabilities over all possible directions of $\mathbf{k}'$, taking into account the angular profiles (4.5) and performing the integration in spherical coordinates, one has for a photon with polarisation $\sigma^{\pm}$

$$\bar{p}_{\pm}(\kappa = \pm k) = \frac{3}{8}\int_0^{\pi} \sin\theta\cos^2\theta\left(1+\cos^2\theta\right)\mathrm{d}\theta = 1/5$$
$$\bar{p}_{\pm}(\kappa = 0) = \frac{3}{8}\int_0^{\pi} \sin\theta\sin^2\theta\left(1+\cos^2\theta\right)\mathrm{d}\theta = 3/5, \tag{4.8}$$

whilst one has for a photon with polarisation π

$$\bar{p}_0(\kappa = \pm k) = \frac{3}{4}\int_0^{\pi} \sin\theta\cos^2\theta\sin^2\theta\mathrm{d}\theta = 1/10$$
$$\bar{p}_0(\kappa = 0) = \frac{3}{4}\int_0^{\pi} \sin\theta\sin^2\theta\sin^2\theta\mathrm{d}\theta = 4/5. \tag{4.9}$$

These developments indicate that the jump operators which should be employed in the dissipator (4.4) are given by

$$\hat{C}_q(\kappa) = \sqrt{\Gamma\bar{p}_q(\kappa)}e^{-ik'\hat{z}}\left(\boldsymbol{\epsilon}_q^* \cdot \hat{\mathbf{S}}^-\right),$$

with the probability $\bar{p}_q(\kappa)$ $(q = 0, \pm)$ for each of the nine jump operators given thereinabove. We use this form for the jump operators in the Doppler cooling and Sisyphus cooling simulations.

4.1.2 Atomic model

We now have to detail the atomic model and the parameters used in our simulations. We consider the 1D cooling of atoms through a $J_g = 1/2 \leftrightarrow J_e = 3/2$ transition for which Clebsch-Gordan coefficients are recalled in Figure 4.4. There are 6 Zeeman sublevels : 4 for the excited state manifold and 2 for the ground state manifold. The parameters we choose in our computations are those of sodium, as summarised in Table 4.1.

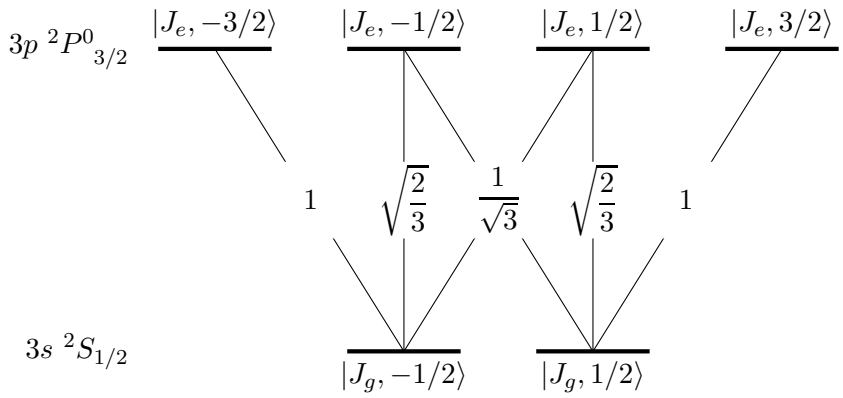

Figure 4.4: Atomic level scheme for a $J_g = 1/2 \leftrightarrow J_e = 3/2$ transition with the associated Clebsch-Gordan coefficients.

As a reminder, a discussion about Clebsch-Gordan coefficients in the rotation group is performed in the appendix A. All atomic parameters have been collected at the National Institute of Standards and Technology (NIST) [80] and are a common feature of all future simulations.

Parameter	Numerical value
λ_0	$588.9950954\,\mathrm{nm}$
ω_0	$1.156991152 \times 10^{15}\,\mathrm{s}^{-1}$
Γ	$6.16 \times 10^7\,\mathrm{Hz}$
ω	$\delta + \omega_0$
λ	$2\pi c/\omega$
k	$2\pi/\lambda$
m	$200\hbar k^2/\Gamma$

Table 4.1: Simulation parameters.

Laser parameters ω, λ and k depend upon the detuning δ which is specific to each simulation.

4.2 Derivation of the system Hamiltonian

In this section, we derive the most general 3D form of the system Hamiltonian, including a quantum treatment of the atomic motion and a Zeeman degeneracy of the angular momenta J_g and J_e considered in the $J_g \leftrightarrow J_e$ transition. Indeed, if we consider the degeneracy of each angular momentum of the transition, then J_g and J_e states are $g_g = 2J_g + 1$-fold and $g_e = 2J_e + 1$-fold degenerate because the quantum number $m_{e/g}$ related to the projection of the corresponding angular momentum onto the quantisation axis can take values in

$$m_{e/g} = -J_{e/g}, -J_{e/g} + 1, \ldots, J_{e/g} - 1, J_{e/g}.$$

The related states are therefore denoted by $|J_{e/g}, m_{e/g}\rangle$. The following derivation is performed for the case of one atom interacting with a single travelling copropagating laser wave. The

generalisation for an atom interacting with several travelling waves is straigthforward and presented at the end of the section. As we already mentioned in the introduction chapter about laser cooling, the system under study is made of one (or several) laser(s) forming the laser field and the atom. Therefore, the system Hamiltonian is a sum of three distinct contributions :

1. The atomic Hamiltonian.
2. If the laser field were treated quantum-mechanically, one would have to consider the laser Hamiltonian. However, since the laser is a widely and densely populated mode of the electric field, consisting in a huge amount of photons, it is sufficient to use a classical description and treat the laser as an external field with no Hamiltonian.
3. The interaction Hamiltonian accounting for the coupling between the laser and the atom.

4.2.1 Derivation of the atomic Hamiltonian

Consider an atomic transition $J_g \leftrightarrow J_e$ of a moving atom with linear momentum $\mathbf{p}$ along the motion axis (chosen here as $\mathbf{e}_z$). One thus has to introduce five quantum numbers : two quantum numbers, $J_{e/g}$ and $m_{e/g}$, that respectively account for the angular momentum considered in the transition and for the projection of that angular momentum onto the quantisation axis and the vector quantum number $\mathbf{p}$ that stands for the atomic linear momentum (one quantum number per direction). Each state is now identified by a unique combination of those quantum numbers and will be denoted as $|J_{e/g}, m_{e/g}, \mathbf{p}\rangle = |J_{e/g}, m_{e/g}\rangle \otimes |\mathbf{p}\rangle$, that is, the tensor product of an internal part by an external part. The atomic Hamiltonian is the sum of a contribution acting on internal variables and another acting on external variables. Hence we can write

$$\hat{H}_A = \hat{H}_{\mathrm{A,int}} + \hat{H}_{\mathrm{A,ext}}.$$

The Hamiltonian describing the atomic internal state admits as an eigenbasis the states $\{|J_e, m_e\rangle, |J_g, m_g\rangle\}$:

$$\begin{cases} \hat{H}_{\mathrm{A,int}} |J_e, m_e\rangle = E_e |J_e, m_e\rangle & m_e = -J_e, -J_e+1, \ldots, J_e-1, J_e \\ \hat{H}_{\mathrm{A,int}} |J_g, m_g\rangle = E_g |J_g, m_g\rangle & m_g = -J_g, -J_g+1, \ldots, J_g-1, J_g. \end{cases}$$

The energy difference between the levels J_e and J_g is given by $\hbar\omega_0$ such that a proper choice of the energy scale allows us to write $E_e = \hbar\omega_0$ and $E_g = 0$. Using the closure relation, one has

$$\hat{\mathbb{1}}_{\mathrm{int}} = \hat{P}_e + \hat{P}_g,$$

where $\hat{P}_e$ and $\hat{P}_g$ are the projectors onto the excited and ground state manifolds, defined as

$$\begin{cases} \hat{P}_e = \displaystyle\sum_{m_e=-J_e}^{J_e} |J_e, m_e\rangle \langle J_e, m_e| \\ \hat{P}_g = \displaystyle\sum_{m_g=-J_g}^{J_g} |J_g, m_g\rangle \langle J_g, m_g| . \end{cases}$$

Using the closure relation, we can simply write the internal Hamiltonian as

$$\hat{H}_{\mathrm{A,int}} = E_e\hat{P}_e + E_g\hat{P}_g = \hbar\omega_0\hat{P}_e.$$

We also have to consider the energy due to the atomic motion. The total atomic Hamiltonian therefore writes

$$\hat{H}_A = \hat{H}_{\mathrm{A,ext}} + \hat{H}_{\mathrm{A,int}} = \frac{\hat{\mathbf{p}}^2}{2m} + \hbar\omega_0\hat{P}_e. \tag{4.10}$$

4.2.2 Derivation of the atom/laser interaction Hamiltonian

In our work, the laser field is treated classically and its coupling with the atom is treated under the electric dipole approximation. In the framework of such an approximation, the interaction Hamiltonian between an electromagnetic field and an atom reads : $\hat{V}_{AL} = -\hat{\mathbf{D}}\cdot\mathbf{E}_L$ where $\mathbf{E}_L$ is the laser electric field. If we consider a travelling laser wave with polarisation $\boldsymbol{\mathcal{E}}$, frequency ω and wavevector $\mathbf{k}$, we have

$$\mathbf{E}_L(\hat{\mathbf{r}},t) = E_0\boldsymbol{\mathcal{E}}\cos\left(\mathbf{k}\cdot\hat{\mathbf{r}}-\omega t\right) = E_0\boldsymbol{\mathcal{E}}\frac{e^{i(\mathbf{k}\cdot\hat{\mathbf{r}}-\omega t)}+e^{-i(\mathbf{k}\cdot\hat{\mathbf{r}}-\omega t)}}{2}, \tag{4.11}$$

where E_0 is the amplitude of the electric laser field. One often introduces the standard spherical basis (3.11) to deal with the polarisation of the laser electric field,

$$\begin{cases}\boldsymbol{\epsilon}_\pm = \mp\dfrac{1}{\sqrt{2}}(\mathbf{e}_x \pm i\mathbf{e}_y)\\ \boldsymbol{\epsilon}_0 = \mathbf{e}_z\end{cases}. \tag{4.12}$$

The polarisation vector $\boldsymbol{\mathcal{E}}$ can always be decomposed onto such a basis as

$$\boldsymbol{\mathcal{E}} = \sum_{q=0,\pm}\mathcal{E}_q\boldsymbol{\epsilon}_q. \tag{4.13}$$

where $\mathcal{E}_q = \boldsymbol{\mathcal{E}}\cdot\boldsymbol{\epsilon}_q$ (with $q=0,\pm$) stands for the projection of the polarisation vector $\boldsymbol{\mathcal{E}}$ onto $\boldsymbol{\epsilon}_q$, the q component of the standard spherical basis (4.12). The subscript $\pm$ in Eq. (4.12) corresponds to a $\sigma^\pm$ polarised wave whilst the 0 subscript stands for a π polarised wave.

The other quantity appearing in the coupling Hamiltonian is $\hat{\mathbf{D}}$, the electric dipole moment operator defined as

$$\hat{\mathbf{D}} = \sum_{m_e=-J_e}^{J_e}\sum_{m_g=-J_g}^{J_g}\left(\mathbf{d}_{m_em_g}\left|J_e,m_e\right\rangle\left\langle J_g,m_g\right| + \mathrm{h.c.}\right).$$

In that expression, we have introduced a fundamental quantity, namely the reduced electric dipole matrix element of the transition $J_e,m_e \leftrightarrow J_g,m_g$. It is defined according to

$$\mathbf{d}_{m_em_g} = \langle J_e,m_e|\hat{\mathbf{D}}|J_g,m_g\rangle. \tag{4.14}$$

Considering the expressions for the laser electric field (4.11) and the electric dipole moment (4.14), the coupling Hamiltonian reads

$$\begin{aligned}\hat{V}_{AL} &= -\hat{\mathbf{D}}\cdot\mathbf{E}_L(\hat{\mathbf{r}},t)\\ &= -\hat{\mathbf{D}}\cdot E_0\boldsymbol{\mathcal{E}}\cos\left(\mathbf{k}\cdot\hat{\mathbf{r}}-\omega t\right)\\ &= -\frac{1}{2}\left[\sum_{m_e=-J_e}^{J_e}\sum_{m_g=-J_g}^{J_g}\left(\boldsymbol{\mathcal{E}}\cdot\mathbf{d}_{m_em_g}\left|J_e,m_e\right\rangle\left\langle J_g,m_g\right| + \mathrm{h.c.}\right)\right]E_0\left(e^{i(\mathbf{k}\cdot\hat{\mathbf{r}}-\omega t)} + \mathrm{h.c.}\right).\end{aligned}$$

In terms of the electric dipole moment operator, the dot product between the polarisation vector $\boldsymbol{\mathcal{E}}$ and the reduced electric dipole matrix elements reads

$$\boldsymbol{\mathcal{E}} \cdot \mathbf{d}_{m_e m_g} = \langle J_e, m_e | \boldsymbol{\mathcal{E}} \cdot \hat{\mathbf{D}} | J_g, m_g \rangle.$$

One can expand this dot product onto the spherical basis (see Eq.(4.13)) and express it as a sum of projections onto each element of that basis in order to write

$$\langle J_e, m_e | \boldsymbol{\mathcal{E}} \cdot \hat{\mathbf{D}} | J_g, m_g \rangle = \sum_{q=0,\pm} \langle J_e, m_e | \mathcal{E}_q \hat{D}_q | J_g, m_g \rangle.$$

Applying the Wigner-Eckart theorem [81], one can write

$$\langle J_e, m_e | \hat{D}_q | J_g, m_g \rangle = \langle J_g, m_g, 1, q | J_e, m_e \rangle \langle J_e \| \hat{D} \| J_g \rangle. \tag{4.15}$$

Therefore, the reduced electric dipole matrix element could be written

$$\boldsymbol{\mathcal{E}} \cdot \mathbf{d}_{m_e m_g} = \langle J_e \| \hat{D} \| J_g \rangle \sum_{q=0,\pm} \langle J_g, m_g, 1, q | J_e, m_e \rangle \mathcal{E}_q. \tag{4.16}$$

Considering this expansion (4.16), one can rewrite the interaction Hamiltonian $\hat{V}_{AL}$ as

$$\hat{V}_{AL} = \frac{\hbar}{2} \left[\sum_{m_e=-J_e}^{J_e} \sum_{m_g=-J_g}^{J_g} \left(\Omega_{m_e m_g} \left| J_e, m_e \right\rangle \left\langle J_g, m_g \right| + \text{h.c.} \right) \right] \left(e^{i(\mathbf{k} \cdot \hat{\mathbf{r}} - \omega t)} + \text{h.c.} \right), \tag{4.17}$$

where we have introduced the Rabi frequencies

$$\Omega_{m_e m_g} = -\frac{\boldsymbol{\mathcal{E}} \cdot \mathbf{d}_{m_e m_g} E_0}{\hbar}.$$

The Rabi frequency characterises the coupling strength between the states $|J_e, m_e\rangle$ and $|J_g, m_g\rangle$. It enables one to understand why some transitions vanish according to the laser polarisation or are forbidden (in the electric dipole approximation) whatever the laser polarisation. For that purpose, let us reuse the result of the Wigner-Eckart theorem (4.15) and (4.16) in order to write the Rabi frequency as

$$\Omega_{m_e m_g} = -\frac{\boldsymbol{\mathcal{E}} \cdot \mathbf{d}_{m_e m_g} E_0}{\hbar} = -\frac{E_0}{\hbar} \langle J_e \| \hat{D} \| J_g \rangle \sum_{q=0,\pm} \langle J_g, m_g, 1, q | J_e, m_e \rangle \mathcal{E}_q. \tag{4.18}$$

We see that there is a direct relationship between the Clebsch-Gordan coefficients, the polarisation of the laser electric field and the related Rabi frequency. The laser polarisation is well defined and usually chosen to be either σ^+, σ^- or π. In particular, the polarisation standard basis (4.12) has been chosen such that $q = 1$ for σ^+, $q = -1$ for σ^- and $q = 0$ for π. Therefore, if it is so, only the term corresponding to the value of q related to the laser polarisation considered plays a role in the summation appearing in (4.18)[1]. The related (square of the)

[1] If one uses different lasers of different polarisations, it is obvious that the terms associated to the values of q representing those laser polarisations will not vanish. However, Rabi frequency only characterises the coupling strength between a single laser and the atom. Therefore, for a given laser, all terms that do not correspond to the laser polarisation will vanish although they will not for other lasers.

Clebsch-Gordan coefficient (obtained by the value of q associated with the polarisation of the laser electric field) informs us about the probability of the considered transition. In conclusion, a Rabi frequency characterises the strength, (notably) through the related Clebsch-Gordan coefficient, of the transition between two atomic levels for a given laser polarisation.

The values of q tell us about the angular momentum of the laser photons projected onto the z axis. From stimulated processes point of view, the z component of the angular momentum of the photon is $q\hbar$, with $q = 0, \pm$. From the spontaneous emission point of view, the roles of the coupled levels are inverted and therefore the z component of the angular momentum of the photon is $-q\hbar$, with $q = 0, \pm$. The same point holds for the terminology used : an emitted photon which has a projection of its angular momentum onto the z axis equal to $-\hbar$ (so that $q = -$) is a σ^+ photon. The time-dependent coupling Hamiltonian (4.17) can be simplified in the interaction picture. By applying the unitary transformation

$$\hat{U}(t) = \exp\left(-i\omega_0 \hat{P}_e t\right) = \sum_{n=0}^{\infty} \frac{1}{n!} \left(-i\omega_0 t\right)^n \hat{P}_e = e^{-i\omega_0 t} \hat{P}_e.$$

to the time-dependent coupling Hamiltonian (4.17), we switch to the interaction picture [82] and we have

$$\begin{aligned} \hat{H}_I(t) &= \hat{U}_0^\dagger(t) \hat{V}_{AL}(t) \hat{U}_0(t) \\ &= \frac{\hbar}{2} \hat{U}_0^\dagger \left[\sum_{m_e=-J_e}^{J_e} \sum_{m_g=-J_g}^{J_g} \left(\Omega_{m_e m_g} \left| J_e, m_e \right\rangle \left\langle J_g, m_g \right| + \text{h.c.} \right) \right] \hat{U}_0 \left(e^{i\mathbf{k}\cdot\hat{\mathbf{r}}} e^{-i\omega t} + \text{h.c.} \right), \end{aligned}$$

which yields

$$\hat{H}_I(t) = \frac{\hbar}{2} \left[\sum_{m_e=-J_e}^{J_e} \sum_{m_g=-J_g}^{J_g} \Omega_{m_e m_g} e^{i\mathbf{k}\cdot\hat{\mathbf{r}}} \left(e^{-i\delta t} + e^{i(\omega+\omega_0)t} \right) \left| J_e, m_e \right\rangle \left\langle J_g, m_g \right| + \text{h.c.} \right]. \quad (4.19)$$

Noting that oscillating terms at frequency $\pm(\omega_0 + \omega)$ oscillate much faster than terms oscillating at frequency $\pm\delta$ if $\omega_0 + \omega \gg \delta$, a good approximation is the rotating wave approximation (RWA) [83] which amounts to neglecting terms involving $\exp[\pm i(\omega_0 + \omega)t]$ in the coupling Hamiltonian (4.19). Indeed, because those terms oscillate much faster compared to terms involving $\exp[\pm i\delta t]$, their mean over a time interval $\Delta t \gg 1/(\omega + \omega_0)$ but small compared to a characteristic of populations evolution $\tau \sim 1/\Omega$ is zero [84]. Within RWA, the coupling Hamiltonian (4.19) in the interaction picture is given by

$$\hat{H}_I(t) \simeq \frac{\hbar}{2} \left[\sum_{m_e=-J_e}^{J_e} \sum_{m_g=-J_g}^{J_g} \Omega_{m_e m_g} e^{i\mathbf{k}\cdot\hat{\mathbf{r}}} e^{-i\delta t} \left| J_e, m_e \right\rangle \left\langle J_g, m_g \right| + \text{h.c.} \right]. \quad (4.20)$$

We also note that the passage to the interaction picture leads to

$$\hat{H}_{\text{int}}(t) = \hat{U}_0^\dagger(t) \hat{H}_{\text{tot}}(t) \hat{U}_0(t) - \hbar\omega_0 \hat{P}_e = \frac{\hat{\mathbf{p}}^2}{2m} + \hat{H}_I(t), \quad (4.21)$$

where $\hat{H}_{\text{tot}}(t) = \hat{H}_A + \hat{V}_{AL}(t)$ is the total Hamiltonian in the Schrödinger picture.

4.2.3 System Hamiltonian in the interaction picture

The time-dependent system Hamiltonian (4.21) which is the sum of the interaction Hamiltonian (4.20) and $\hat{\mathbf{p}}^2/2m$ both in the interaction picture reads

$$\hat{H}_{\text{int}}(t) = \frac{\hat{\mathbf{p}}^2}{2m} + \frac{\hbar}{2}\left[\sum_{m_e=-J_e}^{J_e}\sum_{m_g=-J_g}^{J_g}\Omega_{m_e m_g} e^{i\mathbf{k}\cdot\hat{\mathbf{r}}} e^{-i\delta t}\left|J_e, m_e\right\rangle\left\langle J_g, m_g\right| + \text{h.c.}\right]. \tag{4.22}$$

We shall get rid of the time dependency by working in a rotating reference frame in Hilbert space [82] by applying the unitary transformation

$$\hat{U}(t) = \exp\left(-\frac{i}{\hbar}\hat{S}t\right),$$

where $\hat{S}$ denotes any Hermitian operator. Under such a transformation, the system Hamiltonian becomes

$$\hat{H}_S = \hat{U}^\dagger \hat{H}_{\text{int}}(t)\hat{U} - \hat{S}.$$

We shall choose the Hermitian operator $\hat{S}$ as being

$$\hat{S} = \hbar\delta\hat{P}_e,$$

and the unitary transformation reads

$$\hat{U}(t) = \exp\left(-i\delta\hat{P}_e t\right) = \sum_{n=0}^{\infty}\frac{1}{n!}\left(-i\delta t\right)^n \hat{P}_e = e^{-i\delta t}\hat{P}_e.$$

Therefore, the system Hamiltonian after such a transformation is given by

$$\begin{aligned}\hat{H}_S &= \hat{U}^\dagger \hat{H}_{\text{int}}(t)\hat{U} - \hat{S} \\ &= \frac{\hat{\mathbf{p}}^2}{2m} + \left(e^{i\delta t}\hat{P}_e\right)\hat{H}_I\left(e^{-i\delta t}\hat{P}_e\right) - \hbar\delta\hat{P}_e.\end{aligned}$$

Finally, the system Hamiltonian reads

$$\begin{aligned}\hat{H}_S &= \frac{\hat{\mathbf{p}}^2}{2m} + \frac{\hbar}{2}\left[\sum_{m_e=-J_e}^{J_e}\sum_{m_g=-J_g}^{J_g}\Omega_{m_e m_g} e^{i\mathbf{k}\cdot\hat{\mathbf{r}}}\left|J_e, m_e\right\rangle\left\langle J_g, m_g\right| + \text{h.c.}\right] - \hbar\delta\hat{P}_e \\ &= \frac{\hat{\mathbf{p}}^2}{2m} + \frac{\hbar\Omega}{2}(e^{i\mathbf{k}\cdot\hat{\mathbf{r}}}\hat{S}^+ + e^{-i\mathbf{k}\cdot\hat{\mathbf{r}}}\hat{S}^-) - \hbar\delta\hat{P}_e\end{aligned} \tag{4.23}$$

where we have introduced the raising and the lowering operators related to the dipole operator

$$\begin{cases}\hat{S}^+ = \displaystyle\sum_{m_e=-J_e}^{J_e}\sum_{m_g=-J_g}^{J_g}\frac{\Omega_{m_e m_g}}{\Omega}\left|J_e, m_e\right\rangle\left\langle J_g, m_g\right| \\ \hat{S}^- = \displaystyle\sum_{m_e=-J_e}^{J_e}\sum_{m_g=-J_g}^{J_g}\frac{\Omega^*_{m_e m_g}}{\Omega^*}\left|J_g, m_g\right\rangle\left\langle J_e, m_e\right|.\end{cases} \tag{4.24}$$

and the invariant Rabi frequency

$$\Omega = -\frac{\boldsymbol{\mathcal{E}} \cdot \mathbf{d}_{J_e J_g} E_0}{\hbar},$$

with

$$\mathbf{d}_{J_e J_g} = \langle J_e, m_e = J_e | \hat{\mathbf{D}} | J_g, m_g = J_g \rangle.$$

The invariant Rabi frequency is defined in terms of the reduced electric dipole matrix element between the $m_g = J_g$ ground state and $m_e = J_e$ excited state manifolds. As Dunn and Greene indicate [85], such a definition is convenient because, in general, Rabi frequencies for transitions to different excited state and ground state manifolds will not be the same. We notice that the introduction of Ω leads to

$$\frac{\Omega_{m_e m_g}}{\Omega} = \frac{\boldsymbol{\mathcal{E}} \cdot \mathbf{d}_{m_e m_g}}{\boldsymbol{\mathcal{E}} \cdot \mathbf{d}_{J_e J_g}} = \frac{\sum\limits_{q=0,\pm} \langle J_g, m_g, 1, q | J_e, m_e \rangle \mathcal{E}_q}{\sum\limits_{q=0,\pm} \langle J_g, J_g, 1, q | J_e, J_e \rangle \mathcal{E}_q} \equiv \Xi_{m_e m_g},$$

that is a ratio of sums of Clebsch-Gordan coefficients. The exponentials appearing in the raising and the lowering operators related to the dipole operator (4.24) can be treated either classically, which is the subject of the following paragraphs or quantum mechanically which is detailed just after the classical treatment.

Classical treatment of the atomic motion

In a classical approach, the external degrees of freedom are treated classically such that $\hat{\mathbf{r}} \equiv \mathbf{r}$ and $\hat{\mathbf{p}} \equiv \mathbf{p}$ are classical variables of time : the atom is point-like and its centre-of-mass is in rectilinear motion. In such a case, the system Hamiltonian (4.23) reads

$$\hat{H}_S = \frac{\hbar\Omega}{2} \left[\sum_{m_e=-J_e}^{J_e} \sum_{m_g=-J_g}^{J_g} \left(\Xi_{m_e m_g} e^{i\mathbf{k}\cdot\mathbf{r}} \left| J_e, m_e \right\rangle \left\langle J_g, m_g \right| + \text{h.c.} \right) \right] - \hbar\delta \hat{P}_e.$$

In that expression, exponentials appearing in the definition of the system Hamiltonian are phase factors and do not act upon the atomic internal states. Those phase factors reflect the position dependence of the laser wave. The internal atomic variables are treated using the Monte-Carlo wavefunction approach whilst the external atomic variables are treated classically using a point-like description of the atomic centre-of-mass. The system state is either evolved through the non-Hermitian Hamiltonian $\hat{H} = \hat{H}_S - (i\hbar\Gamma/2)\hat{P}_e$ in which case the position and momentum are evolved through the classical equations

$$\begin{aligned} \mathbf{r}(t+\delta t) &= \mathbf{r}(t) + \frac{\mathbf{p}(t)}{m}\delta t + \mathcal{O}(\delta t^2) \\ \mathbf{p}(t+\delta t) &= \mathbf{p}(t) + \mathbf{F}(t)\delta t, \end{aligned}$$

where the damping force experienced by the atom due to the optical molasse is given by

$$\mathbf{F}(t) = -\left\langle \psi(t) \left| \boldsymbol{\nabla}_{\mathbf{r}} \hat{H} \right| \psi(t) \right\rangle.$$

Otherwise the system is evolved through the application of one of the jump operators in which case the momentum is modified of an amount $\pm\hbar k$ or is not modified according to which jump has occurred.

Quantum treatment of the atomic motion

In the expression (4.24) of the raising and lowering operators, arise the operators $\exp(\pm i\mathbf{k}\cdot\hat{\mathbf{r}})$ which we shall prove are translation operators in momentum space. With that goal in mind, we shall successively derive the action of those operators first on a wavefunction in the momentum representation and then on the momentum eigenstates $|\mathbf{p}\rangle$ themselves. First, let us consider a wavefunction in the momentum basis to which we apply $\exp(\pm i\mathbf{k}_0\cdot\hat{\mathbf{r}})$. Observing that the position operator $\hat{\mathbf{r}}$ reads in the momentum basis $\hat{\mathbf{r}} = -(\hbar/i)\boldsymbol{\nabla}_{\mathbf{p}}$, one can expand in Taylor series the following operator

$$\begin{aligned}
\exp\left(\pm\frac{i}{\hbar}\mathbf{p}_0\cdot\hat{\mathbf{r}}\right)\bar{\psi}(\mathbf{p}) &= \left(\hat{\mathbb{1}} \pm \frac{i}{\hbar}\mathbf{p}_0\cdot\hat{\mathbf{r}} - \frac{1}{2\hbar^2}(\mathbf{p}_0\cdot\hat{\mathbf{r}})^2 \mp \frac{i}{6\hbar^3}(\mathbf{p}_0\cdot\hat{\mathbf{r}})^3 + \dots\right)\bar{\psi}(\mathbf{p}) \\
&= \bar{\psi}(\mathbf{p}) \mp \mathbf{p}_0\cdot\boldsymbol{\nabla}_{\mathbf{p}}\bar{\psi}(\mathbf{p}) + \frac{1}{2}(\mathbf{p}_0\cdot\boldsymbol{\nabla}_{\mathbf{p}})^2\bar{\psi}(\mathbf{p}) \mp \frac{1}{6}(\mathbf{p}_0\cdot\boldsymbol{\nabla}_{\mathbf{p}})^3\bar{\psi}(\mathbf{p}) + \dots \\
&= \bar{\psi}(\mathbf{p}) + \sum_{n=1}^{\infty}\frac{1}{n!}(\mp\mathbf{p}_0\cdot\boldsymbol{\nabla}_{\mathbf{p}})^n\bar{\psi}(\mathbf{p}) \\
&= \bar{\psi}(\mathbf{p}\mp\mathbf{p}_0).
\end{aligned}$$

We observe that the action of operators $\exp(\pm i\mathbf{p}_0\cdot\hat{\mathbf{r}}/\hbar)$ on a wavefunction expressed in the momentum representation is to translate the wavefunction as a whole by an amount $\pm\mathbf{p}_0$. Clearly, it appears that those operators are translation operators in momentum space. We shall now derive their action on momentum eigenstates $|\mathbf{p}\rangle$

$$\exp\left(\pm\frac{i}{\hbar}\mathbf{p}_0\cdot\hat{\mathbf{r}}\right)|\mathbf{p}\rangle\,.$$

Let us express it in the position representation[2]

$$\begin{aligned}
\langle\mathbf{r}|\exp\left(\pm\frac{i}{\hbar}\mathbf{p}_0\cdot\hat{\mathbf{r}}\right)|\mathbf{p}\rangle &= \exp\left(\pm\frac{i}{\hbar}\mathbf{p}_0\cdot\mathbf{r}\right)\langle\mathbf{r}|\mathbf{p}\rangle \\
&= \frac{1}{(2\pi\hbar)^{3/2}}\exp\left(\frac{i}{\hbar}\mathbf{p}\cdot\mathbf{r}\right)\exp\left(\pm\frac{i}{\hbar}\mathbf{p}_0\cdot\mathbf{r}\right) \\
&= \frac{1}{(2\pi\hbar)^{3/2}}\exp\left(\frac{i}{\hbar}(\mathbf{p}\pm\mathbf{p}_0)\cdot\mathbf{r}\right) \\
&= \langle\mathbf{r}|\mathbf{p}\pm\mathbf{p}_0\rangle.
\end{aligned}$$

Since this development is valid for any bra $\langle\mathbf{r}|$, we can conclude that

$$\exp\left(\pm\frac{i}{\hbar}\mathbf{p}_0\cdot\hat{\mathbf{r}}\right)|\mathbf{p}\rangle = |\mathbf{p}\pm\mathbf{p}_0\rangle\,.$$

[2]In the position representation, the position operator $\hat{\mathbf{r}}$ is simply given by $\mathbf{r}$.

The action of those translation operators on a wavefunction and on momentum eigenstates $|\mathbf{p}\rangle$ being known, we can decompose the operators $\exp(\pm i\mathbf{k}\cdot\hat{\mathbf{r}})$ as follows

$$\begin{aligned}\exp(\pm i\mathbf{k}\cdot\hat{\mathbf{r}}) &= \iint \langle\mathbf{p}|e^{\pm i\mathbf{k}\cdot\hat{\mathbf{r}}}|\mathbf{p}'\rangle\,|\mathbf{p}\rangle\langle\mathbf{p}'|\,\mathrm{d}\mathbf{p}\mathrm{d}\mathbf{p}' \\ &= \iint \underbrace{\langle\mathbf{p}|\mathbf{p}'\pm\hbar\mathbf{k}\rangle}_{\delta_{\mathbf{p},\mathbf{p}'\pm\hbar\mathbf{k}}}|\mathbf{p}\rangle\langle\mathbf{p}'|\,\mathrm{d}\mathbf{p}\mathrm{d}\mathbf{p}' \\ &= \int |\mathbf{p}\rangle\langle\mathbf{p}\mp\hbar\mathbf{k}|\,\mathrm{d}\mathbf{p}.\end{aligned}$$

With this latter expression, the system Hamiltonian can be written as

$$\begin{aligned}\hat{H}_S &= \frac{\hat{\mathbf{p}}^2}{2m} + \frac{\hbar\Omega}{2}\left[\int \sum_{m_e=-J_e}^{J_e}\sum_{m_g=-J_g}^{J_g}\Big(\Xi_{m_e m_g}|J_e,m_e,\mathbf{p}\rangle\langle J_g,m_g,\mathbf{p}-\hbar\mathbf{k}| \right.\\ &\qquad\left. + \Xi^*_{m_e m_g}|J_g,m_g,\mathbf{p}\rangle\langle J_e,m_e,\mathbf{p}+\hbar\mathbf{k}|\Big)\mathrm{d}\mathbf{p}\right] - \hbar\delta\hat{P}_e \\ &= \frac{\hat{\mathbf{p}}^2}{2m} + \frac{\hbar\Omega}{2}(\hat{\mathcal{S}}^+ + \hat{\mathcal{S}}^-) - \hbar\delta\hat{P}_e. \end{aligned} \tag{4.25}$$

In the latter Hamiltonian, we have introduced the operators $\hat{\mathcal{S}}^+ = \exp(i\mathbf{k}\cdot\hat{\mathbf{r}})\hat{S}^+$ and $\hat{\mathcal{S}}^- = \exp(-i\mathbf{k}\cdot\hat{\mathbf{r}})\hat{S}^-$ with $\hat{S}^+$ and $\hat{S}^-$ defined in Eq. (4.24). We note that if the derivation were performed for a counterpropagating instead of a copropagating laser, the results are the same provided that $\mathbf{k}\mapsto-\mathbf{k}$.

4.2.4 Interaction Hamiltonian for an arbitrary number of lasers along arbitrary directions

We have derived a general expression for the atom/laser coupling Hamiltonian. In that derivation, we have considered a travelling plane laser wave of arbitrary polarisation interacting with an atom through a $J_g \leftrightarrow J_e$ transition. With the formalism developed in the previous subsections, one can easily derive the system Hamiltonian for an atom placed in a light field of the form

$$\mathbf{E}(\hat{\mathbf{r}},t) = \sum_{l=1}^{\mathcal{L}} E_{0,l}\boldsymbol{\mathcal{E}}_l\cos(\mathbf{k}_l\cdot\hat{\mathbf{r}}-\omega_l t)$$

arising from the superposition of $\mathcal{L}$ laser fields. The system Hamiltonian now reads

$$\begin{aligned}\hat{H}_S &= \frac{\hat{\mathbf{p}}^2}{2m} + \frac{\hbar}{2}\sum_{l=1}^{\mathcal{L}}\Omega_l\left[\int \sum_{m_e=-J_e}^{J_e}\sum_{m_g=-J_g}^{J_g}\Big(\Xi_{m_e m_g}|J_e,m_e,\mathbf{p}\rangle\langle J_g,m_g,\mathbf{p}-\hbar\mathbf{k}| \right.\\ &\qquad\left. + \Xi^*_{m_e m_g}|J_g,m_g,\mathbf{p}\rangle\langle J_e,m_e,\mathbf{p}+\hbar\mathbf{k}|\Big)\mathrm{d}\mathbf{p}\right]_l - \hbar\delta\hat{P}_e. \end{aligned} \tag{4.26}$$

Chapter 5

Simulation results for Doppler and Sisyphus cooling

In this chapter, we apply the MCWF method to the study of laser cooling in one dimension. Hence, we apply the MCWF method to an atom in a 1D σ^+ standing wave in order to assess the equilibrium properties of an atomic gas cooled in a laser field with gradient of intensity (Doppler cooling). After that, we apply the MCWF treatment to the lin⊥lin configuration to predict the temperature of a multilevel atom in a polarisation-gradient field. A comparison between the σ^+ standing wave and the lin⊥lin configuration is then performed. Finally, we also present some results obtained when treating the atomic motion classically, which results are to be compared to the results obtained in a full quantum approach.

5.1 Doppler cooling in a σ^+ standing wave

In this section, we consider the one dimensional cooling of an atom through a $J_g = 1/2 \leftrightarrow J_e = 3/2$ transition driven by a σ^+ standing wave resulting from the superposition of two counter-propagating lasers with the same frequency, detuning, intensity and polarisation. Applying the prescription of Eq. (4.26), the system Hamiltonian reads

$$\begin{aligned}\hat{H}_S &= \frac{\hat{p}^2}{2m} + \hbar\Omega\cos(k\hat{z})\left(\hat{S}^+ + \hat{S}^-\right) - \hbar\delta\hat{P}_e \\ &= \frac{\hat{p}^2}{2m} + \frac{\hbar\Omega}{2}\Big[\underbrace{e^{ik\hat{z}}\left(\hat{S}^+ + \hat{S}^-\right)}_{\hat{\mathcal{S}}^+(k)+\hat{\mathcal{S}}^-(k)} + \underbrace{e^{-ik\hat{z}}\left(\hat{S}^+ + \hat{S}^-\right)}_{\hat{\mathcal{S}}^+(-k)+\hat{\mathcal{S}}^-(-k)}\Big] - \hbar\delta\hat{P}_e,\end{aligned} \tag{5.1}$$

where $\hat{p}$ denotes the momentum operator along the z-direction. In the latter expression, the raising and lowering operators $\hat{\mathcal{S}}^+$ and $\hat{\mathcal{S}}^-$ are given by Eq. (4.25), *i.e.*

$$\begin{cases}\hat{\mathcal{S}}^+(k) = \displaystyle\int \sum_{m_e=-J_e}^{J_e}\sum_{m_g=-J_g}^{J_g} \Xi_{m_e m_g}\left|J_e, m_e, p\right\rangle\left\langle J_g, m_g, p-\hbar k\right| \mathrm{d}p \\ \hat{\mathcal{S}}^-(k) = \displaystyle\int \sum_{m_e=-J_e}^{J_e}\sum_{m_g=-J_g}^{J_g} \Xi^*_{m_e m_g}\left|J_g, m_g, p\right\rangle\left\langle J_e, m_e, p+\hbar k\right| \mathrm{d}p.\end{cases} \tag{5.2}$$

Due to optical pumping in a σ^+ standing wave, only the two substates with the highest magnetic quantum numbers are involved in the dynamics, which allows one to consider only two states which we denote by $|g\rangle \equiv |1/2, 1/2\rangle$ and $|e\rangle \equiv |3/2, 3/2\rangle$. In the definition of the raising and lowering operators $\hat{\mathcal{S}}^+$ and $\hat{\mathcal{S}}^-$, we replace the integral over all momenta by a truncated summation over a finite range of momenta

$$\int_{-\infty}^{\infty} f(p)\,\mathrm{d}p \longrightarrow \sum_{n=-n_{\max}}^{n_{\max}} f(n\hbar k)\hbar k, \tag{5.3}$$

i.e. we discretise the momentum range over $2n_{\max}+1$ values with a step size $\hbar k$. Provided that no momentum component of the atom extends over the considered grid, this approximation yields the same solution as the integral. In the following, we work in the $\{|e,p\rangle, |g,p\rangle\}$ basis where the quantum number p accounts for the atomic momentum along the z axis and extends from $-n_{\max}\hbar k$ to $n_{\max}\hbar k$. Then, we apply the MCWF procedure which involves $2\times(2n_{\max}+1)$ basis states. In the following, we denote by $\alpha_n(t)$ and by $\beta_n(t)$ the components of the excited and ground states with momentum $n\hbar k$ along the z-direction at time t.

Either the system is evolved under the action of the non-Hermitian Hamiltonian $\hat{H} = \hat{H}_S - (i\hbar\Gamma/2)\hat{P}_e$, in which case the coefficients $\alpha_n(t)$ and $\beta_n(t)$ are governed by

$$\begin{aligned}
\alpha_n(t) \to \alpha_n(t+\delta t) &= \left(1 - i\frac{\delta t}{\hbar}\frac{(n\hbar k)^2}{2m} + i\delta t - \frac{\Gamma}{2}\right)\alpha_n(t) - \frac{i\delta t\Omega}{2}(\beta_{n+1}(t) + \beta_{n-1}(t)) \\
\beta_n(t) \to \beta_n(t+\delta t) &= \left(1 - i\frac{\delta t}{\hbar}\frac{(n\hbar k)^2}{2m}\right)\beta_n(t) - \frac{i\delta t\Omega}{2}(\alpha_{n+1}(t) + \alpha_{n-1}(t)),
\end{aligned}$$

or a jump occurs, with probability

$$\delta p(t) = \Gamma \sum_{n=-n_{\max}}^{n_{\max}} |\alpha_n(t)|^2 \delta t.$$

The three possible jump operators to apply are given by

$$\hat{C}_{k'} = \sqrt{\Gamma \bar{p}_+(k')} e^{-ik'\hat{z}} |g\rangle \langle e|, \quad \text{with } k' = 0, \pm k$$

and $\bar{p}_+(k')$ is given by Eq. (4.8), that is

$$\hat{C}_0 = \sqrt{\frac{3\Gamma}{5}} |g\rangle \langle e|, \qquad \hat{C}_{\pm k} = \sqrt{\frac{\Gamma}{5}} e^{\mp ik\hat{z}} |g\rangle \langle e|.$$

The action of one of those operators on the wavefunction yields the wavefunction at time $t + \delta t$ with

$$\begin{aligned}
\alpha_n(t) \to \alpha_n(t+\delta t) &= 0, \\
\beta_n(t) \to \beta_n(t+\delta t) &= \mu\alpha_{n+m}(t),
\end{aligned}$$

where μ is a normalisation coefficient and $m = 0, \pm 1$ according to the direction of emission ($m = 1$ if $k' = k$, $m = 0$ if $k' = 0$ and $m = -1$ otherwise). Therefore, after the action of such an operator, the atom is found in its ground state and the momentum distribution has been shifted from an amount $\hbar k'$. Contrarily to a semiclassical approach, the centre-of-mass motion and the recoil due to spontaneous emission are treated quantum mechanically.

5.1.1 Numerical results

In this subsection, we provide a series of numerical results based on the MCWF method. We consider two distinct cases :

1. the initial momentum distribution is not centered on 0 and has a small standard deviation,
2. the initial momentum distribution is centered on 0 and has a large standard deviation.

We show, in both cases, that the mean momentum tends to zero and the width of the momentum distribution tends to a few $\hbar k$ for large times compared to Γ^{-1}.

Slowing of atoms

In order to demonstrate slowing of atoms, we take as initial state $|\psi(0)\rangle = |e, p = 40\hbar k\rangle \equiv |J_e, m_e = 3/2, p = 40\hbar k\rangle$ corresponding to an atom in the excited state $|J_e, m_e = 3/2\rangle$ with an initial momentum $p = 40\hbar k$. Figure 5.1 shows the time evolution of the momentum expectation value averaged over many trajectories $\overline{\langle\hat{p}\rangle(t)} = \overline{\langle\psi(t)|\hat{p}|\psi(t)\rangle}$.

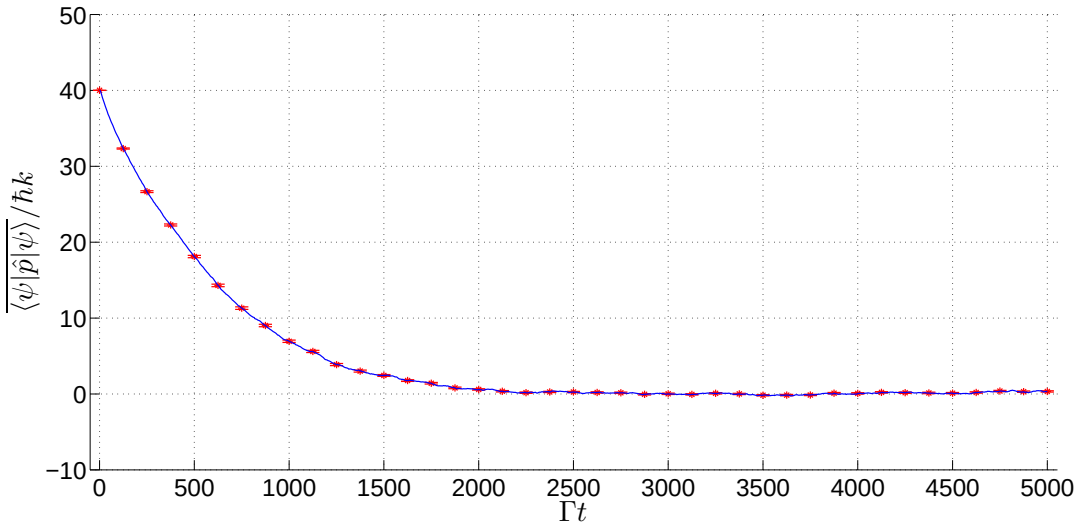

Figure 5.1: Time evolution of $\overline{\langle\hat{p}\rangle}$ averaged over 1000 trajectories in the case of a $J_g = 1/2 \leftrightarrow J_e = 3/2$ transition driven by a σ^+-polarised 1D standing wave. Error bars show the statistical error. Simulation parameters are : $\delta = -\Gamma/2$, $\Omega = \Gamma$, $\Gamma t_f = 5000$, $n_{\max} = 50$, $\Gamma\delta t = 0.0005$ and $|\psi(0)\rangle = |e, p = 40\hbar k\rangle$.

The momentum expectation value decreases with time to reach a steady state for which $\overline{\langle\hat{p}\rangle} = 0$. We present a single MCWF trajectory in order to emphasise the residual motion due to fluorescence cycles. Note that the steady state is reached after a transient period whose duration is here about $2000\Gamma^{-1}$ but depends on the initial state.

In Figure 5.2, we show the time evolution of $\langle \hat{p} \rangle$ for a single trajectory.

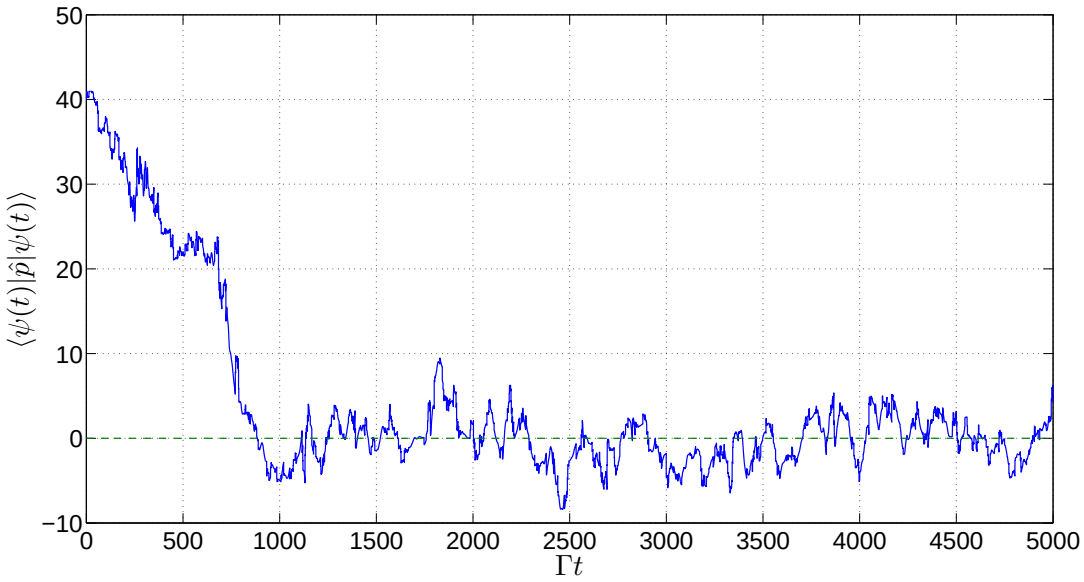

Figure 5.2: Time evolution of $\langle \hat{p} \rangle$ for a single trajectory in the case of a $J_g = 1/2 \leftrightarrow J_e = 3/2$ transition driven by a σ^+-polarised 1D standing wave. Simulation parameters are : $\delta = -\Gamma/2$, $\Omega = \Gamma$, $\Gamma t_f = 5000$, $n_{\max} = 50$, $\Gamma \delta t = 0.0005$ and $|\psi(0)\rangle = |e, p = 40\hbar k\rangle$.

The residual motion is due to linear momentum exchanges resulting from fluoresence cycles. Indeed, each absorbed or emitted photon cause a recoil that translates the wavefunction as a whole, without any modification of its shape.

In Figure 5.3, we plot our results for the momentum distribution at the initial time $t = 0$ and final time $t_f = 5000\Gamma^{-1}$.

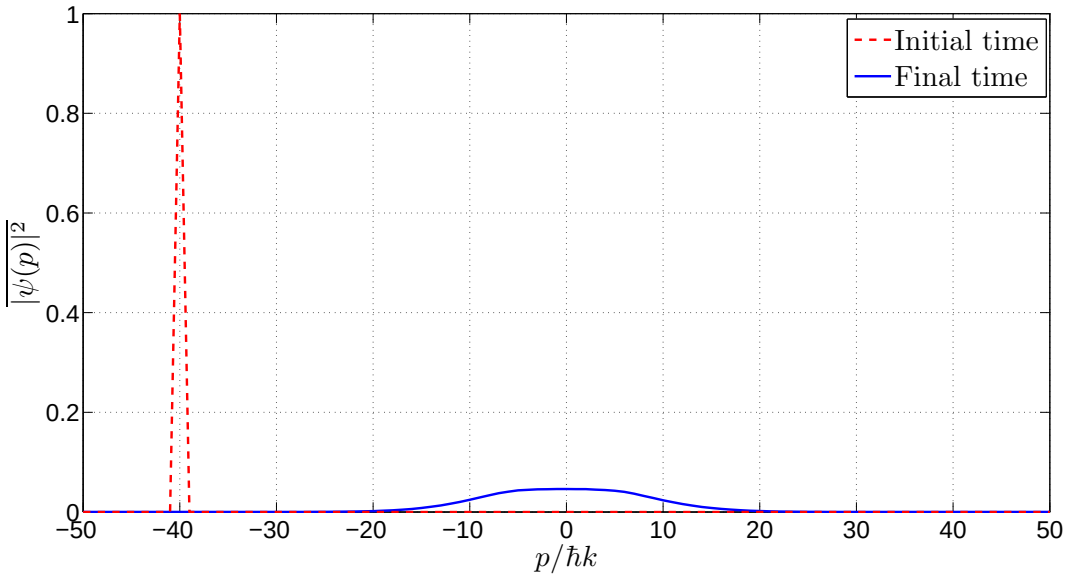

Figure 5.3: Momentum distribution in the case of a $J_g = 1/2 \leftrightarrow J_e = 3/2$ transition driven by a σ^+-polarised 1D standing wave at $t = 0$ and in steady state averaged over 1000 trajectories. The distribution at final time is also averaged over time in the range $\Gamma t \in [4500, 5000]$. Simulation parameters are : $\delta = -\Gamma/2$, $\Omega = \Gamma$, $\Gamma t_f = 5000$, $n_{\max} = 50$, $\Gamma\delta t = 0.0005$ and $|\psi(0)\rangle = |e, p = 40\hbar k\rangle$.

The wavepacket in the momentum representation initially centered on $p = 40\hbar k$ has moved around $p = 0$ and displays a standard deviation $\sigma \approx 9.7\hbar k$ as Figure 5.4 shows on a different scale.

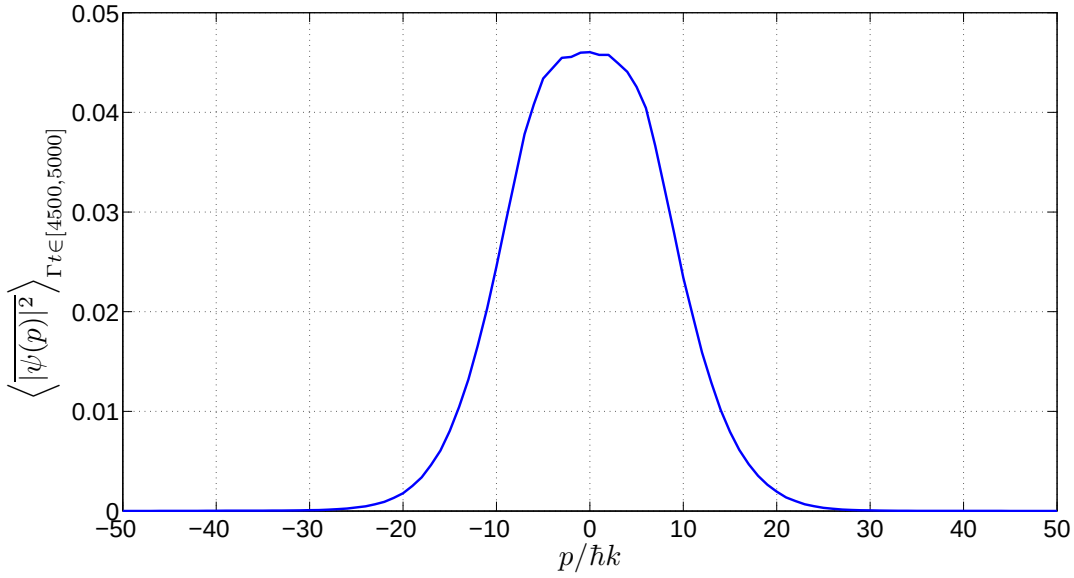

Figure 5.4: Steady state momentum distribution in the case of a $J_g = 1/2 \leftrightarrow J_e = 3/2$ transition driven by a σ^+-polarised 1D standing wave. The average has been taken over 1000 trajectories and over time in the range $\Gamma t \in [4500, 5000]$. Simulation parameters are : $\delta = -\Gamma/2$, $\Omega = \Gamma$, $\Gamma t_f = 5000$, $n_{\max} = 50$, $\Gamma \delta t = 0.0005$ and $|\psi(0)\rangle = |e, p = 40\hbar k\rangle$.

Such a picture shows that the momentum distribution is bell-shaped. From the width of that curve, one can compute the temperature of the cooled gas. The temperature is related to the root mean square value of the momentum

$$p_{\text{rms}} = \Delta p = \sqrt{\overline{\langle\psi|\hat{p}^2|\psi\rangle} - \overline{\langle\psi|\hat{p}|\psi\rangle}^2}$$

via the classical formula

$$T = \frac{p_{\text{rms}}^2}{k_B m}.$$

We have used this formula to obtain the curve plotted in Figure 5.5, where T_D is the Doppler temperature given by Eq. (1.12).

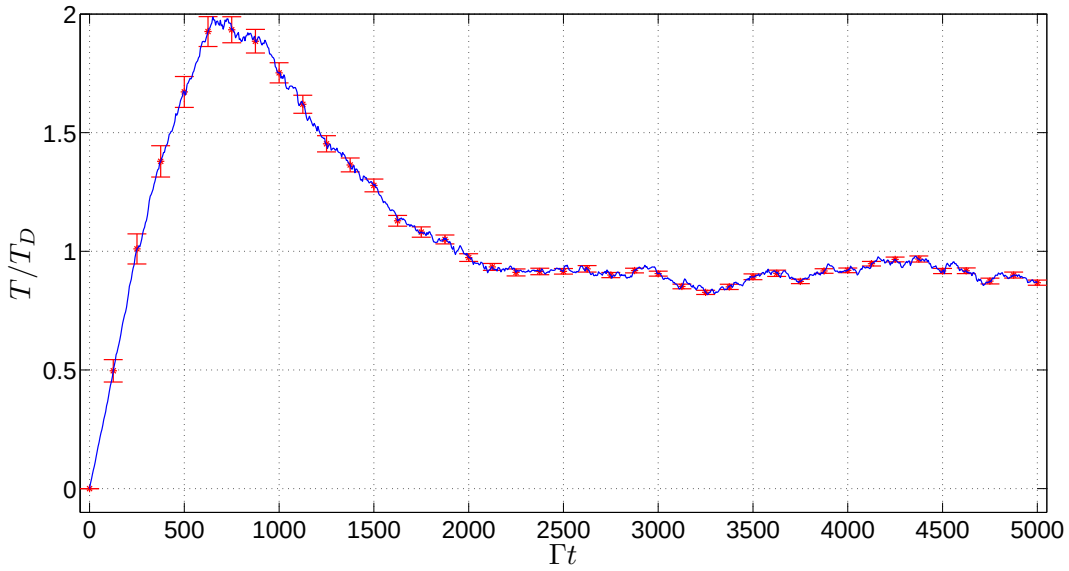

Figure 5.5: Time evolution of the temperature ratio T/T_D with T_D the Doppler temperature in the case of a $J_g = 1/2 \leftrightarrow J_e = 3/2$ transition driven by a σ^+-polarised 1D standing wave. The average has been taken over 1000 trajectories, error bars showing the statistical error. Simulation parameters are : $\delta = -\Gamma/2$, $\Omega = \Gamma$, $\Gamma t_f = 5000$, $n_{\max} = 50$, $\Gamma\delta t = 0.0005$ and $|\psi(0)\rangle = |e, p = 40\hbar k\rangle$.

The temperature starts at $T = 0$ K because the initial state is a momentum eigenstate and the momentum distribution has zero width. The wavepacket needs time to spread and the temperature to increase before gradually decreasing until it reaches the steady state where it is of the same order of magnitude as the Doppler temperature.

Cooling of atoms

In order to demonstrate cooling of atoms, we now choose the initial state as a Gaussian distribution over the momentum eigenstates

$$|\psi(0)\rangle = \sum_{n=-n_{\max}}^{n_{\max}} f_n \, |J_e, m_e = 3/2, p = n\hbar k\rangle \,, \tag{5.4}$$

with f_n a weigthing coefficient whose distribution law is gaussian,

$$f_n = \frac{1}{\sigma\sqrt{2\pi}} e^{\dfrac{-(n\hbar k + p_0)^2}{2\sigma^2}} .$$

In the following, we take $p_0 = 0$ and $\sigma = 15\hbar k$. We show, in Figure 5.6, the results for $p_{\mathrm{rms}}(t)$.

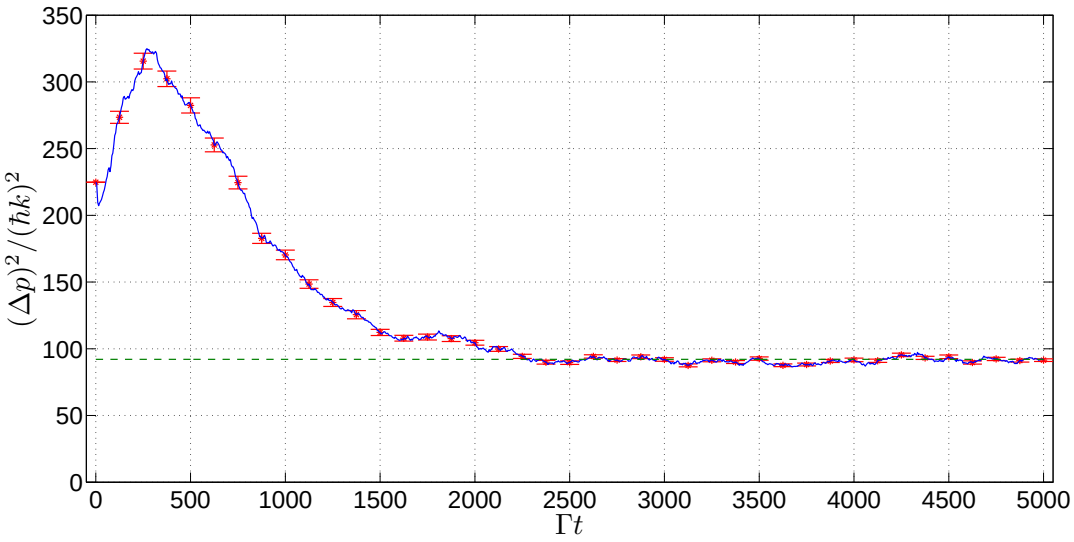

Figure 5.6: Time evolution of $(\Delta p)^2$ in the case of a $J_g = 1/2 \leftrightarrow J_e = 3/2$ transition driven by a σ^+-polarised 1D standing wave, averaged over 1000 trajectories. Error bars show the statistical error. Simulation parameters are : $\delta = -\Gamma/2$, $\Omega = \Gamma$, $\Gamma t_f = 5000$, $n_{\max} = 50$, $\Gamma\delta t = 0.0005$ and $|\psi(0)\rangle$ given by Eq. (5.4) with $p_0 = 0$ and $\sigma = 15\hbar k$.

We have seen in Figure 5.1 that the steady state value for $\langle\hat{p}\rangle(t)$ was $\langle\hat{p}\rangle = 0$. Since we start with a gaussian distribution over the momentum eigenstates with mean $p_0 = 0$ and standard deviation $\sigma = 15\hbar k$, it is expected that $\langle\hat{p}\rangle$ does not display large variations but only fluctuations around the steady state, which has been emphasised in Figure 5.2. However, the standard deviation of the momentum distribution is expected to decrease until it reaches a steady state value to prove cooling. Once again, the momentum distribution displays a standard deviation $\sigma \approx 9.7\hbar k$ in steady state, which clearly demonstrates the cooling.

In Figure 5.7, we plot the results for the momentum distribution at the initial time $t = 0$ and final time $t = 5000\Gamma^{-1}$.

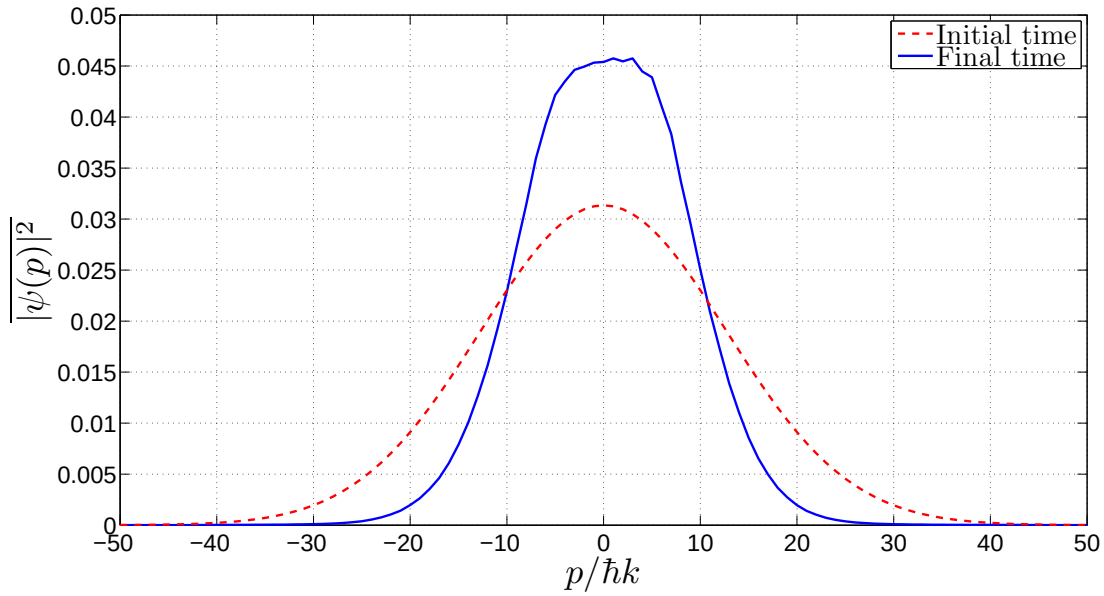

Figure 5.7: Steady state momentum distribution in the case of a $J_g = 1/2 \leftrightarrow J_e = 3/2$ transition driven by a σ^+-polarised 1D standing wave. The average has been made over 1000 trajectories and over time in the range $\Gamma t \in [4500, 5000]$. Simulation parameters are : $\delta = -\Gamma/2$, $\Omega = \Gamma$, $\Gamma t_f = 5000$, $n_{\max} = 50$, $\Gamma \delta t = 0.0005$ and $|\psi(0)\rangle$ given by Eq. (5.4) with $p_0 = 0$ and $\sigma = 15\hbar k$.

In this case, the centre of the wavepacket in the momentum representation has not moved but the standard deviation of the wavepacket has decreased and the final distribution is thiner than the initial one. Once again, the momentum distribution displays a bell-shape.

The related temperature is displayed in Figure 5.8 as a function ot time.

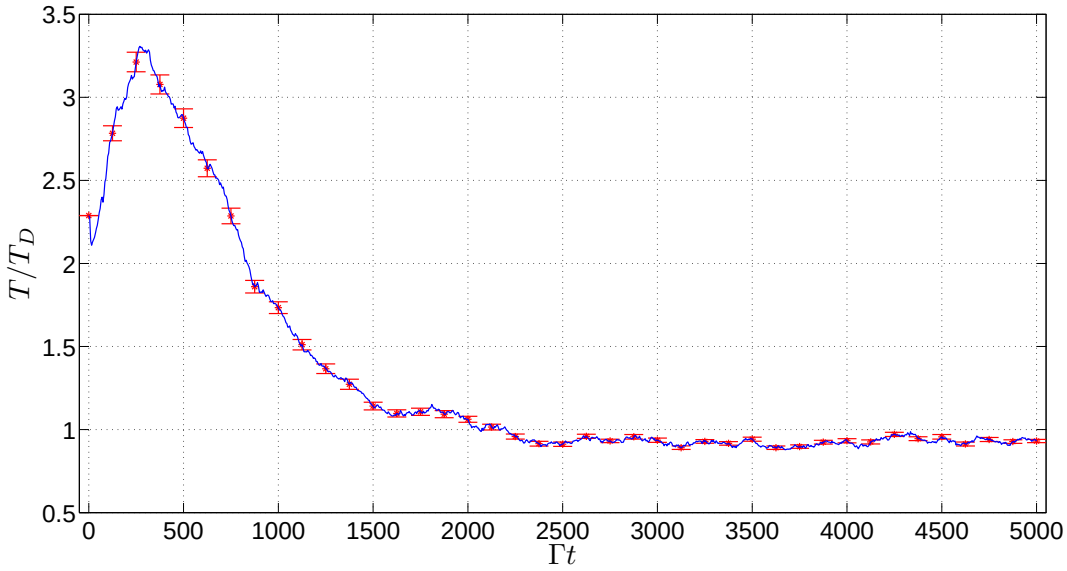

Figure 5.8: Time evolution of the temperature ratio T/T_D with T_D the Doppler temperature in the case of a $J_g = 1/2 \leftrightarrow J_e = 3/2$ transition driven by a σ^+-polarised 1D standing wave. The average has been taken over 1000 trajectories, error bars showing the statistical error. Simulation parameters are : $\delta = -\Gamma/2$, $\Omega = \Gamma$, $\Gamma t_f = 5000$, $n_{\max} = 50$, $\Gamma\delta t = 0.0005$ and $|\psi(0)\rangle$ given by Eq. (5.4) with $p_0 = 0$ and $\sigma = 15\hbar k$.

Once again, there is a transient period before the temperature reaches the steady state where it is close to the Doppler temperature. In Figure 5.9, we show a curve illustrating the steady state temperature averaged over 100 MCWF as a function of the detuning δ and compare it with the theoretical predictions (1.13) [27]

$$k_B T = \frac{\hbar\Gamma}{4}\left(\frac{2|\delta|}{\Gamma} + \frac{\Gamma}{2|\delta|}\right). \tag{5.5}$$

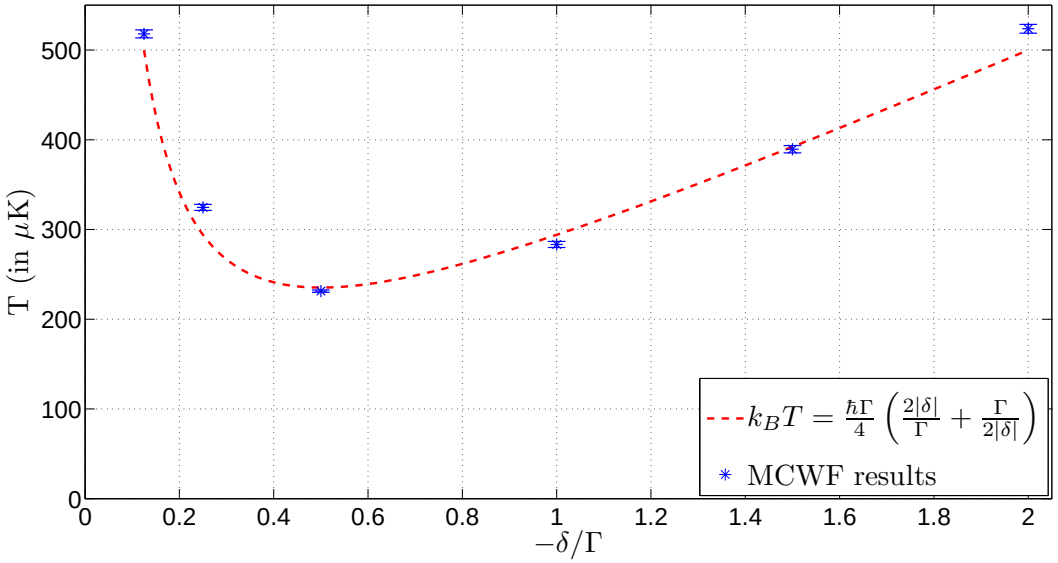

Figure 5.9: Steady state temperature as a function of the detuning δ in the case of a $J_g = 1/2 \leftrightarrow J_e = 3/2$ transition driven by a σ^+-polarised 1D standing wave. Error bars show the statistical error. The temperature is averaged over 100 trajectories and in time over $500\Gamma^{-1}$. Simulation parameters are : $\delta = -\Gamma/2$, $\Omega = \Gamma$, $\Gamma t_f = 5000$, $n_{\max} = 50$, $\Gamma\delta t = 0.0005$ and $|\psi(0)\rangle = |e, p = 0\rangle$.

The results shown in Figure 5.9 are in excellent agreement with Eq. (5.5). The minimal achievable temperature in a σ^+ standing wave is thus, as expected, obtained for $\delta = -\Gamma/2$ and amounts $T \simeq 235$ µK for sodium atoms. When the detuning becomes larger or smaller, the temperature increases and the momentum distribution becomes larger in both cases. In the following section, we analyse the effect of choosing two crossed linear polarisations instead of a σ^+ standing wave. We shall see that this change of laser polarisation leads to a dramatic decrease of the steady state temperature.

5.2 Sisyphus cooling in a lin⊥lin configuration

The lin⊥lin configuration refers to a laser configuration where two counterpropagating lasers of identical intensity have perpendicular linear polarisations. As Nienhuis, de Kloe and van der Straten [86] noticed, an equivalent picture is provided by two standing waves with opposite circular polarisations σ^+ and σ^- that are spatially shifted by a quarter wavelength. Indeed, the field $\mathbf{E}(z,t)$ resulting from the superposition of two counterpropagating laser of crossed polarisations

$$\begin{cases} \mathbf{E}_L(z,t) = E_0 \mathbf{e}_x \left(e^{i(kz-\omega t)} + e^{-i(kz-\omega t)} \right) \\ \mathbf{E}_R(z,t) = E_0 \mathbf{e}_y \left(e^{i(-kz-\omega t-\pi/2)} + e^{-i(-kz-\omega t-\pi/2)} \right) \end{cases},$$

reads

$$\mathbf{E}(z,t) = E_0 \left(\mathbf{e}_x e^{ikz} - i\mathbf{e}_y e^{-ikz} \right) e^{-i\omega t} + \text{c.c.}.$$

Since $e^{\pm ikz} = \cos(kz) \pm i\sin(kz)$, we also have

$$\begin{aligned}\mathbf{E}(z,t) &= E_0\Big[\mathbf{e}_x\big(\cos(kz) + i\sin(kz)\big) - i\mathbf{e}_y\big(\cos(kz) - i\sin(kz)\big)\Big]e^{-i\omega t} + \text{c.c.} \\ &= E_0\Big[\big(\mathbf{e}_x - i\mathbf{e}_y\big)\cos(kz) + i\big(\mathbf{e}_x + i\mathbf{e}_y\big)\sin(kz)\Big]e^{-i\omega t} + \text{c.c.} \\ &= E_0\sqrt{2}\Big(\boldsymbol{\epsilon}_-\cos(kz) + i\boldsymbol{\epsilon}_+\sin(kz)\Big)e^{-i\omega t} + \text{c.c.}.\end{aligned}$$

Applying the treatment described in chapter 4, we find that the Hamiltonian of the system reads

$$\hat{H}_S = \frac{\hat{p}^2}{2m} + \frac{\hbar\Omega}{\sqrt{2}}\Big[\cos(k\hat{z})(\hat{S}^+_{q=+} + \hat{S}^-_{q=+}) + \sin(k\hat{z})(\hat{S}^+_{q=-} + \hat{S}^-_{q=-})\Big] - \hbar\delta\hat{P}_e, \tag{5.6}$$

that is the Hamiltonian used by Nienhuis, de Kloe and van der Straten [86]. In Eq. (5.6), the subscripts appearing in $\hat{S}^+$ and $\hat{S}^-$ indicate the value of q related to the polarisation of each standing wave. In the following, we work in the $\{|J_e, m_e, p\rangle, |J_g, m_g, p\rangle\}$ basis where the quantum number p still accounts for the atomic momentum along the z axis and extends from $-n_{\max}\hbar k$ to $n_{\max}\hbar k$. Quantum numbers $J_{e/g}$ and $m_{e/g}$ still stand for the angular momentum of the excited/ground state and its projection onto the quantisation axis. Then, we apply the MCWF procedure which implies $[(2J_e+1)+(2J_g+1)] \times (2n_{\max}+1)$ basis states, that is $6 \times (2n_{\max}+1)$ basis states for the $J_g = 1/2 \leftrightarrow J_e = 3/2$ transition considered. Compared to Doppler cooling where we have restricted the discussion to only two levels, we have to consider all sublevels for the Sisyphus cooling and we have 3 times more basis states, which is numerically much heavier.

Either the system is evolved under the action of the non-Hermitian Hamiltonian $\hat{H} = \hat{H}_S - (i\hbar\Gamma/2)\hat{P}_e$, or a jump occurs, in which case we have to apply the proper jump operator amongst the nine possible operators (that is, three times more jump operators than for Doppler cooling)

$$\hat{C}_{k',q} = \sqrt{\Gamma\bar{p}_q(k')}e^{-ik'\hat{z}}(\boldsymbol{\epsilon}^*_q \cdot \hat{\mathbf{S}}^-), \tag{5.7}$$

with $k' = 0, \pm k$, $q = 0, \pm$ and $\bar{p}_q(k')$ is given by Eqs. (4.8) and (4.9). Those operators read

$$\hat{C}_{0,+} = \sqrt{\frac{3\Gamma}{5}}(\boldsymbol{\epsilon}^*_+ \cdot \hat{\mathbf{S}}^-), \qquad \hat{C}_{0,0} = \sqrt{\frac{4\Gamma}{5}}(\boldsymbol{\epsilon}^*_0 \cdot \hat{\mathbf{S}}^-), \qquad \hat{C}_{0,-} = \sqrt{\frac{3\Gamma}{5}}(\boldsymbol{\epsilon}^*_- \cdot \hat{\mathbf{S}}^-),$$

$$\hat{C}_{\pm k,+} = \sqrt{\frac{\Gamma}{5}}e^{\mp ik\hat{z}}(\boldsymbol{\epsilon}^*_+ \cdot \hat{\mathbf{S}}^-), \quad \hat{C}_{\pm k,0} = \sqrt{\frac{\Gamma}{10}}e^{\mp ik\hat{z}}(\boldsymbol{\epsilon}^*_0 \cdot \hat{\mathbf{S}}^-), \quad \hat{C}_{\pm k,-} = \sqrt{\frac{\Gamma}{5}}e^{\mp ik\hat{z}}(\boldsymbol{\epsilon}^*_- \cdot \hat{\mathbf{S}}^-).$$

5.2.1 Numerical results

In Figure 5.10, we plot the steady state temperature for different values of both the detuning and the Rabi frequency.

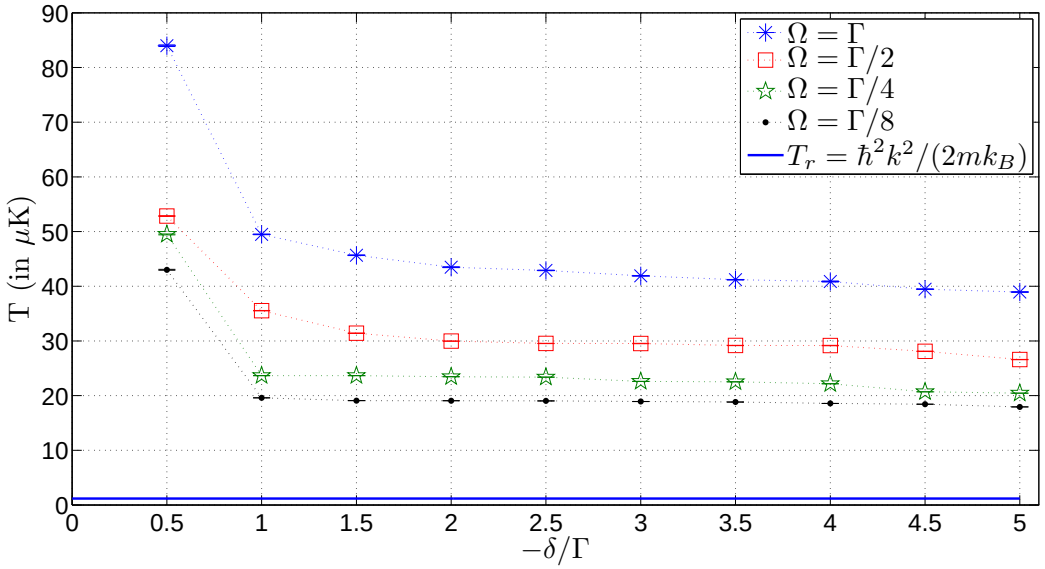

Figure 5.10: Steady state temperature as a function of the detuning δ in the case of a $J_g = 1/2 \leftrightarrow J_e = 3/2$ transition driven by a lin⊥lin laser field. Error bars show the statistical error and are so small that they are systematically within the marker. Each point represents an amount of computation time of approximately 1000 hours if all realisations were run serially. With a cluster accepting $\simeq 30$ jobs at the same time, the computation time is still approximately 30 hours per point. The temperature is averaged over 100 trajectories and in time over $500\Gamma^{-1}$. Simulation parameters are : $\delta = -\Gamma/2$, $\Omega = \Gamma$, $\Gamma t_f = 5000$, $n_{\max} = 25$, $\Gamma\delta t = 0.0005$ and $|\psi(0)\rangle = |J_e, m_e = 3/2, p = 0\rangle$.

Because we have performed 100 trajectories for each point, the related statistical errors are small and contained within the marker size. We observe that the temperature decreases when the intensity of the laser decreases and when the detuning increases. As expected, the Sisyphus cooling mechanism is more efficient at low intensity. We have also plotted the recoil temperature [27] defined as

$$T_r = \frac{\hbar k^2}{2mk_B},$$

which for sodium atoms amounts $T_R \simeq 1\,\mu\text{K}$. The recoil temperature is the temperature corresponding to the kinetic energy kick the spontaneously emitted photon delivers to the atom. We observe that the steady state temperature, even when the detuning is large and the Rabi frequency small, is the recoil temperature multiplied by a rather large numerical factor (comprised between 18 and 84 for the parameters of our simulations).

In Table 5.1, we give the numerical values for the temperatures plotted in Figure 5.10.

δ \ Ω	Γ	$\Gamma/2$	$\Gamma/4$	$\Gamma/8$
$-\Gamma/2$	83.99 ± 1.46	52.83 ± 0.74	49.48 ± 0.63	43.00 ± 0.46
$-\Gamma$	49.49 ± 0.54	35.53 ± 0.26	23.65 ± 0.14	19.59 ± 0.08
$-3\Gamma/2$	45.67 ± 0.47	31.41 ± 0.22	23.65 ± 0.12	19.08 ± 0.06
-2Γ	43.47 ± 0.47	29.96 ± 0.22	23.45 ± 0.11	19.06 ± 0.05
$-5\Gamma/2$	42.90 ± 0.46	29.54 ± 0.21	23.37 ± 0.11	19.03 ± 0.04
-3Γ	41.90 ± 0.43	29.53 ± 0.21	22.60 ± 0.11	18.92 ± 0.04
$-7\Gamma/2$	41.20 ± 0.41	29.17 ± 0.20	22.52 ± 0.10	18.83 ± 0.04
-4Γ	40.86 ± 0.39	29.16 ± 0.19	22.17 ± 0.10	18.57 ± 0.04
$-9\Gamma/2$	39.46 ± 0.38	28.10 ± 0.19	20.70 ± 0.09	18.43 ± 0.04
-5Γ	38.94 ± 0.37	26.59 ± 0.18	20.45 ± 0.07	17.93 ± 0.03

Table 5.1: Steady state temperature (in μK) for sodium atoms in a lin⊥lin laser configuration as a function of δ and Ω with the related statistical error.

When the detuning is small, the steady state temperature is very detuning sensitive. For example, for $\Omega = \Gamma$, we go from $T \simeq 84$ μK when $\delta = -\Gamma/2$ to $T \simeq 49$ μK when $\delta = -\Gamma$. However, when the detuning becomes larger, the steady state temperature seems to saturate and to reach a minimal value.

We also present the same data in log-log scale in Figure 5.11.

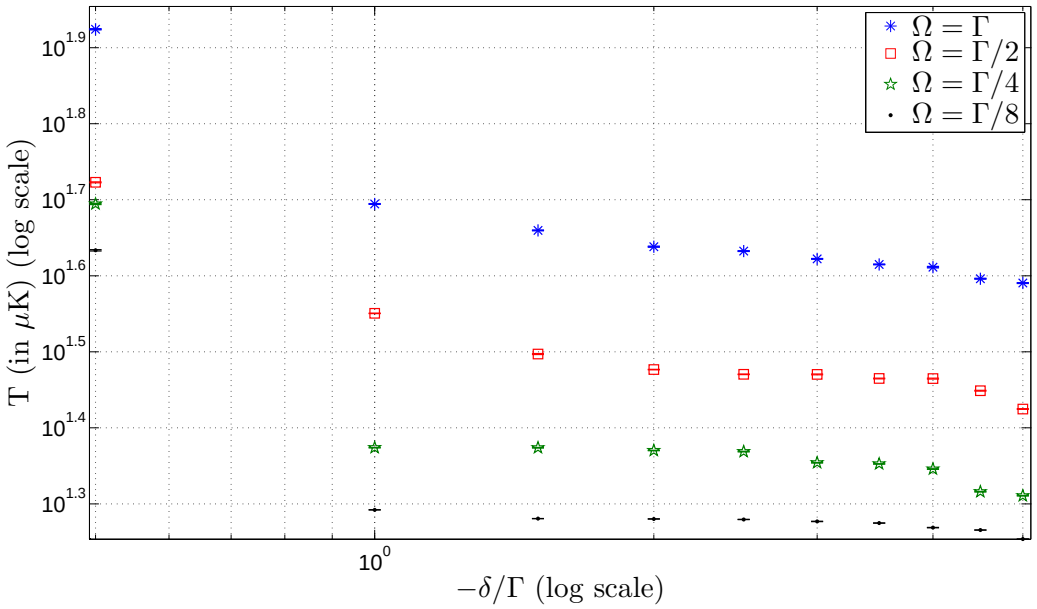

Figure 5.11: Steady state temperature as a function of the detuning δ (log-log scale) in the case of a $J_g = 1/2 \leftrightarrow J_e = 3/2$ transition driven by a lin⊥lin laser field. Error bars show the statistical error and are so small that they are systematically within the marker. The temperature is averaged over 100 trajectories and in time over $500\Gamma^{-1}$. Simulation parameters are : $\delta = -\Gamma/2$, $\Omega = \Gamma$, $\Gamma t_f = 5000$, $n_{\max} = 50$, $\Gamma\delta t = 0.0005$ and $|\psi(0)\rangle = |J_e, m_e = 3/2, p = 0\rangle$.

The steady state temperature is now being compared to theoretical predictions given *e.g.* in [26, 27, 87]

$$T_S \propto \frac{\hbar\Omega^2}{\alpha|\delta|k_B}, \tag{5.8}$$

where α is a multiplicative factor equal to 3 in [26], 4 in [27] and 8 in [87]. We plot those 3 curves in Figure 5.12 for $\Omega = \Gamma/2$ and we compare the theoretical predictions to numerical results.

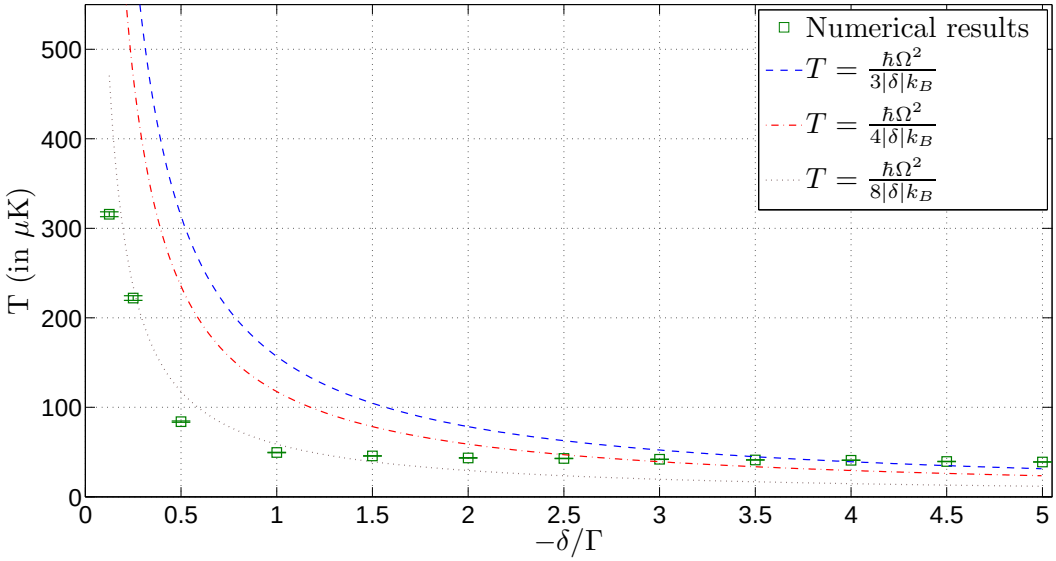

Figure 5.12: Steady state temperature as a function of the detuning δ in the case of a $J_g = 1/2 \leftrightarrow J_e = 3/2$ transition driven by a lin$\perp$lin laser field. Error bars show the statistical error and are so small that they are systematically within the marker. The temperature is averaged over 100 trajectories and in time over $500\Gamma^{-1}$. Simulation parameters are : $\delta = -\Gamma/2$, $\Omega = \Gamma$, $\Gamma t_f = 5000$, $n_{\max} = 50$, $\Gamma\delta t = 0.0005$ and $|\psi(0)\rangle = |J_e, m_e = 3/2, p = 0\rangle$.

Numerical results display the same kind of behaviour as the analytical predictions (5.8) except for the saturation value of the temperature that is higher for the numerical results. Indeed, Eq. (5.8) suggests that arbitrarily small temperatures are obtained for arbitrary large detuning or arbitrary small Rabi frequency. In the limit where the Rabi frequency is zero, which amounts to a zero atom/laser coupling, the steady state temperature would be $T = 0\,\mathrm{K}$. Equation (5.8) is manifestly not suitable for the description of the steady state temperature at very low laser intensity due to departure hypotheses which are no more verified. However, the tendency followed by the numerical results is in a good agreement with Eq. (5.8).

We also present the same data in log-log scale in Figure 5.13.

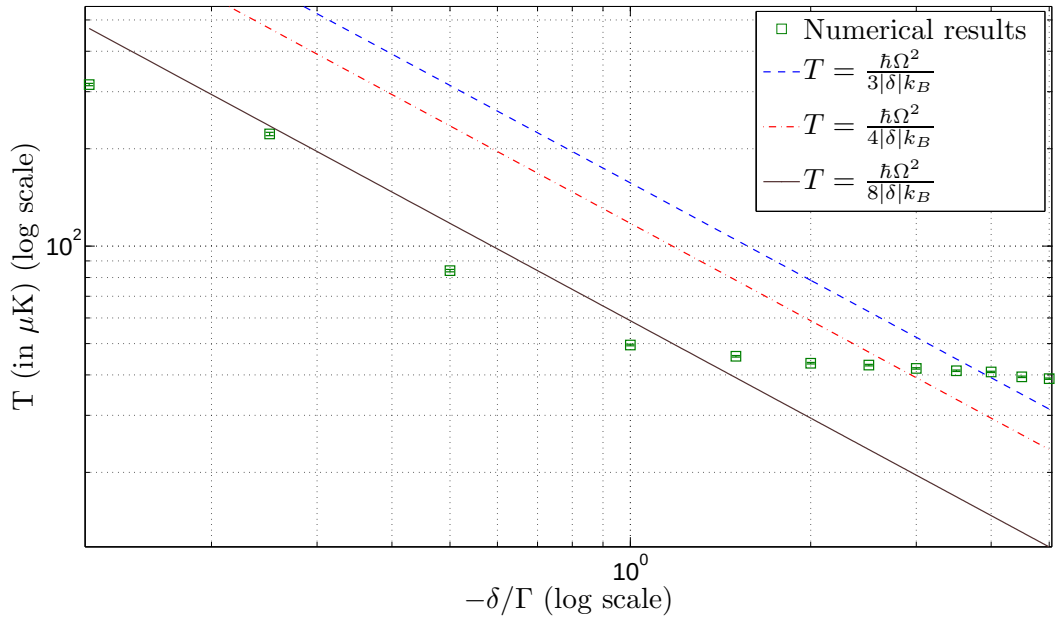

Figure 5.13: Steady state temperature as a function of the detuning δ (log-log scale) in the case of a $J_g = 1/2 \leftrightarrow J_e = 3/2$ transition driven by a lin⊥lin laser field. Error bars show the statistical error and are so small that they are systematically within the marker. The temperature is averaged over 100 trajectories and in time over $500\Gamma^{-1}$. Simulation parameters are : $\delta = -\Gamma/2$, $\Omega = \Gamma$, $\Gamma t_f = 5000$, $n_{\max} = 50$, $\Gamma\delta t = 0.0005$ and $|\psi(0)\rangle = |J_e, m_e = 3/2, p = 0\rangle$.

We observe that the data are best fitted when $\alpha = 8$ in Eq. (5.8) and that our results are in good agreement with the theoretical prediction (5.8) for small detunings. However, for the reasons explained previously, this is no more the case as soon as the detuning becomes large.

In Figure 5.14, we show the momentum distributions corresponding to the highest and lowest temperatures displayed in Figure 5.10 and Table 5.1.

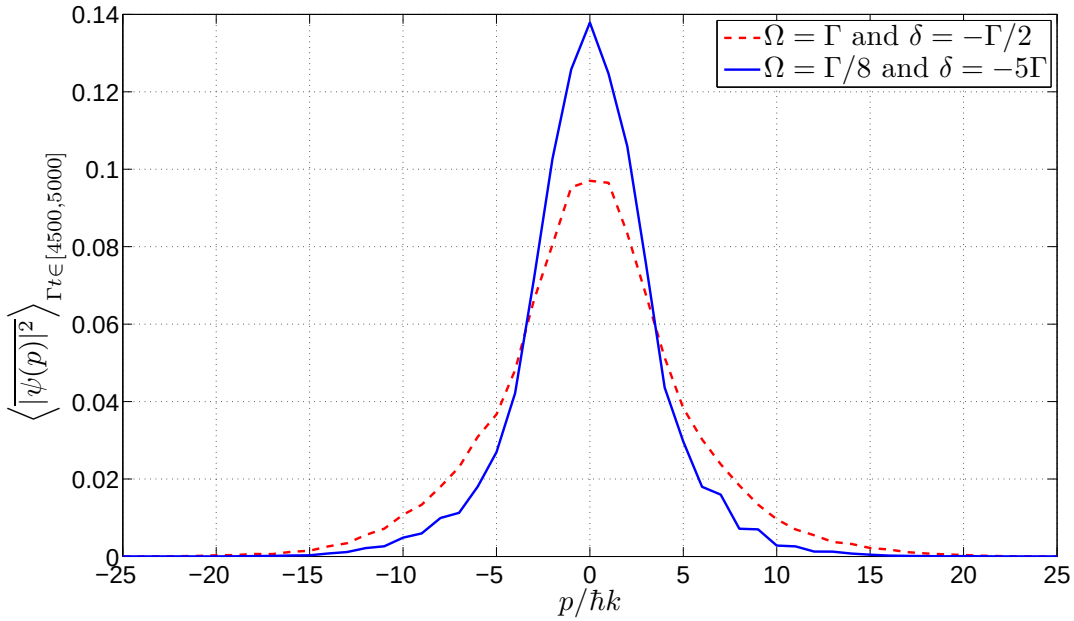

Figure 5.14: Final momentum distributions as a function of the detuning δ in the case of a $J_g = 1/2 \leftrightarrow J_e = 3/2$ transition driven by a lin⊥lin laser field. Results are averaged over 100 trajectories and in time over $500\Gamma^{-1}$. Simulation parameters are : $\delta = -\Gamma/2$ and $\Omega = \Gamma$ for the dashed red curve and $\delta = -5\Gamma$ and $\Omega = \Gamma/8$ for the solid blue curve, and with $\Gamma t_f = 5000$, $n_{\max} = 50$, $\Gamma \delta t = 0.0005$, $|\psi(0)\rangle = |J_e, m_e = 3/2, p = 0\rangle$ for both curves.

The distribution corresponding to $\Omega = \Gamma/8$ and $\delta = -5\Gamma$ is obviously thiner than the one corresponding to $\Omega = \Gamma$ and $\delta = -\Gamma/2$. In the first case, the standard deviation is $\sigma \approx 5.9\hbar k$ whilst in the second case, the standard deviation is $\sigma \approx 2.8\hbar k$. Once again, we can conclude that the Sisyphus cooling is more efficient at low laser intensity.

5.3 Comparison between Doppler and Sisyphus cooling results

In this subsection, we compare the results obtained for both cooling schemes treated in this master thesis. We begin by displaying in Figure 5.15 the steady state momentum distributions for a σ^+ standing wave configuration with $\Omega = \Gamma$ and $\delta = -\Gamma/2$ (blue solid curve) and to a lin⊥lin configuration with $\Omega = \Gamma/16$ and $\delta = -5\Gamma$ (green dashed curve).

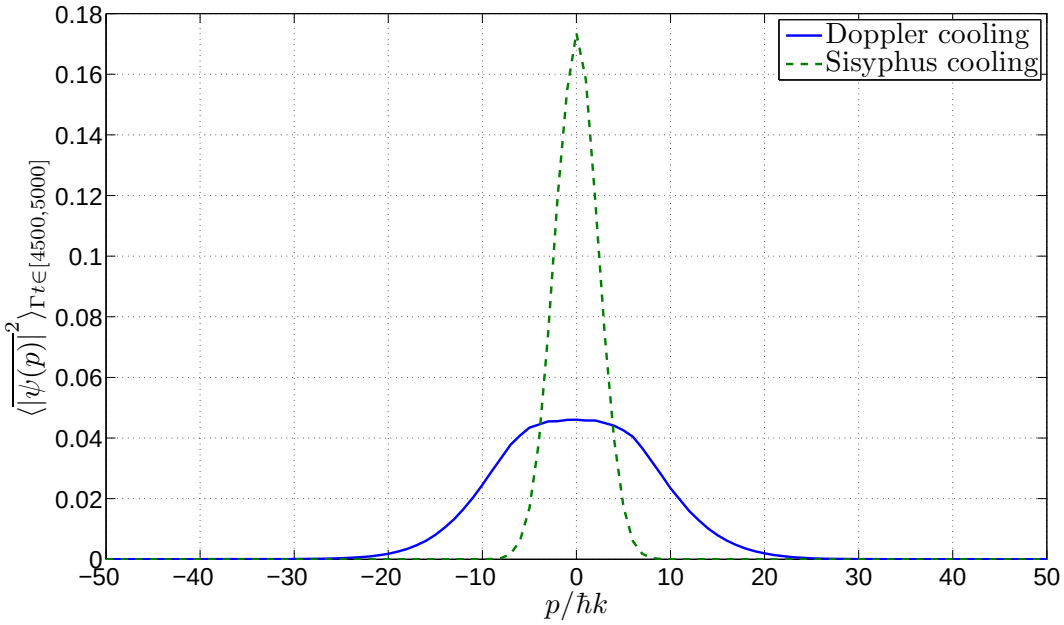

Figure 5.15: Final momentum distributions averaged over 100 trajectories and in time over $500\Gamma^{-1}$ in the case of a $J_g = 1/2 \leftrightarrow J_e = 3/2$ transition driven by a σ^+ standing wave (blue solid curve) and by a lin⊥lin laser field (red dashed curve). Simulation parameters are : $n_{\max} = 50$, $\delta = -\Gamma/2$ and $\Omega = \Gamma$ for the solid blue curve and $n_{\max} = 20$, $\delta = -5\Gamma$ and $\Omega = \Gamma/16$ for the green dashed curve, and with $\Gamma t_f = 5000$, $\Gamma\delta t = 0.0005$, $|\psi(0)\rangle = |J_e, m_e = 3/2, p = 0\rangle$ for both curves.

Whereas the distribution has a standard deviation is $\sigma \approx 9.7\hbar k$ in the σ^+ standing wave, we see that the momentum distribution has a standard deviation much smaller $\sigma \approx 2.6\hbar k$ in the lin⊥lin configuration, indicating that smaller temperatures are reached.

The temperature separation due to the change of laser configuration clearly indicates that the Doppler cooling theory fails at predicting temperatures produced in some schemes. For example, in Figure 5.16, we plot the steady state temperature both for the σ^+ standing wave and for the lin⊥lin configuration as a function of the detuning.

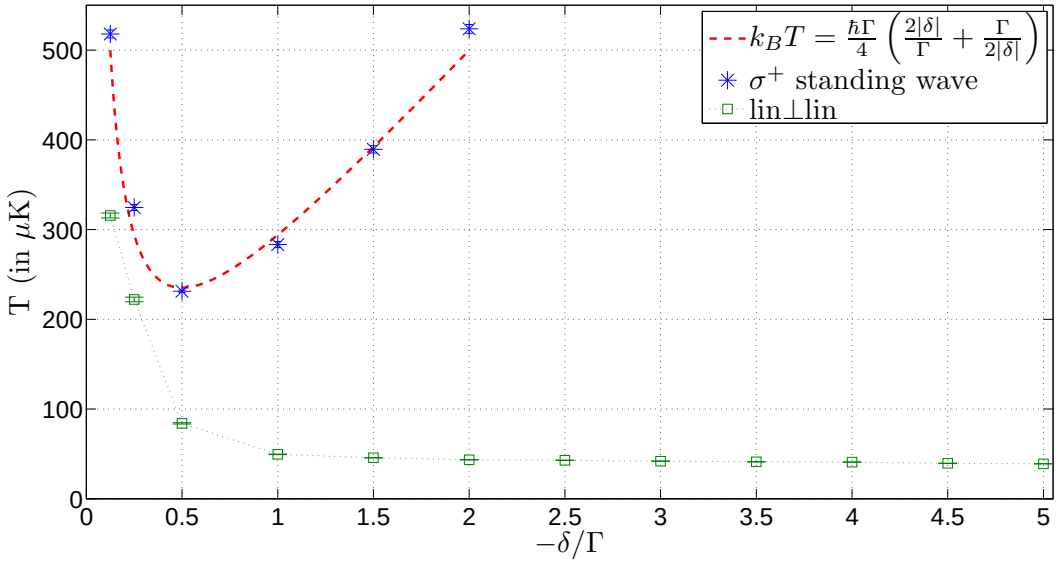

Figure 5.16: Steady state temperatures as a function of the detuning δ, for $\Omega = \Gamma$. Results are averaged over 100 trajectories and over $500\Gamma^{-1}$ both for the σ^+ standing wave and the lin⊥lin configuration. The temperature separation is clearly due to the gradient of polarisation produced by the lin⊥lin configuration. Error bars are contained within markers for the Sisyphus cooling whilst they are a little larger for Doppler cooling.

Figure 5.16 clearly illustrates the difference of regime in which Doppler and Sisyphus cooling act. Those results are in excellent agreement with theoretical predictions Eq. (5.5) for Doppler cooling and follow the same tendency for Sisyphus cooling as Eq. (5.8). For the latter, results predicted by semiclassical theories are often referred to as magnitude scale in the literature because the underlying hypotheses are often not verified. For such cases, MCWF method appears as a good alternative to semiclassical theories or to the full integration of the master equation.

The goal we had in mind was to compare the curves in Figure 5.16 with the experimental data of Phillips *et al.* [88].

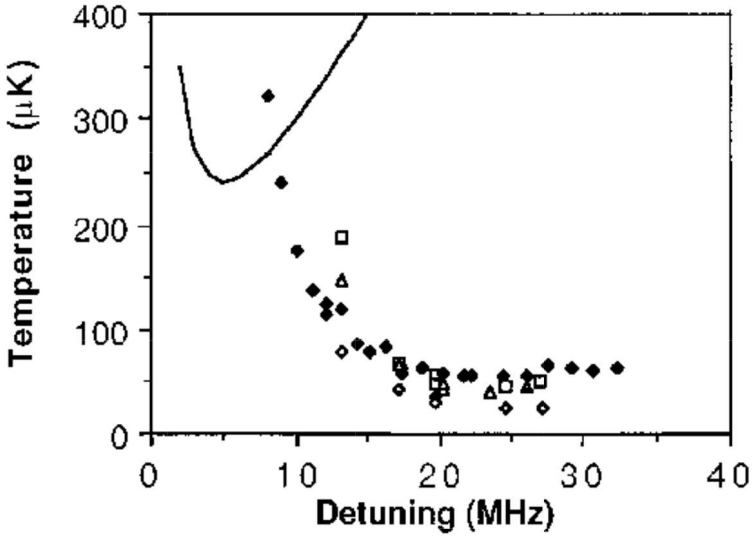

Figure 5.17: Temperature measurements in an optical molasse by Phillips *et al.* in 1988 [88].

We conclude that our numerical results display the same behaviour as those observed by Phillips *et al.* [88].

5.4 Comparison between the classical and the quantum treatment of the atomic motion

In the following, we apply the semiclassical treatment described in chapter 4 which considers that atomic position and momentum are classical variables of time. Due to optical pumping occurring in a σ^+ standing wave, only the levels $|J_e = 3/2, 3/2\rangle \equiv |e\rangle$ and $|J_g = 1/2, 1/2\rangle \equiv |g\rangle$ play a role in the system dynamics. The system Hamiltonian for an atom interacting with a σ^+ standing laser wave is obtained from Eq. (5.1) and reads

$$\begin{aligned}\hat{H}_S &= \hbar\Omega\cos(kz)\left(\hat{S}^+ + \hat{S}^-\right) - \hbar\delta\hat{P}_e \\ &= \frac{\hbar\Omega}{2}\left[e^{ikz}\left(\hat{S}^+ + \hat{S}^-\right) + e^{-ikz}\left(\hat{S}^+ + \hat{S}^-\right)\right] - \hbar\delta\hat{P}_e,\end{aligned}$$

where the exponentials are no more translation operators but phase factors that reflect the position dependence of the laser wave and where the kinetic energy operator has disappeared. When no quantum jump occurs, the system internal states are evolved by the action of $\hat{H} = \hat{H}_S - (i\hbar\Gamma/2)\hat{P}_e$ during a time step δt and the external variables follow the classical equations (valid for small δt)

$$z(t+\delta t) = z(t) + \frac{p_z(t)}{m}\delta t + \mathcal{O}(\delta t^2) \tag{5.9}$$

$$p_z(t+\delta t) = p_z(t) + F(t)\delta t + \mathcal{O}(\delta t^2), \tag{5.10}$$

with

$$F(t) = -\left\langle \psi(t) \left| \frac{\partial \hat{H}}{\partial z} \right| \psi(t) \right\rangle$$

the damping force experienced by the atom due to the optical molasse. When a quantum jump occurs, the internal wavefunction is projected onto the ground state in which case the classical momentum is modified according to

$$p_z(t + \delta t) = p_z(t) + \hbar k'$$

and the classical position is modified according to the prescription of Eq. (5.9). The quantum jump operators read

$$\hat{C}_0 = \sqrt{\frac{3\Gamma}{5}} |g\rangle \langle e| , \qquad \hat{C}_{\pm k} = \sqrt{\frac{\Gamma}{5}} |g\rangle \langle e|$$

and the atomic momentum is subsequentely modified by an amount $\mp\hbar k$ for $\hat{C}_{\pm k}$ and is left unchanged for $\hat{C}_0$.

We had in mind to compare the curve depicted in Figure 5.9 with results obtained by applying the previous prescription, which is presented in Figure 5.18.

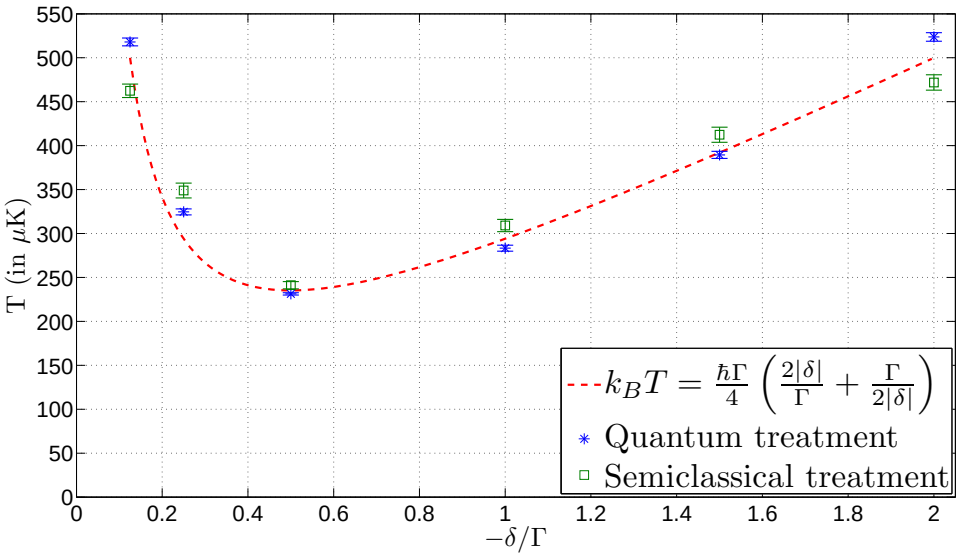

Figure 5.18: Comparison of the steady state temperature as a function of the detuning δ in the case of a $J_g = 1/2 \leftrightarrow J_e = 3/2$ transition driven by a σ^+-polarised 1D standing wave for a classical and a quantum treatment of the atomic motion. Error bars show the statistical error. The temperature is averaged over 100 trajectories and in time over $500\Gamma^{-1}$. For the quantum treatment, simulation parameters are : $\Gamma t_f = 5000$, $n_{\max} = 50$ and $|\psi(0)\rangle = |e, p = 0\rangle$. For the classical treatment, $\Gamma t_f = 6000$, $z(0) = 0$, $p_z(0) = 0$ and $|\psi(0)\rangle = |e\rangle$. In both cases : $\Omega = \Gamma$ and $\Gamma\delta t = 0.0005$.

We observe that apart from the fluctuations due to the finite number of trajectories, the data depicted in Figure 5.18 for the semiclassical approach and the full quantum approach

are very close together and in rather good agreement with the analytical prediction. We also show in Figure 5.19 a histogram of the final classical momentum averaged over time. Contrarily to the quantum treatment where one can associate a momentum distribution to each trajectory, in the semiclassical approach, the momentum is described by a single value instead of a distribution. However, momenta resulting from each trajectory at final time form a distribution which is presented as a histogram. Those histograms are averaged over $1000/\Gamma$ in time after the steady state is reached for more accuracy. In Figure 5.19, we plot the momentum distribution related to the lowest temperature displayed in Figure 5.18, that is when $\delta = -\Gamma/2$.

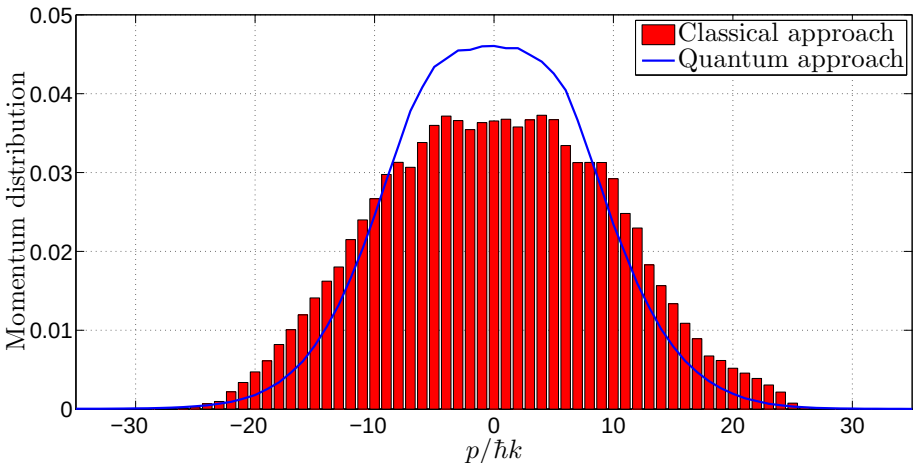

Figure 5.19: Histogram representing the steady state classical momentum distribution in the case of a $J_g = 1/2 \leftrightarrow J_e = 3/2$ transition driven by a σ^+-polarised 1D standing wave averaged over time in the range $\Gamma t \in [5000, 6000]$. Simulation parameters are : $\delta = -\Gamma/2$, $\Omega = \Gamma$, $\Gamma t_f = 6000$, $\Gamma \delta t = 0.0005$, $z(0) = 0$, $p_z(0) = 0$ and $|\psi(0)\rangle = |e\rangle$.

As in the quantum treatment, the momentum distribution is bell-shaped. However, contrarily to the results related to the quantum approach, the results within a semiclassical treatment are not so smooth. As we already mentioned, this is due to the classical nature of the momentum. This can be enhanced by averaging over more than 100 trajectories. Unfortunately, this also involves a much more important computational cost. Once again, we observe that the semiclassical treatment of the centre-of-motion leads to the same kind of behaviour as the one observed with a full quantum approach. The semiclassical results are in good qualitative agreement with those of Smeets *et al.* [89]. In the model used by Smeets *et al.* [89], based after the work of Hoogerland *et al.* [90], the motion is governed by a Fokker-Planck equation. Finally, we conclude that semiclassical approach works rather well in the case of a σ^+ standing wave.

Conclusion

The purpose of this master thesis was to present an original synthesis of the Monte-Carlo wavefunction (MCWF) method in quantum optics and its application to laser cooling of atoms with a particular focus on Doppler and Sisyphus cooling mechanisms. We introduced the MCWF method which is used to solve master equations describing the dynamics of open quantum systems in quantum optics. This method turns out to be much more efficient than a method based on the full integration of the density matrix. We performed laser cooling simulations in 1D both with a classical and a quantum treatment of the atomic centre-of-mass motion.

In chapter 1, we presented a review about the semiclassical theory of laser cooling in which the centre-of-mass motion is treated classically. This theory explains the slowing and cooling in terms of a damping force exerted by the optical molasse on atoms. We introduced the three systems in interaction : an atom which is coupled both to a laser field which we treat classically and to the quantised electromagnetic field. The laser/atom system evolves unitarily and coherently whilst the coupling with the quantised field is responsible for damping (spontaneous emission) and decoherence. We finally introduced the Doppler and Sisyphus cooling theories and presented the underlying limits of such mechanisms.

In chapter 2, we detailed the density operator formalism suitable for treating open quantum systems. Indeed, systems exhibiting decoherence cannot be treated as closed systems whose dynamics is governed by Schrödinger's equation. We introduced master equations whose purpose is to describe the evolution of the reduced density operator $\hat{\rho}_S$ and we also presented the underlying hypotheses of derivation. We finally introduced the Lindblad equation which is a generic form every superoperator considered in a master equation must subscribe to in order for that master equation to preserve the properties of $\hat{\rho}_S$ as a density operator.

In chapter 3, we introduced the MCWF method which we have used to solve master equations. We detailed thoroughly the principle of the method. The method consists in evolving a wavefunction in time with two possible types of evolution at each time step. Either the wavefunction is evolved through a non-Hermitian Hamiltonian, or it is evolved through a jump operator that projects the wavefunction on the proper ground substate. We then explained that, as every statistical method, MCWF method has to be repeated over a large number of realisations, each of which represents a possible history for the atom. We also showed the equivalence between the MCWF method averaged over many realisations and the master equation. We illustrated the physical content of the MCWF method through the example of spontaneous emission. We also presented the related numerical results for an atom at rest driven by a laser field.

In chapter 4, we determined the master equations to solve with a quantisation of the atomic centre-of-mass motion. Starting from a continuum of directions of spontaneous emission, we restricted the discussion to a discrete set of possible directions of emission and we derived the related discrete probabilities of emission of a spontaneous photon, which probabilities explicitely appear in the quantum jump operators. We then derived the system Hamiltonian that appears in the non-Hermitian Hamiltonian, which is one the two possible evolutions for the wavefunction at each time step. These derivations are original inasmuch they never appear in the literature.

In chapter 5, we presented our numerical results about laser cooling. We showed our results about Doppler cooling in a σ^+ standing wave which turned out to be in excellent agreement with semiclassical predictions. We then considered the dramatic change caused by a passage from a σ^+ standing wave to the lin$\perp$lin configuration which consists in two crossed linear polarisations resulting from the superposition of σ^+ and σ^- standing waves. Once again, our numerical results turned out to be in very good agreement with those predicted by semiclassical theories, except for large detuning and/or low intensity laser where semiclassical theories fail. For such cases, our method provided a good alternative and predicted temperatures much larger than the recoil temperature. Finally, we considered the classical treatment of the centre-of-mass motion and compared the subsequent results with those obtained with a full quantum approach. In the σ^+ standing wave, the semiclassical treatment we applied allowed one to compute temperatures in reasonable good agreement with the quantum results.

In this master thesis, we have mainly focussed on 1D laser cooling although the MCWF method allows one as well to perform 3D calculations. Its versatility actually makes it a powerful tool for laser cooling simulations, especially in 3D. All derivations and master equations we considered are derived in a general form and can be easily extended to 3D. However, the computation time which is already rather important in the 1D case literally becomes prohibitive in 3D in the scope of a master thesis. It might be interesting to carry out such computations in order to get 3D distributions of momentum and to have a further insight of the underlying physics. The semiclassical treatment of the atomic motion could also be extended to the lin$\perp$lin configuration. Because the viscous force experienced by the atom depends onto the internal state, optical potentials should act through the viscous force. Such a treatment is not expected to be reliable as soon as the de Broglie wavelength $\lambda_{\mathrm{dB}} = h/p$ becomes of the same order as the laser wavelength. Indeed, the atomic wavepacket spreads over more than one optical potential, in which case the atom does not feel the optical potentials as individual potentials. More complicated transitions than the simple $J_g = 1/2 \leftrightarrow J_e = 3/2$ transition we considered should also be envisaged to study cooling of more complicated atomic species. For example, because a thorough literature is still missing, iron is a promising species that could be a good (master) thesis subject. Indeed, experiments are currently ongoing at the cold atom laboratory of Prof. Thierry Bastin at ULg. A generalisation of this work could also be to add a magnetic field which could be at the basis of a magneto optical trap (MOT). For a proper choice of magnetic field configuration, that turns out to be the anti-Helmholtz configuration, it would add a position-dependent force exerted on the atom that would drive it to the centre of the MOT. MCWF method thus also provides a way to compute steady state properties of a cold atom gas trapped in a MOT. However, because the quantisation axis is determined by the magnetic field, the treatment becomes much more complex and is far beyond the scope of this work.

Appendix A

Clebsch-Gordan coefficients

In the particular case of the rotation group $SO(3)$, Clebsch-Gordan coefficients, named after the German mathematicians Alfred Clebsch and Paul Gordan, are sets of numbers related to the coupling of angular momenta. We first present those coefficients in the framework of the general theory of angular momentum without giving any too advanced demonstration. We then explain how those coefficients come into play when one deals with atomic transitions. We also give a table with these coefficients computed and explain how to use this table. In particular, a distinction between coefficients for spontaneous emission and for stimulated processes has to be made and explained. At last, we provide some examples of the use of those coefficients in order to clearly establish the way to use them.

A.1 Clebsch-Gordan coefficients in the angular momentum coupling theory

We consider two angular momenta, $\hat{\mathbf{J}}_1$ and $\hat{\mathbf{J}}_2$ from two distinct systems. We recall the fundamental theorem about eigenvalues and eigenvectors of $\hat{\mathbf{J}}^2$ and $\hat{J}_z$ which are the Hermitian operators associated to the square and to the projection of the total angular momentum $\hat{\mathbf{J}} = \hat{\mathbf{J}}_1 + \hat{\mathbf{J}}_2$ on a quantisation axis that we choose as being $\mathbf{e}_z$.

Fundamental theorem of angular momentum

- The eigenvalues of $\hat{\mathbf{J}}^2$ take the form $J(J+1)\hbar^2$ with j being positive integer or positive half-integer. All possible values for J are not necessarily realised.
- The eigenvalues of $\hat{J}_x, \hat{J}_y, \hat{J}_z$ take the form $m\hbar$ with m integer or half-integer. The quantum number m is called the quantum magnetic number.
- The operators $\hat{\mathbf{J}}^2$ and $\hat{J}_z$ commute and there is a common eigenvectors basis to both operators. We call $\{|J,m\rangle\}$ such a basis

$$\begin{cases} \hat{\mathbf{J}}^2 |J,m\rangle = J(J+1)\hbar^2 |J,m\rangle \\ \hat{J}_z |J,m\rangle = m\hbar |J,m\rangle \end{cases} . \tag{A.1}$$

- For any given J, there are only $2J+1$ values for m for which there are eigenvectors $|J,m\rangle$ that fulfil the relation (A.1), that is : $m = -J, -J+1, \ldots, J-1, J$.

The two angular momentum operators $\hat{\mathbf{j}}_1$ and $\hat{\mathbf{j}}_2$ follow explicitely that fundamental theorem (as any angular momentum operator), which allows one to write (with $i = 1, 2$)

$$\begin{cases} \hat{\mathbf{j}}_i^2 \left|j_i, m_i\right\rangle = j_i(j_i+1)\hbar^2 \left|j_i, m_i\right\rangle \\ \hat{j}_{iz} \left|j_i, m_i\right\rangle = m_i \hbar \left|j_i, m_i\right\rangle \end{cases} .$$

Consequently, those two momentum operators admit the quantum number J_i and also admit $2J_i + 1$ values for the quantum magnetic number : $m_i = -j_i, -j_i + 1, \ldots, j_i - 1, j_i$. Now, we consider the vector sum of those two momenta $\hat{\mathbf{J}} = \hat{\mathbf{j}}_1 + \hat{\mathbf{j}}_2$. The resulting operator $\hat{\mathbf{J}}$ remains an angular momentum operator and must therefore fulfil the fundamental theorem recalled thereinbefore.

Therefore, our goal consists in finding the eigenvalues J and M and eigenvectors $|JM\rangle$ satisfying the fundamental theorem of angular momentum. The solution which can be found *e.g.* in the quantum mechanics book of A. Messiah [91] is given here without any proof and lies in the *fundamental addition theorem*.

Fundamental addition theorem
In the subspace $\mathcal{E}(\alpha, j_1, j_2)$, where α represents the additionnal quantum numbers required to specify the dynamical state completely [91], of dimension $(2j_1 + 1) \times (2j_2 + 1)$ spanned by the vectors $|\alpha, j_1, j_2, m_1, m_2\rangle$ (with only m_1 and m_2 variable, the rest being fixed) :

1. The possible eigenvalues for the quantum orbital number J associated to the total angular momentum operator $\hat{\mathbf{J}}$ are :

$$J = |j_1 - j_2| < |j_1 - j_2| + 1 < \ldots < j_1 + j_2 - 1 < j_1 + j_2.$$

2. To each value of J given hereinbefore corresponds one, and only one, series of $(2J+1)$ eigenvectors $|JM\rangle$ of the total angular momentum operator $\hat{\mathbf{J}}$.

The first of these two assertions have led some authors [91,92] to state that J takes all values such that $j_1 + j_2 + J$ is an integer with j_1, j_2 and J forming the sides of a triangle (see Figure A.1).

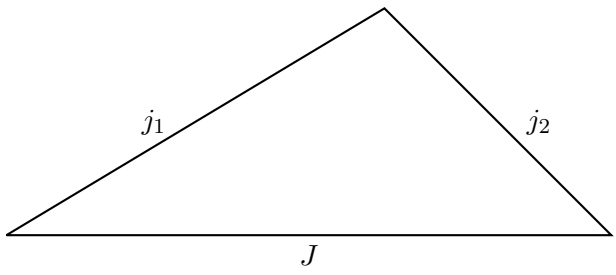

Figure A.1: Triangle rule for the quantum angular momentum numbers j_1, j_2 and J.

Therefore, one can write, for the operators associated to the projection on $\mathbf{e}_z$ and to the square of the resulting momentum operator $\hat{\mathbf{J}}$ that

$$\begin{cases} \hat{\mathbf{J}}^2 \left|J,M\right\rangle = J(J+1)\hbar^2 \left|J,M\right\rangle \\ \hat{J}_z \left|J,M\right\rangle = M\hbar \left|J,M\right\rangle \end{cases},$$

with J taking values satisfying the fundamental addition theorem ($J = |j_1 - j_2|, \ldots, j_1 + j_2$) and M taking $2J+1$ values satisfying the fundamental angular momentum theorem ($M = -J, \ldots, J$). Considering the fact that the Hilbert space $\mathcal{H}$ spanned by the vectors $|JM\rangle$ admits the orthogonal basis $\{|j_1, m_1\rangle \otimes |j_2, m_2\rangle\}$, any state vector $|J, M\rangle$ of $\mathcal{H}$ can be decomposed on that basis

$$|J,M\rangle = \sum_{m_1+m_2=M} C^{j_1 j_2 J}_{m_1 m_2 M} \left|j_1,m_1\right\rangle \otimes \left|j_2,m_2\right\rangle . \tag{A.2}$$

Coefficients[1] $C^{j_1 j_2 J}_{m_1 m_2 M} = \langle j_1, j_2, m_1, m_2 | j_1, j_2, J, M\rangle$ are the so-called Clebsch-Gordan coefficients. Therefore, those coefficients are nothing more than the coefficients of the spectral decomposition of the total angular momentum operator eigenstates on a tensor product basis of momenta that give rise to $\hat{\mathbf{J}}$. The decomposition (A.2) can be inverted in order to produce the tensor product basis of the initial momenta as follows

$$\left|j_1,m_1\right\rangle \otimes \left|j_2,m_2\right\rangle = \sum_J C^{j_1 j_2 J}_{m_1 m_2 M} \left|J,M\right\rangle . \tag{A.3}$$

Remark : in the literature, one often finds the final state marked as $|J, M\rangle$ instead of the full notation $|j_1, j_2, J, M\rangle$.

A.2 Example

Before coming to the introduction of the Clebsch-Gordan coefficients in atomic transitions, we shall give a simple example of expansion of the eigenvectors $|J, M\rangle$ on the tensor product basis of uncoupled momenta $|j_1, m_1\rangle \otimes |j_2, m_2\rangle$. We shall also provide a table in which the coefficients have been computed and explain how to read that table. For the purpose of our example, let us consider that we want to couple the momenta $j_1 = 3/2$ and $j_2 = 1$ in order to produce $|j_1, j_2, J = 1/2, M = 1/2\rangle \equiv |J = 1/2, M = 1/2\rangle$. The possible values for m_1 and m_2 are : $m_1 = -3/2, -1/2, 1/2, 3/2$ and $m_2 = -1, 0, 1$. The spectral decomposition theorem allows one to write

$$\begin{aligned} \left|\frac{3}{2},1,\frac{1}{2},\frac{1}{2}\right\rangle &= \sum_{m_1+m_2=\frac{1}{2}} C^{\frac{3}{2}1\frac{1}{2}}_{m_1 m_2 \frac{1}{2}} \left|\frac{3}{2},m_1\right\rangle \otimes \left|1,m_2\right\rangle \\ &= C^{\frac{3}{2}1\frac{1}{2}}_{-\frac{1}{2}1\frac{1}{2}} \left|\frac{3}{2},-\frac{1}{2}\right\rangle \otimes \left|1,1\right\rangle + C^{\frac{3}{2}1\frac{1}{2}}_{\frac{1}{2}0\frac{1}{2}} \left|\frac{3}{2},\frac{1}{2}\right\rangle \otimes \left|1,0\right\rangle + C^{\frac{3}{2}1\frac{1}{2}}_{\frac{3}{2}-1\frac{1}{2}} \left|\frac{3}{2},\frac{3}{2}\right\rangle \otimes \left|1,-1\right\rangle \\ &= \frac{1}{\sqrt{6}} \left|\frac{3}{2},-\frac{1}{2}\right\rangle \otimes \left|1,1\right\rangle - \frac{1}{\sqrt{3}} \left|\frac{3}{2},\frac{1}{2}\right\rangle \otimes \left|1,0\right\rangle + \frac{1}{\sqrt{2}} \left|\frac{3}{2},\frac{3}{2}\right\rangle \otimes \left|1,-1\right\rangle . \end{aligned}$$

[1] In the litterature, one can find two equivalent and alternative notations for the Clebsch-Gordan coefficients $C^{j_1 j_2 J}_{m_1 m_2 M} = \langle j_1, j_2, m_1, m_2 | j_1, j_2, J, M\rangle$. Those notations are used interchangeably according to the purpose of the problem.

If one wants to invert the decomposition, then for $m_1 = 1/2$ and for $m_2 = 0$, one can write

$$\begin{aligned}\left|\frac{3}{2},\frac{1}{2}\right\rangle \otimes |1,0\rangle &= \sum_{J=1/2}^{5/2} C^{\frac{3}{2}1J}_{\frac{1}{2}0\frac{1}{2}} \left|J, m_1+m_2=\frac{1}{2}\right\rangle \\ &= C^{\frac{3}{2}1\frac{1}{2}}_{\frac{1}{2}0\frac{1}{2}} \left|\frac{1}{2},\frac{1}{2}\right\rangle + C^{\frac{3}{2}1\frac{3}{2}}_{\frac{1}{2}0\frac{1}{2}} \left|\frac{3}{2},\frac{3}{2}\right\rangle + C^{\frac{3}{2}1\frac{5}{2}}_{\frac{1}{2}0\frac{1}{2}} \left|\frac{5}{2},\frac{5}{2}\right\rangle \\ &= -\frac{1}{\sqrt{3}} \left|\frac{1}{2},\frac{1}{2}\right\rangle + \frac{1}{\sqrt{15}} \left|\frac{3}{2},\frac{3}{2}\right\rangle + \sqrt{\frac{3}{5}} \left|\frac{5}{2},\frac{5}{2}\right\rangle .\end{aligned}$$

Now that it has been illustrated through this example how the eigenvectors of the resulting momentum are decomposed on a basis of tensor product of uncoupled momenta, we still have to show how to compute the Clebsch-Gordan coefficients. A formal computation of these coefficients requires the repeated action of the raising and lowering operators on the total angular momentum operator and leads to the so-called Racah recursion formula [92]

$$\begin{aligned}&\sqrt{J(J+1)-M(M\pm 1)}\,\langle j_1, j_2, m_1, m_2 | J, M\pm 1\rangle \\ &\qquad = \sqrt{j_1(j_1+1)-m_1(m_1\mp 1)}\,\langle j_1, j_2, m_1\mp 1, m_2 | J, M\rangle \\ &\qquad\quad + \sqrt{j_2(j_2+1)-m_2(m_2\mp 1)}\,\langle j_1, j_2, m_1, m_2\mp 1 | J, M\rangle .\end{aligned}$$

In this recursion formula, if $M = \pm J$, the left hand side vanishes, in accordance with the fundamental theorem of angular momentum. If we take into account the fact that the sum of the square of all coefficients must be equal to one (in order to ensure the normalisation of the state $|J, \pm J\rangle$), we can compute all coefficients by using that relation. Such a recursive computation has already been done for a long time and is reachable in Table A.1.

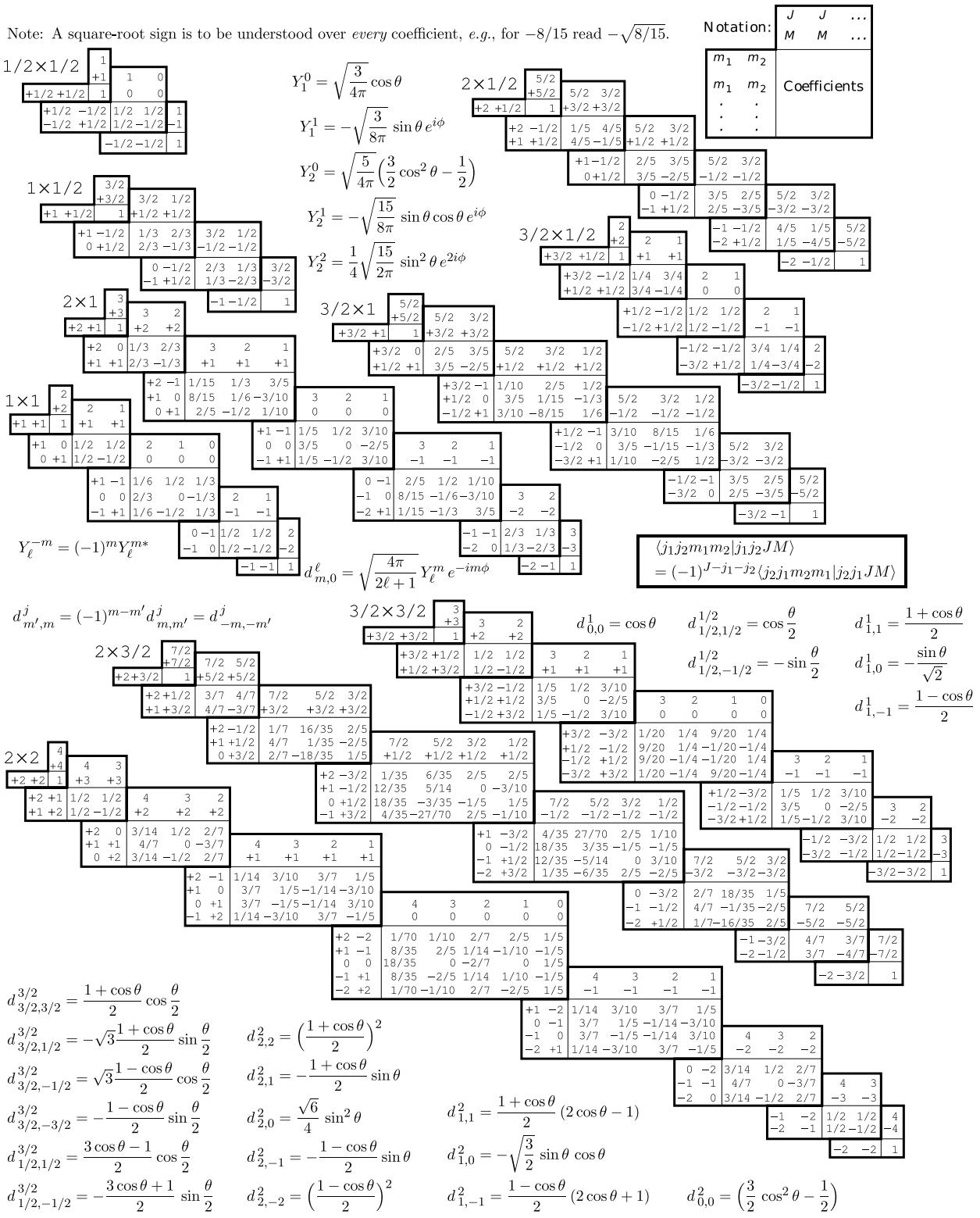

Table A.1: Clebsch-Gordan coefficients table [93]. The sign convention is that of Wigner [94] also sometimes referred to as Condon and Shortley phase convention [95] and has been used by Rose [96] and Cohen [97].

Such a table is simpler to use than it looks but we however explain how to use it through a simple example. For example, consider that we want to couple the momenta $\hat{\mathbf{j}}_1$ and $\hat{\mathbf{j}}_2$ exhibiting the quantum numbers j_1 and j_2 and the quantum magnetic numbers m_1 and m_2 satisfying the conditions mentioned previously. That coupling gives rise to the state $|J, M\rangle$ which can be, as we have seen, expanded onto the $|j_1, m_1\rangle \otimes |j_2, m_2\rangle$ basis. Suppose we want to get one of the coefficient of that expansion, say $C^{\frac{3}{2},\frac{1}{2},2}_{\frac{1}{2},\frac{1}{2},1}$. That example is illustrated on Figure A.2.

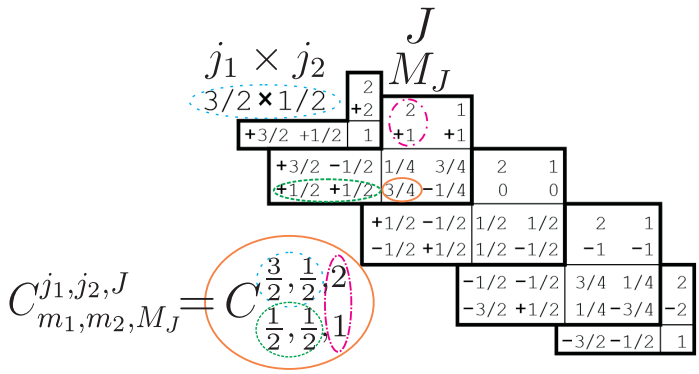

Figure A.2: How to read the Clebsch-Gordan coefficients table through the simple example of $m_1 = m_2 = 1/2, j_1 = 3/2, j_2 = 1/2, J = 2$ and $M = 1$.

First of all, we have to find the proper table amongst all given in Table A.1. That table is given by the product of the two quantum numbers $j_1 \times j_2$ and is indicated in the upper left corner of each table (surrounded in dotted blue in the Table A.2). Then one has to find the column to look at, which is given by the quantum number J and M (surrounded in dot-dashed pink in the Table A.2). At last, one must find the correct line, which is performed by looking at the two quantum numbers m_1 and m_2 (surrounded in dashed green in the Table A.2). Those three informations yield a single number which is (at a sign apart) the square root of the wanted Clebsch-Gordan coefficient. In case a permutation of j_1 and j_2 occurs (i.e. their product is not in the same order as the one in the table), then the coefficient is the following one

$$\langle j_1, j_2, m_1, m_2 | j_1, j_2, J, M\rangle = (-1)^{J-j_1-j_2} \langle j_2, j_1, m_1, m_2 | j_2, j_1, J, M\rangle.$$

In the following, we apply this prescription to compute coefficients appearing in Figure 4.4.

A.2.1 Absorption or stimulated emission of light

Clebsch-Gordan coefficients in case of stimulated process, for example for a $|J, M_J\rangle \to |J', M'_J\rangle$ transition, read $C^{J,1,J'}_{M_J,q,M'_J}$, where J and M_J stands for the angular momentum and its projection onto the quantisation axis of the related ground (resp. excited) substate, J' and M'_J stands for the angular momentum and its projection onto the quantisation axis of the related excited (resp. ground) substate and q for the polarisation of the absorbed photon. For example, if we consider the absorption of σ^--polarised light from $|1/2, 1/2\rangle$ to $|3/2, -1/2\rangle$, we find $J = 1/2$, $M_J = 1/2$, $J' = 3/2$, $M'_J = -1/2$ and $q = -1$. Following the example of Figure A.2,

we find that $C^{1/2,1,3/2}_{1/2,-1,-1/2} = 1/\sqrt{3}$. This procedure is then repeated for all possible absorptions of light. Coefficients are the same for stimulated emission.

A.2.2 Spontaneous emission of light

Because spontaneous and stimulated processes do not have the same nature, the related Clebsch-Gordan coefficients are different. For a $|J', M'_J\rangle \rightarrow |J, M_J\rangle$ transition, they read $C^{J',1,J}_{M'_J,q,M_J}$, where J and M_J stands for the angular momentum and its projection onto the quantisation axis of the related ground substate, J' and M'_J stands for the angular momentum and its projection onto the quantisation axis of the related excited substate and q for the polarisation of the emitted photon, considered from the absorption point of view. For example, if we consider the emission of σ^+-polarised light from $|3/2, 3/2\rangle$ to $|1/2, 1/2\rangle$, we find $J = 1/2$, $M_J = 1/2$, $J' = 3/2$, $M'_J = 3/2$ and $q = -1$ (because it is considered from the absorption point a view, the sign of q is inverted). Following the example of Figure A.2, we find that $C^{3/2,1,1/2}_{3/2,-1,1/2} = 1/\sqrt{2}$. This procedure is then repeated for all possible spontaneous emissions of light. Although the coefficients are not the same as for stimulated processes, their squares are in the same ratio.

A.3 Raising and lowering operators

Thanks to the discussion led hereinbefore, we are now able to compute all Clebsch-Gordan coefficients appearing in the raising and lowering operators defined in Eq. (4.24). The non-vanishing components of the raising operator appearing in Eq. (4.24) read

$$\begin{aligned}\hat{S}^+ = {} & C^{3/2,1,1/2}_{3/2,1,1/2} \left|3/2, 3/2\right\rangle \left\langle 1/2, 1/2\right| \mathcal{E}_+ + C^{3/2,1,1/2}_{1/2,0,1/2} \left|3/2, 1/2\right\rangle \left\langle 1/2, 1/2\right| \mathcal{E}_0 \\ & + C^{3/2,1,1/2}_{1/2,1,-1/2} \left|3/2, 1/2\right\rangle \left\langle 1/2, -1/2\right| \mathcal{E}_+ + C^{3/2,1,1/2}_{-1/2,-1,1/2} \left|3/2, -1/2\right\rangle \left\langle 1/2, 1/2\right| \mathcal{E}_- \\ & + C^{3/2,1,1/2}_{-1/2,0,-1/2} \left|3/2, -1/2\right\rangle \left\langle 1/2, -1/2\right| \mathcal{E}_0 + C^{3/2,1,1/2}_{-3/2,-1,-1/2} \left|3/2, -3/2\right\rangle \left\langle 1/2, -1/2\right| \mathcal{E}_-\end{aligned}$$

Therefore, the system Hamiltonian (4.23) reads

$$\begin{aligned}\hat{H}_S &= \frac{\hat{\mathbf{p}}^2}{2m} + \frac{\hbar\Omega}{2}(e^{i\mathbf{k}\cdot\hat{\mathbf{r}}}\hat{S}^+ + e^{-i\mathbf{k}\cdot\hat{\mathbf{r}}}\hat{S}^-) - \hbar\delta\hat{P}_e \\ &= \frac{\hat{\mathbf{p}}^2}{2m} + \frac{\hbar\Omega}{2}\Bigg[e^{i\mathbf{k}\cdot\hat{\mathbf{r}}}\Bigg(C^{3/2,1,1/2}_{3/2,1,1/2} \left|3/2, 3/2\right\rangle \left\langle 1/2, 1/2\right| \mathcal{E}_+ + C^{3/2,1,1/2}_{1/2,0,1/2} \left|3/2, 1/2\right\rangle \left\langle 1/2, 1/2\right| \mathcal{E}_0 \\ &\quad + C^{3/2,1,1/2}_{1/2,1,-1/2} \left|3/2, 1/2\right\rangle \left\langle 1/2, -1/2\right| \mathcal{E}_+ + C^{3/2,1,1/2}_{-1/2,-1,1/2} \left|3/2, -1/2\right\rangle \left\langle 1/2, 1/2\right| \mathcal{E}_- \\ &\quad + C^{3/2,1,1/2}_{-1/2,0,-1/2} \left|3/2, -1/2\right\rangle \left\langle 1/2, -1/2\right| \mathcal{E}_0 + C^{3/2,1,1/2}_{-3/2,-1,-1/2} \left|3/2, -3/2\right\rangle \left\langle 1/2, -1/2\right| \mathcal{E}_-\Bigg) \\ &\quad + \text{h.c.}\Bigg] - \hbar\delta\hat{P}_e. \end{aligned} \tag{A.4}$$

In the appendix B, we show how such a form is implemented.

Appendix B

Numerical implementation

In this appendix, we explain how to implement the MCWF method numerically using all expressions derived in chapter 4. In the following, we still restrict the discussion to 1D and we stress the points where the generalisation to the 3D case has to be performed. The discussion remains nontechnical and is performed for one laser to avoid unnecessary complications.

As a reminder, we consider a $J_g \leftrightarrow J_e$ atomic transition. To each angular momentum quantum numbers $J_{e/g}$ considered, are associated $2J_{e/g}+1$ Zeeman sublevels labelled by the value of the quantum magnetic number $m_{e/g}$ related to the projection of the angular momentum onto the quantisation axis. This amounts to considering $(2J_e+1)+(2J_g+1)$ internal substates. Because the wavefunction of the system is a tensor product between the internal and external states, $|\psi\rangle = |J_{e/g}, m_{e/g}\rangle \otimes |p\rangle$, one also has to consider the linear momentum of the atom along the z axis, which we denote by p. In Eq. (5.3), we had explained that we restricted the momentum space to a finite set of discrete values separated by $\hbar k$ and extending from $-n_{\max}\hbar k$ to $n_{\max}\hbar k$: we discretise the momentum range over $2n_{\max}+1$ values with a step size $\hbar k$. Therefore, to all of the $(2J_e+1)+(2J_g+1)$ internal substates, are associated $2n_{\max}+1$ values that account for the atomic linear momentum along the axis of motion.

A state is univocally determined by the quantum numbers $J_{e/g}$, $m_{e/g}$ and p : they form a basis denoted by $\{|J_e, m_e, p\rangle, |J_g, m_g, p\rangle\}$ which counts $[(2J_e+1)+(2J_g+1)] \times (2n_{\max}+1)$ basis states. In the following, we restrict the discussion to the transition we considered in this master thesis, that is a $J_g = 1/2 \leftrightarrow J_e = 3/2$ transition. In that case, we work with six internal substates and $2n_{\max}+1$ external momentum eigenstates per internal substate.

B.1 Definition of all suitable quantities in the $\{|J_e, m_e, p\rangle, |J_g, m_g, p\rangle\}$ basis

When the basis is chosen, all quantities must be expressed within that basis and all future calculations reduce to matrix calculations.

Wavefunction

The wavefunction $|J_{e/g}, m_{e/g}, p\rangle = |J_{e/g}, m_{e/g}\rangle \otimes |p\rangle$ consists in six blocks, each of $2n_{\max}+1$ values that represent the momentum related to each internal substate and reads

$$|\psi(t)\rangle \mapsto \begin{pmatrix} \begin{pmatrix} n_{\max}\hbar k \\ (n_{\max}-1)\hbar k \\ \vdots \\ (-n_{\max}+1)\hbar k \\ -n_{\max}\hbar k \end{pmatrix} \\ \vdots \\ \begin{pmatrix} n_{\max}\hbar k \\ (n_{\max}-1)\hbar k \\ \vdots \\ (-n_{\max}+1)\hbar k \\ -n_{\max}\hbar k \end{pmatrix} \end{pmatrix} \begin{matrix} \left.\vphantom{\begin{pmatrix} a \\ b \\ c \\ d \\ e \end{pmatrix}}\right\} J_e = \frac{3}{2}, m_e = \frac{3}{2} \\ \\ \left.\vphantom{\begin{pmatrix} a \\ b \\ c \\ d \\ e \end{pmatrix}}\right\} J_g = \frac{1}{2}, m_g = -\frac{1}{2} \end{matrix} \tag{B.1}$$

that is a block structure beginning by $|J_e = 3/2, m_e = 3/2\rangle$ and ending by $|J_g = 1/2, m_g = -1/2\rangle$, each of which with all possible values for p.

System and non-Hermitian Hamiltonians

As a reminder, the system Hamiltonian given in Eq. (4.25) particularised to 1D and with momentum discretised as in Eq. (5.3) reads

$$\begin{aligned} \hat{H}_S = \frac{\hat{p}^2}{2m} + \frac{\hbar\Omega}{2} \Bigg[\sum_{n=-n_{\max}}^{n_{\max}} \sum_{m_e=-J_e}^{J_e} \sum_{m_g=-J_g}^{J_g} \Big(& \Xi_{m_e m_g} |J_e, m_e, n\hbar k\rangle \langle J_g, m_g, n\hbar k - \hbar k| \\ & + \Xi^*_{m_e m_g} |J_g, m_g, n\hbar k\rangle \langle J_e, m_e, n\hbar k + \hbar k| \Big) \Bigg] - \hbar\delta \hat{P}_e \\ = \frac{\hat{p}^2}{2m} + \frac{\hbar\Omega}{2}(\hat{\mathcal{S}}^+ + \hat{\mathcal{S}}^-) - \hbar\delta \hat{P}_e. & \end{aligned}$$

Such a form gives rise to a block matrix constituted of submatrices for each transition between substates, as it clearly arises from (A.4). The term $\hbar\delta\hat{P}_e$ simply consists in a diagonal term appearing for each block related to excited substates. The kinetic energy is discretised over the momentum space and consists in diagonal terms for each diagonal block, starting from $p = n_{\max}\hbar k$ for the first diagonal term and going to $p = -n_{\max}\hbar k$ for the last diagonal term, with step $\hbar k$. Finally, the atom/laser coupling parts consist in off diagonal blocks coupling two substates. Those blocks are labelled by the quantum numbers identifying internal substates in play, as Figure B.1 illustrates. This figure displays the matrix form of the system Hamiltonian in the case of an atom interacting with a copropagating laser. The translation operators involved in the coupling are such that each non-diagonal block has only non-zero terms either on the first secondary diagonal (if $p \to p + \hbar k$) or on the second secondary diagonal (if $p \to p - \hbar k$) or finally on the main diagonal (if $p \to p$). Each block is therefore made of 1

or 0 that should be multiplied by the proper Clebsch-Gordan coefficient coupling the related substates, by the Rabi frequency (that could possibly be zero for certain laser polarisations) and by $\hbar/2$. The non-Hermitian Hamiltonian is obtained by subtracting $i\hbar\Gamma/2$ to diagonal terms of the submatrices related to excited state sublevels.

Quantum jump operators

As a reminder, quantum jump operators are defined according to (5.7)

$$\hat{C}_{k',q} = \sqrt{\Gamma \bar{p}_q(k')} e^{-ik'\hat{z}} (\boldsymbol{\epsilon}_q^* \cdot \hat{\mathbf{S}}^-),$$

with $k' = 0, \pm k$, $q = 0, \pm$ and $\bar{p}_q(k')$ defined in Eqs. (4.8) and (4.9). Once again, quantum jump operators explicitely involve translation operators whose action is the same as for the atom/laser coupling part, that is either shifting non-zero terms from the main diagonal to one of the two secondary diagonal or possibly leaving them unchanged. For the rest, by contrast with the atom/laser coupling matrix where submatrices related to all possible transitions between sublevels have non-zero terms, only the block related to the quantum jump which has occurred contains non-zero terms. Those terms are given by the proper Clebsch-Gordan coefficient multiplied by the numerical prefactor $\sqrt{\Gamma \bar{p}_q(k')}$. In Figure B.2, we also give the matrix form of the first operator, that is

$$\hat{C}_{-k,+} = \sqrt{\frac{3\Gamma}{5}} e^{ik\hat{z}} (\boldsymbol{\epsilon}_q^* \cdot \hat{\mathbf{S}}^-).$$

Once all suitable quantities are expressed under matrix form, all subsequent computations are matrix calculations.

B.2 Computational cost

Due to the size of the matrices involved in the computations, that is for $J_e = 3/2$, $J_g = 1/2$ and $n_{\max} = 50$ a total number of elements $606^2 = 367236$ and to the number of matrix products at each time step, computations are quite expensive. At each time step, a matrix product is performed for the system evolution (either the wavevector is evolved by the action of $\hat{H}$ or by a quantum jump operator). At time steps where where the expectation value of physical observables is computed, there are as many additional matrix products as there are physical observables we want to know the expectation value. Therefore, because of the huge amount of matrix products, even a single trajectory requires at least 25 hours of calculation.

Even when we restricted the momentum range discretisation to $n_{\max} = 25$ for Sisyphus cooling related calculations, because we did not expect the wavepacket to overcome such values, a single trajectory still requires at least 10 hours of calculation. Because we systematically performed 100 trajectories, the computational time increases to 1000 hours per simulation. Thanks to the "Consortium des Équipements de Calcul Intensif" (`http://www.ceci-hpc.be/`), we were able to launch several trajectories at the same time (from 10 to 50, depending on the cluster load) which drastically reduced the computational time requested by the MCWF method.

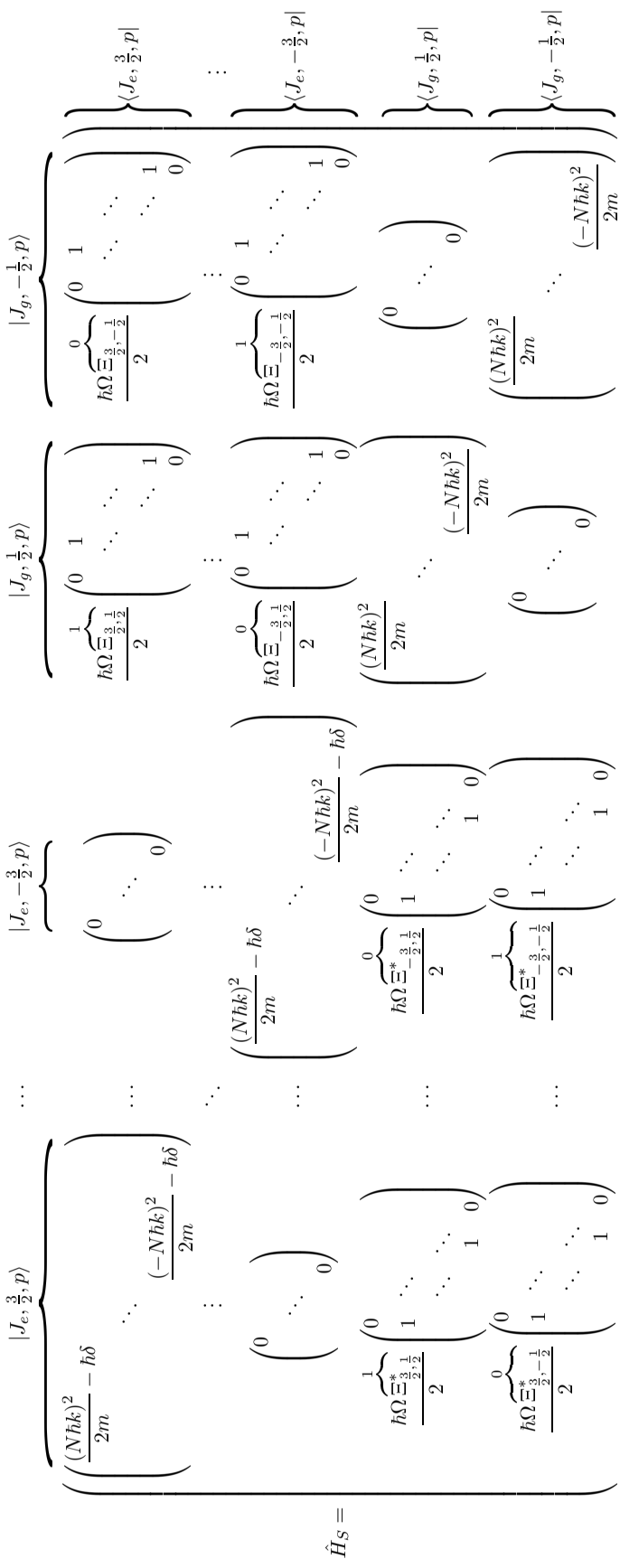

Figure B.1: Matrix form of the system Hamiltonian $\hat{H}_S$ for $J_e = 3/2$ and $J_g = 1/2$, with $N \equiv n_{\max}$.

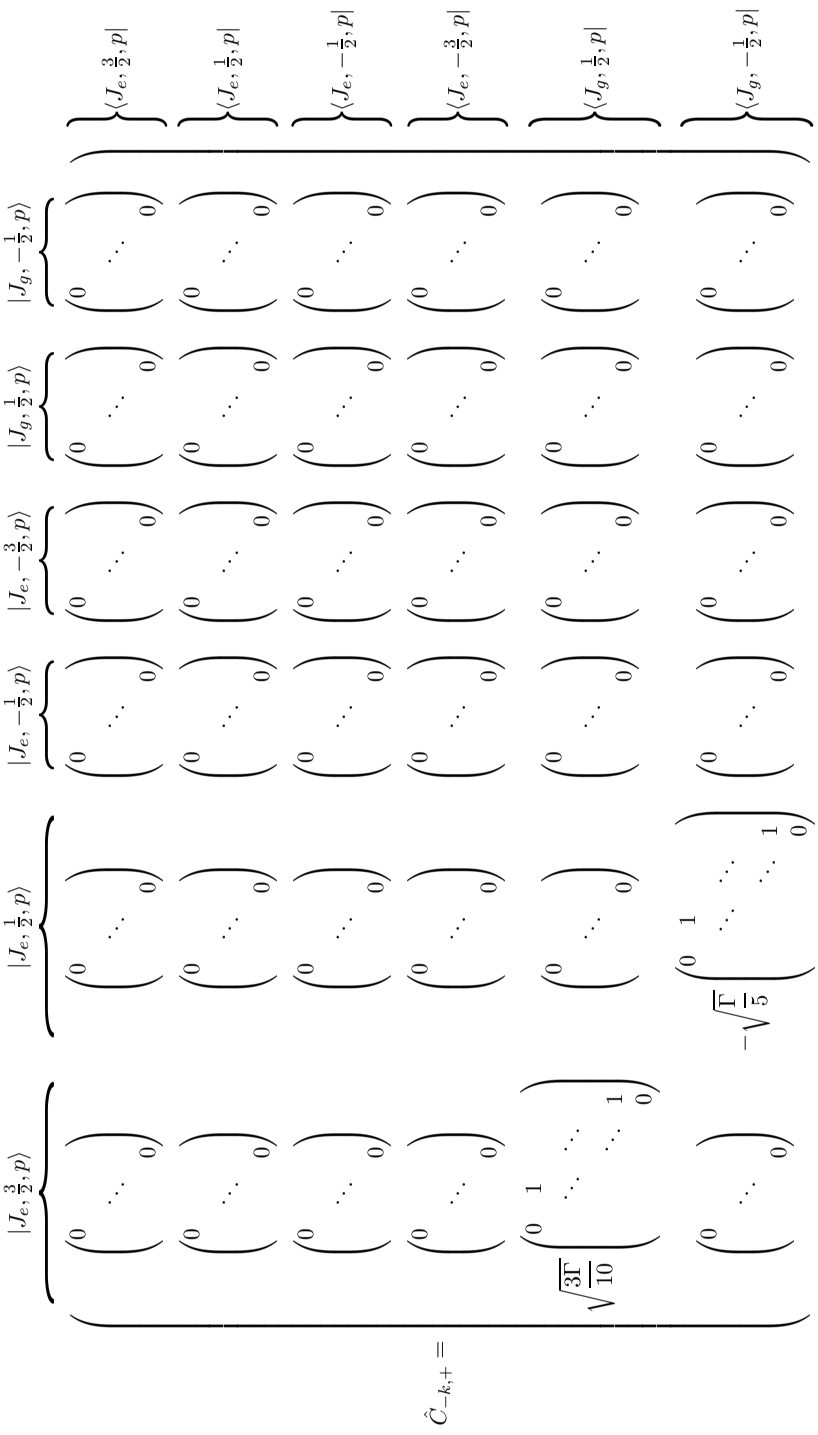

Figure B.2: Matrix form of the quantum jump operator $\hat{C}_{k',q}$ for $J_e = 3/2$ and $J_g = 1/2$.

Bibliography

[1] C. S. Adams and E. Riis, *Prog. Quant. Electr.* **21**, 1 (1997).

[2] D. J. Wineland and H. Dehmelt, *Bull. Am. Phys. Soc.* **20**, 637 (1975).

[3] T. W. Hänsch and A. L. Shawlow, *Opt. Comm.* **13**, 68 (1975).

[4] A. Aspect, E. Arimondo, R. Kaiser, N. Vansteenkiste and C. Cohen-Tannoudji, *Phys. Rev. Lett.* **61**, 826 (1988).

[5] W. Ketterle and N. J. van Druten, *Evaporative cooling of trapped atoms in : Advances in Atomic, Molecular and Optical Physics*, San Diego Academic Press (1996).

[6] H. F. Hess, *Bull. Am. Phys. Soc.* **30**, 854 (1985).

[7] H. F. Hess, *Phys. Rev. B* **34**, 3476 (1986).

[8] E. A. Cornell, C. E. Wieman, *Int. J. Mod. Phys B* **16**, 4503 (2002).

[9] M. H. Anderson, J. Ensher, M. Matthews, C. Wieman, and E. Cornell, *Science* **269**, 198 (1995).

[10] K. B. Davis, M. O. Mewes, N. Van Druten, D. Durfee, D. Kurn, and W. Ketterle, *Phys. Rev. Lett.* **75**, 3969 (1995).

[11] C. C. Bradley, C. A. Sackett, and R. G. Hulet, *Phys. Rev. Lett.* **78** 985 (1997).

[12] C. C. Bradley, C. A. Sackett, J. J. Tollett, and R. G. Hulet, *Phys. Rev. Lett.* **75** 1687 (1995).

[13] D. Fried, T. Killian, L. Willmann, D. Landhuis, S. Moss, D. Kleppner and T. Greytak, *Phys. Rev. Lett.* **81**, 3811 (1998).

[14] M. Inguscio, S. Stringari, and C. E. Wieman, *Proceedings of the International School of Physics Enrico Fermi, Course CXL, Bose-Einstein Condensation in Atomic Gases*, IOS Press, Amsterdam, (1999).

[15] K. Mølmer and Y. Castin, *Quantum and Semiclass. Opt.* **8**, 49 (1996).

[16] K. Mølmer, Y. Castin and J. Dalibard, *J. Opt. Soc. Am. B* **10**, 524 (1993).

[17] Y. Castin and K. Mølmer, *Phys. Rev. Lett.* **74**, 3772-3775 (1995).

[18] Y. Castin and J. Dalibard, *Europhys. Lett.* **14**, 761 (1991).

[19] K. Berg-Sørensen, Y. Castin, K. Mølmer and J. Dalibard, *Europhys. Lett.* **22**, 663 (1993).

[20] K. Mølmer, Y. Castin and J. Dalibard, *Phys. Rev. Lett.* **68**, 580 (1992).

[21] K. Mølmer, in Winter School on Quantum Optics, International Centre of Theoretical Physics (1994).

[22] J. Dalibard and Y. Castin, *Proc. of the Int. School of Physics "Enrico Fermi", Course CXX, Frontiers in Laser Spectroscopy* (1992).

[23] F. Damanet, *Dissipative Quantum Dynamics and Application to Superradiance*, Master Thesis, ULg (2011).

[24] J. Dalibard and C. Cohen-Tannoudji, *Laser cooling and trapping of neutral atoms*, `http://www.phys.ens.fr/~dalibard/publi2/laser_cooling.pdf`

[25] W. D. Phillips, *Rev. Mod. Phys.* **70**, 721 (1998).

[26] J. Dalibard, *Ultracold atoms, Course notes*, (2005). `http://www.phys.ens.fr/~dalibard/Notes_de_cours/DEA_atomes_froids_actuel.pdf`

[27] C. Cohen-Tannoudji and D. Guéry-Odelin, *Advances in Atomic Physics : An Overview*, World Scientific (2011).

[28] C. Cohen-Tannoudji, *Forces exerted by photons on atoms, Course notes*, Collège de France (1982). `http://www.phys.ens.fr/~Claude%20Cohen-Tannoudji/college-de-france/1982-83/1982-83.pdf`

[29] H. J. Metcalf and P. van der Straten, *Laser Cooling and Trapping*, Springer, (1999).

[30] P. Gordon and A. Ashkin, *Phys. Rev. A* **21**, 1606 (1980).

[31] V. S. Letokhov, V. G. Minogin and B. D. Pavlik, *Zh. Eksp. Teor. Fiz.* **72**, 1328 (1977).

[32] D. J. Wineland and W. Itano, *Phys. Rev. A* **20**, 1521 (1979).

[33] Y. Castin, H. Wallis and J. Dalibard, *J. Opt. Soc. Am. B* **6**, 2046 (1989).

[34] P. Lett, R. Watts, C. Westbrook, W. D. Philipps, P. Gould and H. J. Metcalf, *Phys. Rev. Lett.* **61**, 169 (1988).

[35] J. Dalibard and C. Cohen-Tannoudji, *J. Opt. Soc. Am. B* **6**, 2023 (1989).

[36] S. Chu, D. Weiss, Y. Shevy, and P. Ungar, *Atomic Physics* **11**, 636 (1989).

[37] J. Dalibard, C. Salomon, A. Aspect, E. Arimondo, R. Kaiser, N. Vansteenkiste and C. Cohen-Tannoudji, *Atomic Physics* **11**, 199 (1989).

[38] Fl. Stancu, *Group Theory in Subnuclear Physics*, Oxford University Press, (1996).

[39] P. J. Ungar, D. S. Weiss, E. Riis and S. Chu, *J. Opt. Soc. Am. B* **6**, 2058 (1989).

[40] V. Finkelstein, P. R. Berkman and J. Guo, *Phys. Rev. A* **45**, 1829 (1992).

[41] A. Kastler, *J. Phys. Rad.* **11**, 255 (1950).

[42] C. Salomon, J. Dalibard, W. D. Philipps, A. Clairon and S. Guelatti, *Europhys. Lett.* **12**, 683 (1990).

[43] S. Banerjee and R. Srikanth, *Phys. Rev. A* **75**, 062106 (2007).

[44] S. Banerjee and R. Srikanth, *Mod. Phys. Lett. B* **24**, 2485 (2010)..

[45] C. Cohen Tannoudji, in *Les Houches : Fundamental Systems in Quantum Optics*, (1990).

[46] P. Meystre and M. Sargent III, *Elements of Quantum Optics*, Springer Verlag (1991).

[47] M. Sargent III, M. O. Scully and W. E. Lamb Jr., *Laser Physics*, Addison Wesley (1992).

[48] C. Cohen-Tannoudji, J. Dupont-Roc and G. Grynberg, *Atom-Photon Interactions*, Wiley (1992).

[49] L. Allen and J. Eberly, *Optical Resonance and Two-Level Atoms*, Dover (1987).

[50] W. H. Louisell, *Quantum Statistical Properties of Radiation*, Wiley, New-York (1973).

[51] H.-P. Breuer and F. Petruccione, *The Theory of Open Quantum Systems*, Oxford University Press (2006).

[52] R. Alicki and K. Lendi, *Lect. Notes. Phys.* 717, Springer (2007).

[53] V. Bužek, *Phys. Rev. A* **58**, 1723 (1998).

[54] M. Le Bellac, *Quantum Physics*, Cambridge University Press (2006).

[55] S. Kryszewski and J. Czechowska-Kryszk, arXiv:0801.1757v1 (2008).

[56] A. Rivas, A. Douglas, K. Plato, S. F. Huelga and M. B. Plenio, *New. J. Phys.* **12**, 113032 (2010).

[57] G. C. Hegerfeldt and T. S. Wilser, in Proceedings of the II International Wigner Symposium, Goslar, 1991, edited by H. D. Döbner, W. Scherer, and F. Schröck (World Scientific, Singapore, 1992).

[58] B. Misra and E. C. G. Sudarshan, *J. Math. Phys.* **18**, 756 (1977).

[59] V. Gorini, A. Kossakowski and E. C. G. Sudarshan, *J. Math. Phys.* **17**, 821 (1976).

[60] G. Lindblad, *Commun. Math. Phys.*
textbf48, 119 (1976).

[61] H. Gutmann, *Description and control of decoherence in quantum bit systems*, PhD Thesis (2005).

[62] C. A. Brasil, F. F. Fanchini, and R. de Jesus Napolitano, arXiv:1110.2122v2 (2012).

[63] H. J. Carmichael, *An Open Systems Approach to Quantum Optics*, LNIP m18, edited by W. Beiglböck (Springer, New York, 1993).

[64] R. Dum, P. Zoller and H. Ritsch, *Phys. Rev. A* **45**, 315 (1992).

[65] N. Gisin and I. Percival, *Phys. Rev. Lett. A* 167, 315 (1992); *J. Phys. A* **25**, 5677 (1992).

[66] D. Bohm, *Phys. Rev.* **85**, 166 (1952).

[67] H. J. Carmichael : lecture notes at U.L.B., unpublished (1991).

[68] H. J. Carmichael and L. Tian, in OSA Annual Meeting Technical Digest (1990).

[69] R. H. Dicke, *Am. J. Phys.* **49**, 925 (1981).

[70] C. Cohen-Tannoudji and J. Dalibard, *Europhys. Lett.* **1**, 441 (1986).

[71] P. Zoller, M. Marte and D. F. Walls, *Phys. Rev. A* **35**, 198 (1987).

[72] F. Bardou, J.-P. Bouchaud, O. Emile, A. Aspect and C. Cohen-Tannoudji, *Phys. Rev. Lett.* **72**, 203 (1994).

[73] R. Blatt, W. Ertmer, P. Zoller and J. L. Hall, *Phys. Rev. A* **34**, 3022 (1986).

[74] C. Cohen-Tannoudji, F. Bardou and A. Aspect, in Laser Spectroscopy X (1991).

[75] C. Cohen-Tannoudji, B. Zambon and E. Arimondo, *C. R. Acad. Sci.* **314**, 1139, 1293 (1992).

[76] K. Berg-Sørensen, Y. Castin, K. Mølmer and J. Dalibard, poster at ICAP XIII (1992).

[77] P. Marte, R. Dum, R. Taieb, P. Lett and P. Zoller, *Phys. Rev. Lett.* **71**, 1335 (1993).

[78] J. Javanainen and S. Stenholm, *Appl. Phys.* **21** 35 (1980).

[79] D. Budker, D. F. Kimball and D. P. DeMille, *Atomic Physics : An Exploration through Problems and Solutions*, Oxford University Press (2004).

[80] `http://www.nist.gov/`

[81] J. J. Sakurai, *Modern Quantum Mechanics*, Addison Wesley (1994).

[82] S. A. Gardiner, *Quantum Measurement, Quantum Chaos and Bose-Einstein Condensates*, Phd Thesis, Leopold-Franzens-Universität Innsbruck (2000).

[83] M. O. Scully and S. Zubairy, *Quantum Optics*, Cambridge University Press (1997).

[84] A. Cesa, *Contribution to the theory of artificial gauge fields : study of a two-atom system with dipole-dipole interactions*, Master Thesis, ULg (2012).

[85] J. W. Dunn and C. H. Greene, *Phys. Rev. A* **73**, 033421 (2006).

[86] G. Nienhuis, J. de Kloe and P. van der Straten, *J. Opt. Soc. Am. B* **12**, 520 (1995).

[87] P. Hamilton, G. Kim, T. Joshi, B. Mukherjee, D. Tiarks and H. Müller, *Phys. Rev. A* **89**, 023409 (2014).

[88] P. D. Lett, R. N. Watts, C. I. Westbrook, W. D. Phillips, P. L. Gould, and H. J. Metcalf, *Phys. Rev. Lett.* **61**, 169 (1988).

[89] B. Smeets, R. W. Herfst, E. te Sligte, P. van der Straten, H. C. W. Beijerinck, and K. A. H. van Leeuwen, *J. Opt. Soc. A* **22**, 11 (2005).

[90] M. D. Hoogerland, H. F. P. de Bie, H. C. W. Beijerinck, E. J. D. Vredenbregt, K. A. H. van Leeuwen, P. van der Straten and H. J. Metcalf, *Phys. Rev. A* **54**, 3206 (1996).

[91] A. Messiah, *Quantum Mechanics (Volume II)*, New York : North Holland Publishing, (1981).

[92] C. Cohen-Tannoudji, B. Diu, and F. Laloë, *Quantum mechanics (Volume II)*, Paris, (1973).

[93] `http://pdg.lbl.gov/2002/clebrpp.pdf`

[94] E. P. Wigner, *Group Theory*, Academic Press, New York, (1959).

[95] E. U. Condon and G. H. Shortley, *The Theory of Atomic Spectra*, Cambridge University Press, New York, (1953).

[96] M. E. Rose, *Elementary Theory of Angular Momentum*, Wiley, New York, (1957).

[97] E. R. Cohen, *tables of the Clebsch-Gordan Coefficients*, North American Rockwell Science Center, Thousand Oaks, Calif., (1974).

[98] C. Cohen-Tannoudji, in *Frontiers in Laser Spectroscopy*, Les Houches (1975).